Study of the Effect of Sensor Position on the Forced Response Characteristics of Rotors with Active Magnetic Bearings

by

Dharamendra Niranjan Rawal

Thesis submitted to the Faculty of the

Virginia Polytechnic Institute and State University

in partial fulfillment of the requirements for the degree of

Master of Science

in

Mechanical Engineering

APPROVED:

R. G. Kirk, Chairman

D. A. Elrod

L. D. Mitchell

August, 1990

Blacksburg, Virginia

Study of the Effect of Sensor Position on the Forced Response Characteristics of Rotors with Active Magnetic Bearings

by

Dharamendra Niranjan Rawal

R. G. Kirk, Chairman

Mechanical Engineering

(ABSTRACT)

The need for better performance of turbomachinery with active magnetic bearings has necessitated a study of such systems for accurate prediction of their vibrational characteristics. This research presents a modification of existing transfer matrix methods for rotor analysis, to predict the response of rotor systems with active magnetic bearings. The position of the magnetic bearing sensors is taken into account and the effect of changing sensor position on the vibrational characteristics of rotor systems is studied. The modified algorithm is validated using a simpler modified Jeffcott model. The effect of changing from a rotating unbalance excitation to a constant excitation in a single plane is also studied. An eight-stage centrifugal compressor rotor is analyzed using the modified transfer matrix code. The results for a two-mass Jeffcott model are presented as plots of critical frequency vs. sensor position and amplitude at critical frequency vs. sensor position. Plots of amplitude vs. frequency and phase angle vs. frequency for different cases of sensor location are also presented. The results obtained by analyzing this two-mass model with the modified transfer matrix method have been compared with the results of the modified Jeffcott analysis for the purpose of verification. Also included are plots of amplitude vs. frequency and phase angle vs. frequency for the eight-stage centrifugal compressor rotor. These plots will demonstrate the significant influence that sensor location has on the critical frequencies and the amplitudes at the critical frequencies of the rotor system.

Acknowledgements

My thanks go to Dr. Kirk for giving me an opportunity to work on this interesting project and for guiding me throughout the course of it. I also thank John Keesee with whom it has been such a pleasure to work. His comments and suggestions have proved very useful. Dr. Mitchell and Dr. Elrod have given me their valuable time and expertise and I acknowledge their help and support. Finally I sincerely thank my parents for helping and supporting me throughout the duration of my study, and for always being there when I needed them.

Table of Contents

List of Illustrations

List of Tables

Nomenclature

a	eccentricity in 2 DOF Jeffcott model (mm)
a_x	eccentricity component in transfer matrix equation (mm)
a_y	eccentricity component in transfer matrix equation (mm)
C	damping (N-sec/mm)
E	modulus of elasticity (N/mm^2)
e	exponential constant = 2.7182818 (dim)
F_{xc}	externally applied planar excitation force in the transfer matrix equations (N)
F_{xs}	externally applied planar excitation force in the transfer matrix equations (N)
F_ϕ	constant excitation force in Jeffcott model (N)
I	moment of inertia of massless shaft (mm^4)
I_p	polar moment of inertia (mm^4)
I_t	transverse moment of inertia (mm^4)
i	complex constant (dim)
K	stiffness ratio, k_1/k_2 (dim)
K	stiffness in transfer matrix equations (N/mm)
k_1	AMB stiffness (N/mm)
k_2	shaft stiffness (N/mm)

L	length of shaft in 2 DOF Jeffcott model (mm)
l	length of massless shafts in transfer matrix equations (mm)
M	mass ratio, m_1/m_2 (dim)
M_1	effective journal mass in Jeffcott model (Kg)
M_2	mid-span mass in Jeffcott model (Kg)
M_{xc}	moment component in transfer matrix equation (N-mm^2)
M_{xs}	moment component in transfer matrix equation (N-mm^2)
m_i	point masses in transfer matrix equations (Kg)
R_i	complex solution of the Jeffcott model
r_i	whirl deflection in Jeffcott model
r_s	whirl deflection at sensor location in Jeffcott model
s	frequency of shaft rotation (rad/sec)
t	time (sec)
V_{xc}	shear component in transfer matrix equation (N)
V_{xs}	shear component in transfer matrix equation (N)
x_i	x component of the whirl deflection in the Jeffcott model (mm)
xc	deflection component in transfer matrix equations (mm)
xs	deflection component in transfer matrix equations (mm)
y_i	y component of the whirl deflection in the Jeffcott model (mm)
z	axial distance between sensor location and bearing sensor (mm)
α	ratio of the distance between bearing centerline and sensor to half-span of the rotor (dim)
θ_{xc}	slope component in the transfer matrix equation (rad)
θ_{xs}	slope component in the transfer matrix equation (rad)
ω	frequency of shaft excitation (rad/sec)

Chapter 1

INTRODUCTION AND LITERATURE SEARCH

The use of active magnetic bearings in turbomachinery is a comparatively new development but one which has shown great promise for better control of rotating equipment. The idea behind these bearings is not new however. The use of magnetic attraction to levitate the rotor shaft free of the bearing has been tried before, but because the system is inherently unstable (Hustak, 1985) unless a real-time control system is used, these attempts were not successful. The first actively controlled bearing was developed in the 1950's (Keesee, 1989). Since then the use of active magnetic bearings has gained widespread acceptance particularly in North America and Canada. Hendrickson et al (1987) give some examples of the varied uses to which active magnetic bearings have been applied. Kirk (1988) lists a number of turbomachinery installations where active magnetic bearings have been used.

The principle of how active magnetic bearings work is very simple. A magnet will attract any ferromagnetic material. Thus, the rotor shaft is wound with ferromagnetic lamination near the journal location. The stator is made up of slotted lamination stack and has coils wound around the

slots. When an electric current is supplied to the coils of lamination in the stator, the lamination acts as an electromagnet and attracts the ferromagnetic material on the rotor shaft. One such electromagnet is located in each of the four quadrants inclined at 45°. The attraction of each of these four electromagnets is varied by a control system to levitate the rotor shaft and keep it levitated while it is rotating. In order to enable the control system to decide the amount of attraction to be applied to the rotor shaft through each electromagnet, sensors are placed at some distance from the stator along the axis of the rotor shaft. These sensors sense the location of the shaft. The configuration is illustrated in Figs. 1 and 2.

Magnetic bearings possess a number of advantages compared to conventional bearings. They give an almost unlimited control over rotor vibrational characteristics due to adjustable stiffness and damping. Automatic balancing is possible by allowing the rotor to spin on its inertial axis. This leads to decreased vibrations and noise. Active magnetic bearings do not require lubrication, and since they are non-contact bearings, they eliminate the possibility of wear and tear of the stator and rotor surfaces. Hendrickson et al (1987) demonstrates the tolerance of magnetic bearings to a wide range of temperatures and also their insensitivity to hostile environments. Zlotykamien (1988) gives a good description of the various advantages of active magnetic bearings.

One of the main disadvantages of active magnetic bearings is the relatively high costs involved due to the presence of a complex control system. Since magnetic bearings require electricity to generate the magnetic field that keeps the rotor levitated, the possibility of power failure has to be taken into account and conventional backup bearings have to be provided. The weight of the rotor shaft has to be within the limits of the carrying capacity of magnetic bearings. Being a comparatively new development, the vibrational behaviour of rotor systems with magnetic bearings needs furthur study specially with respect to their stability characteristics.

Figure 1. Picture of Active Magnetic Bearing (Courtesy of Magnetic Bearings, Inc., USA)

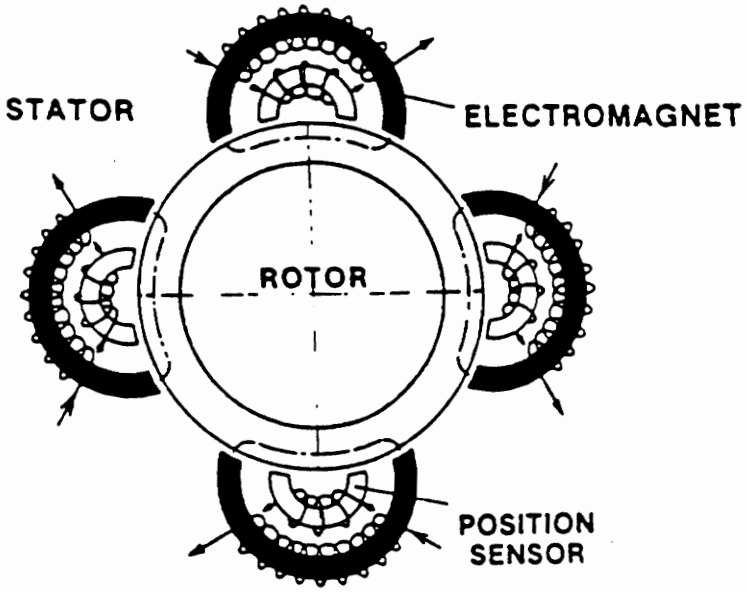

Figure 2. Active Magnetic Bearing Configuration (Zlotykamien, 1988)

Previous Research

Most of the research in active magnetic bearings has been in the control systems used. Schweitzer (1985) shows a method for controlling an elastic rotor so that it can be represented by a low-order model amenable to control techniques. Williams, Keith, and Allaire (1990) have developed theoretical relationships to relate the characteristics of a controller transfer function to the stiffness and damping properties of an active magnetic bearing. Burrows and Sahinkaya (1988) evaluate various strategies for applying a magnetic bearing to control the synchronous vibration of a flexible rotor. Kirk et al (1988) present the results of shop tests on a high-speed eight-stage centrifugal compressor supported by active magnetic bearings along with some design recommendations. Keesee (1989) examines the effects of sensor position on the critical frequencies of rotors with active magnetic bearing.

Research Objective

The sensors are not located at the place where the attraction forces are applied on the rotor shaft but at some distance away along the axis of the shaft. Due to this "non-colocation" of the sensors from the bearing position, the deflection sensed by the sensors is not the same as the actual deflection at the bearing but differs from it by some magnitude and phase, dictated by the mode shape of the rotor shaft. Because of this, the stiffness and damping forces of the active magnetic bearing depend not on the deflection at the bearing location, but on the deflection at the sensor location. For such cases, the vibrational characteristics of the rotor system is different from that obtained using conventional analysis programs. The objective of this research is to take into account the effect of sensor non-colocation on the vibrational characteristics of rotors with active magnetic bearings.

This research is an extension of the work done by Keesee (1989) and involves the modification of an existing transfer matrix code to account for sensor non-colocation. Sensor non-colocation effects on forced response amplitudes and phase angles are studied. The other objective of this research is to compare the vibrational characteristics of rotor systems, when they are subject to unbalance excitation with circular synchronous shaft rotation and excitation in one plane with no shaft rotation or whirling. The effect of changing the mass at the bearing locations with respect to the mass at midspan is studied. The effect of changing the stiffness of the bearings with respect to the stiffness of the shaft is studied. The effect of changing the amount of damping in the system is also studied.

Two models of rotor systems are used for this study. One is a simple two-mass Jeffcott model. The other is an eight-stage centrifugal compressor rotor model. The modification of the transfer matrix program is validated by comparing its results for the two-mass model with the results obtained from a simple program written to specifically analyze the two-mass model. Chapter 2 gives the theory of the Jeffcott model as well as the modification made to account for sensor non-colocation. It also gives the results obtained from the two-mass Jeffcott model. Chapter 3 details the theory of transfer matrices and the different modifications necessary to account for sensor non-colocation and excitation forces. The results of the typical eight-stage centrifugal rotor system are also illustrated in Chapter 3. These results provide the validation of the modifications made in the transfer matrix code. Chapter 4 gives the recommendations and conclusions of this research.The Appendix contains the Jeffcott model code, the data for the two-mass model and the eight-stage compressor rotor system model, guidelines for the use of the AMB (Active Magnetic Bearing) modified transfer matrix code and additional plots illustrating the effect of a change in sensor position on the vibrational characteristics of a two-mass rotor system.

Chapter 2

THE JEFFCOTT MODEL

Jeffcott (1919) has analyzed a simple rotor model composed of a long thin massless elastic shaft with a given stiffness and a central disk mass with a given unbalance. Since the unbalance force rotates at shaft speed, the frequency of whirl will be the same as the frequency of shaft rotation. Jeffcott assumes that the bearings are radially rigid. Thus, the system reduces to a single-degree-of-freedom vibrations problem as shown in Figs. 3-5.

The equations of motion for the system shown in Fig. 3 and Fig. 4 are as follows

$$M\frac{d^2}{dt^2}(x + a\cos\omega t) + C\frac{dx}{dt} + Kx = 0 \qquad [2.1]$$

$$M\frac{d^2}{dt^2}(y + a\sin\omega t) + C\frac{dy}{dt} + Ky = 0 \qquad [2.2]$$

These equations can be simplified and rewritten as follows

$$M\ddot{x} + C\dot{x} + Kx = M\omega^2 a\cos\omega t \qquad [2.3]$$

$$M\ddot{y} + C\dot{y} + Ky = M\omega^2 a\sin\omega t \qquad [2.4]$$

Henceforward, the complex variable $r = x + iy$ will be used to indicate the whirl radius in the Jeffcott model, and all the equations will be stated in terms of r. Equations 2.3 and 2.4 can be combined and written as a single equation by using complex algebra as follows

$$M\ddot{r} + C\dot{r} + Kr = M\omega^2 r \qquad [2.5]$$

The AMB Modification

To modify the Jeffcott model for active magnetic bearings, four additional factors are assumed.

- First, the stiffness and damping of the magnetic bearing are considered. This is because the forces due to bearing stiffness and damping depend on the deflection of shaft sensed by the active magnetic bearing sensor, and thus, are subject to change as the sensor position changes. A change in the excitation frequency will also change the shaft deflection sensed by the sensor and and consequently change the bearing stiffness and damping forces.

- Second, the presence of journal masses at the bearing locations is assumed. Thus, a central disk mass at midspan and the two journal masses at the bearings are considered in the formulation of the equations of motion.

- A harmonic excitation force in one plane F_ϕ that can be applied at the bearing locations is considered. This is so that a magnetic bearing rig can be tested without rotating the rotor shaft. Instead, the journal masses are excited at a particular frequency and the vibrational characteristics of the rig are examined. Unlike an unbalance force where the amplitude of the force changes with the rotor spinning speed, the amplitude of the planar harmonic excitation force remains constant irrespective of the rotor spinning speed and hence this force can also be termed as a constant magnitude excitation force.

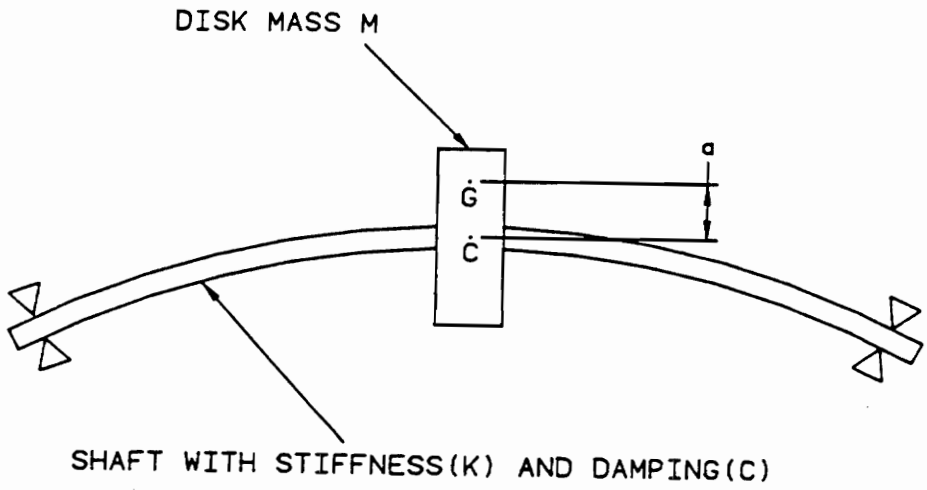

Figure 3. Original Jeffcott Model

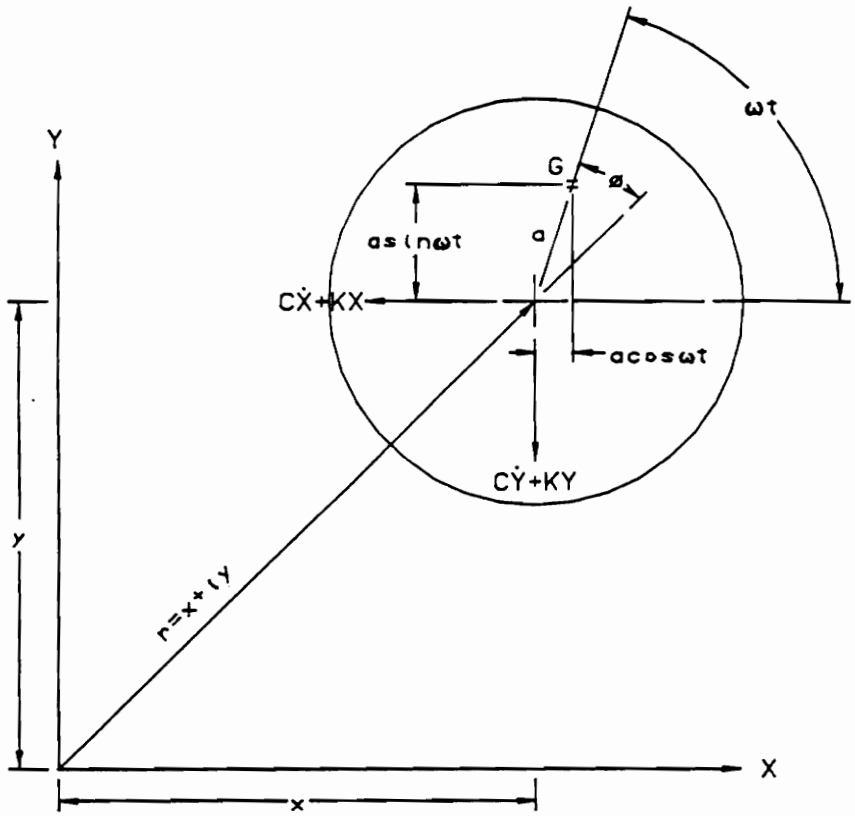

Figure 4. Geometry of Original Jeffcott Model

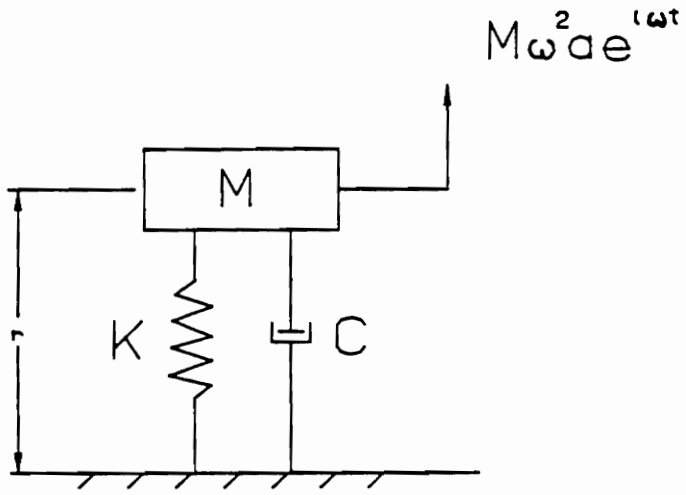

Figure 5. Single DOF Representation of the Jeffcott Model

- Lastly, consideration is given to the sensors that detect the deflection of the shaft at some distance from the bearings. This deflection is then used to modify the stiffness and damping characteristics of the active magnetic bearings.

The bearing pedestal is assumed to be rigid. The entire configuration after modification is illustrated in Figs. 6-8.

Since the unbalance force and the planar harmonic excitation force are applied symmetrically along the longitudinal axis of the rotor, only the first and third modes are observed. The second mode cannot be observed in the reduced two-mass model.

Derivation of Modified Equations

To formulate the equations of motion, consider the freebody diagram shown in Fig. 9.
Note that the forces on the mass M_1 depend on the deflection and velocity at the sensor location. To express the deflection at the sensor location (r_s) as a function of the deflection at the disk (r_2) and at the bearing (r_1), it is assumed that the first and third modes of vibration are half-sine curves. These modes are illustrated in Fig. 10. Thus

$$r_s = r_1 + (r_2 - r_1)\sin(\frac{\pi z}{L}) \qquad [2.6]$$

so that when $z = 0 \quad r_s = r_1$ and

when $z = L/2 \quad r_s = r_2$

The two equations of motion will be

$$M_2\ddot{r}_2 = M_2\omega^2 a e^{i\omega t} - C_2(\dot{r}_2 - \dot{r}_1) - K_2(r_2 - r_1) \qquad [2.7]$$

$$M_1\ddot{r}_1 = F_\phi e^{i\omega t} + C_2(\dot{r}_2 - \dot{r}_1) + K_2(r_2 - r_1) - C_1\dot{r}_s - K_1 r_s \qquad [2.8]$$

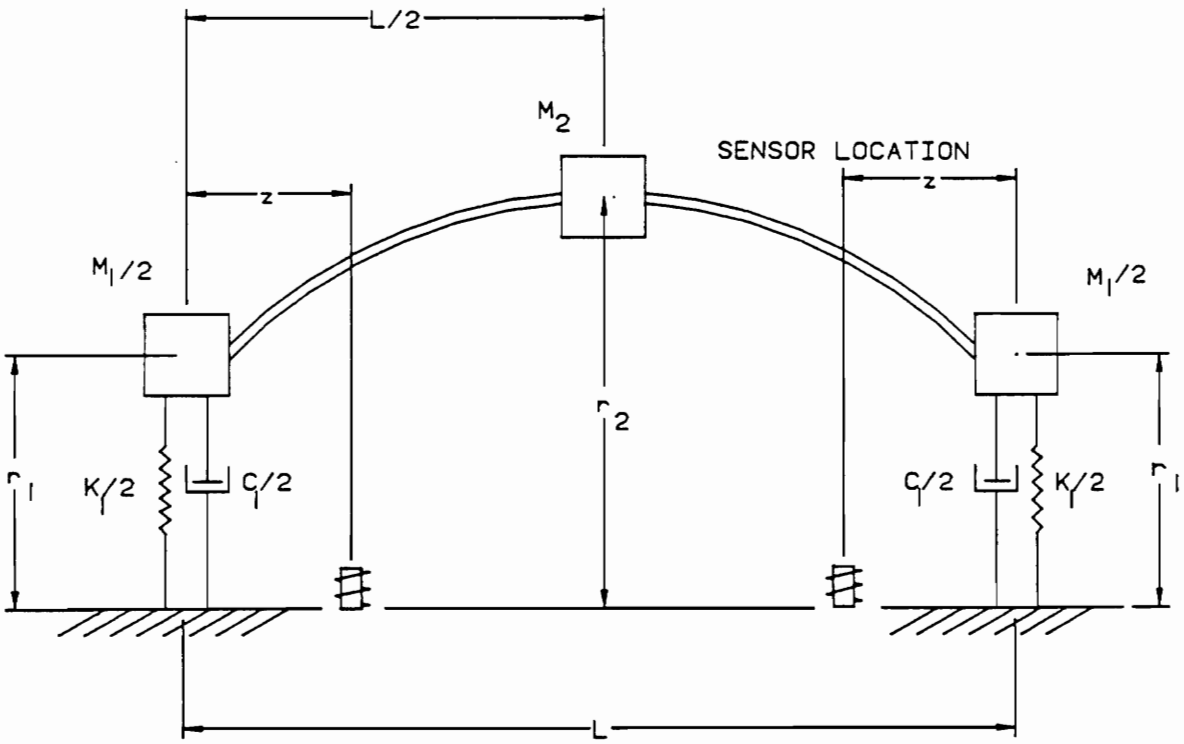

Figure 6. The Modified Jeffcott Model

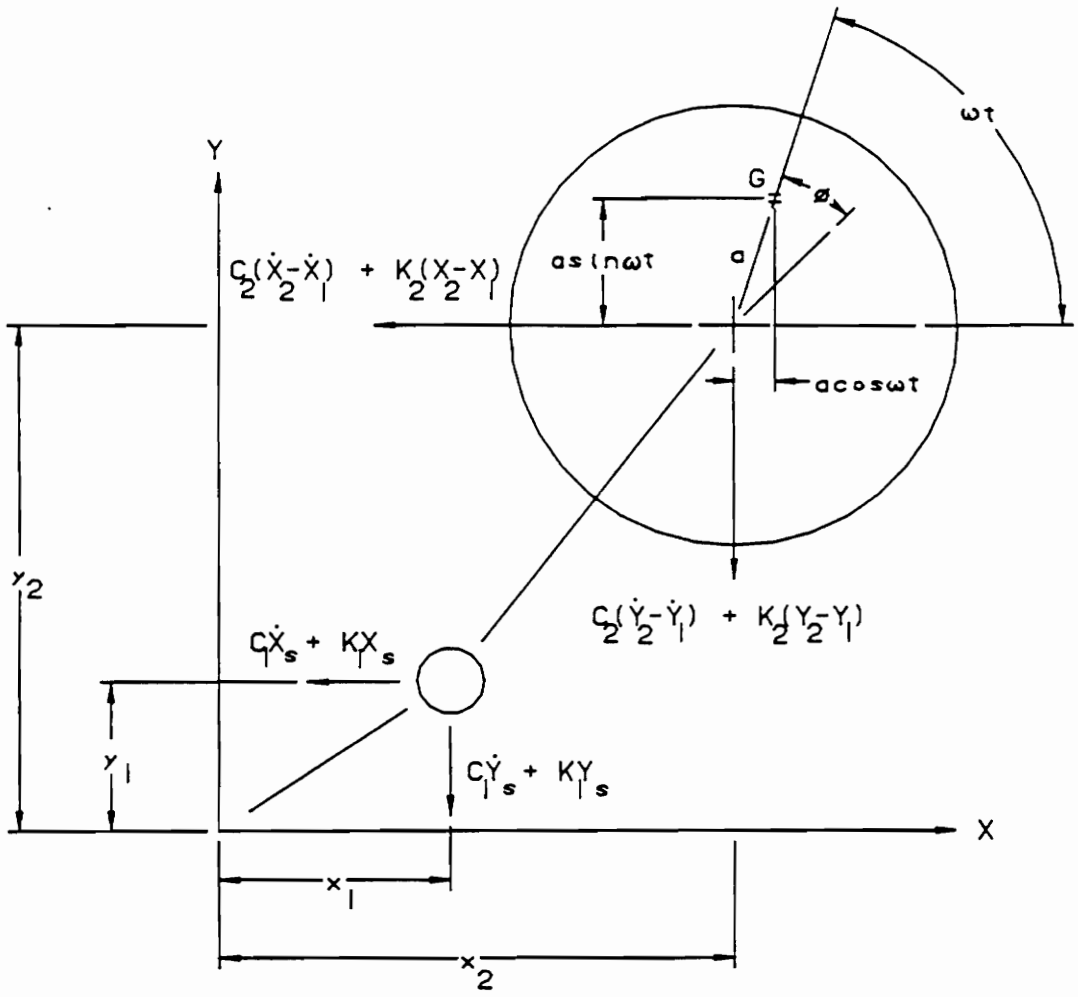

Figure 7. Geometry of the Modified Jeffcott Model

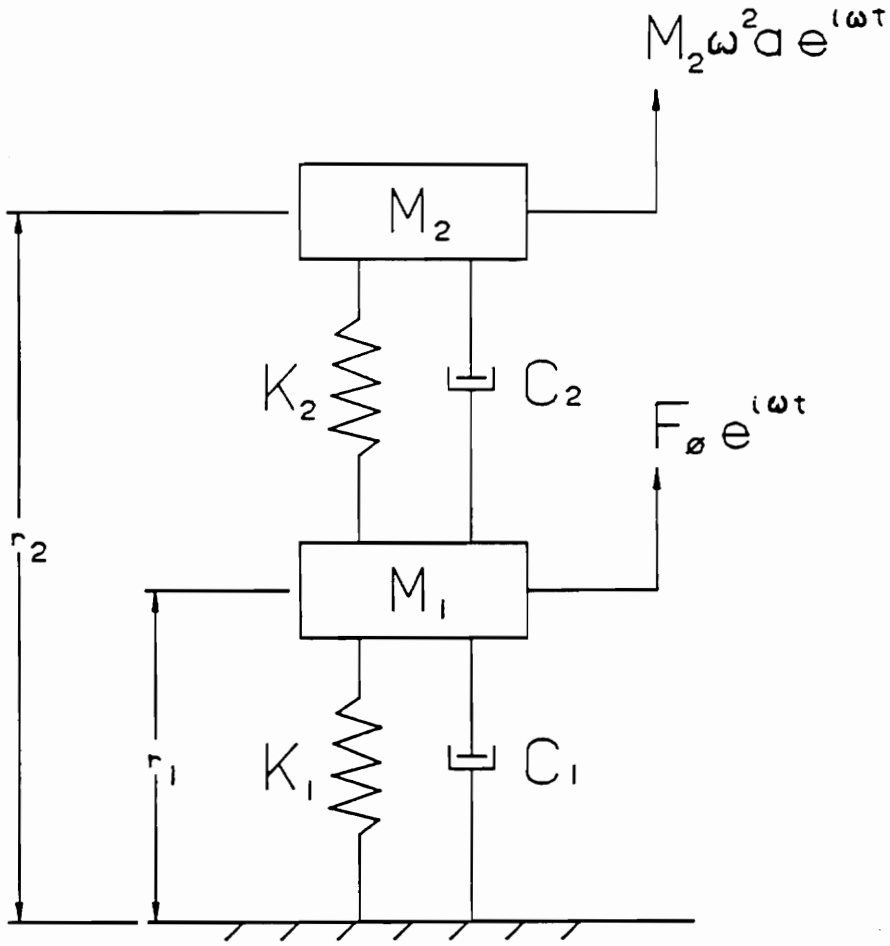

Figure 8. Reduced Two DOF Representation of the Modified Jeffcott Model

Let $\alpha = \frac{z}{(L/2)}$. We have $\sin\frac{\pi z}{L} = \sin\frac{\pi\alpha}{2}$ Let $\beta = \sin\frac{\pi\alpha}{2}$.

Now substituting for r_s in equation [2.8] using equation [2.6] and simplifying,

$$M_2\ddot{r}_2 + C_2\dot{r}_2 - C_2\dot{r}_1 + K_2r_2 - K_2r_1 = M_2\omega^2 a e^{i\omega t} \qquad [2.9]$$

$$M_1\ddot{r}_1 + (C_2 + C_1 - C_1\beta)\dot{r}_1 - (C_2 - C_1\beta)\dot{r}_2 + (K_2 + K_1 - K_1\beta)r_1 - (K_2 - K_1\beta)r_2 = F_\phi e^{i\omega t}$$

[2.10]

Assuming $r = Re^{i\omega t}$

$\dot{r} = i\omega Re^{i\omega t}$

$\ddot{r} = -\omega^2 Re^{i\omega t}$

Expressing in matrix form and simplifying,

$$-\omega^2\begin{bmatrix} M_1 & 0 \\ 0 & M_2 \end{bmatrix} - \omega^2\begin{bmatrix} i\omega(C_2 + C_1 - C_1\beta) + K_2 + K_1 - K_1\beta & i\omega(C_1\beta - C_2) + K_1\beta - K_2 \\ -i\omega(C_2) - K_2 & i\omega(C_2) + K_2 \end{bmatrix}\begin{bmatrix} R_1 \\ R_2 \end{bmatrix}$$

$$= \begin{bmatrix} F_\phi \\ M_2\omega^2 a \end{bmatrix}$$

[2.11]

Solving this system of equations for R_1 and R_2

$$\begin{bmatrix} R_1 \\ R_2 \end{bmatrix} = \frac{1}{S_{22} \times S_{11} - S_{21} \times S_{12}} \begin{bmatrix} S_{11}F_\phi + S_{12}M_2\omega^2 a \\ S_{21}F_\phi + S_{22}M_2\omega^2 a \end{bmatrix} \qquad [2.12]$$

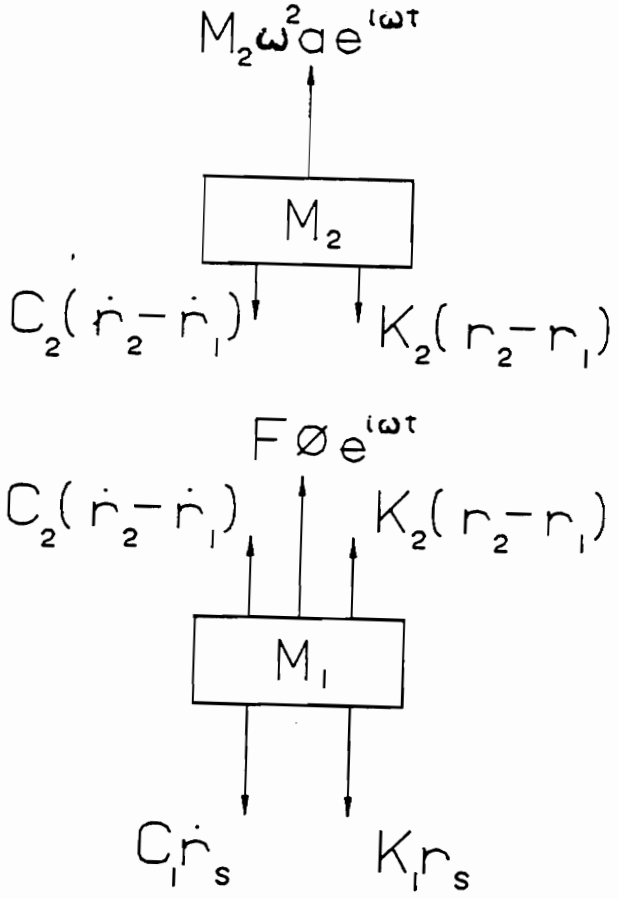

Figure 9. Freebody Diagram of the Modified Jeffcott Model

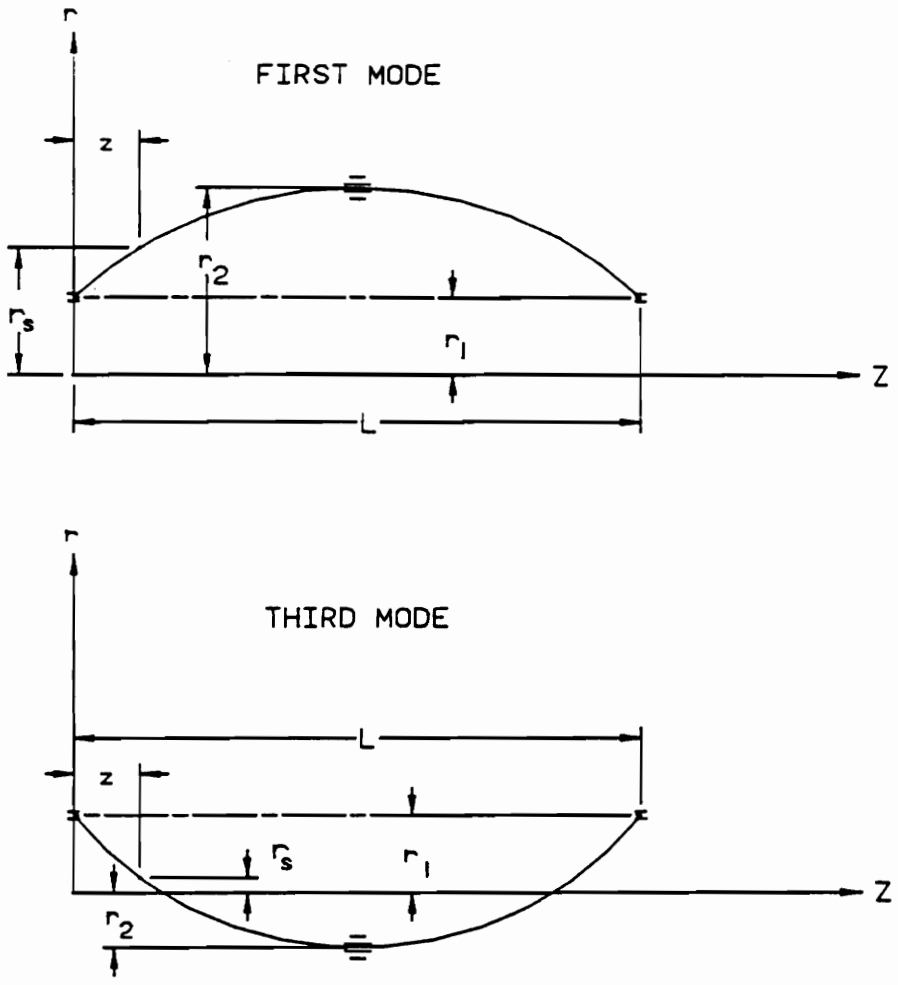

$$r_s = (r_2 - r_1)\sin(\pi z/L) + r_1$$

Figure 10. Mode Shapes for the Modified Jeffcott Model

where $S_{12} = K_2 - K_1\beta + i[\omega(C_2 - C_1\beta)]$

$S_{22} = -M_1\omega^2 + K_1 + i(\omega C_1) + S_{12}$

$S_{21} = K_2 + i(\omega C_2)$

$S_{11} = -M_2\omega^2 + S_{21}$

The phase angles are obtained as follows

$$\theta_2 = \cos^{-1}\left[\frac{real(R_2)}{\sqrt{\{real(R_2)\}^2 + \{imag(R_2)\}^2}}\right] \qquad \theta_1 = \cos^{-1}\left[\frac{real(R_1)}{\sqrt{\{real(R_1)\}^2 + \{imag(R_1)\}^2}}\right]$$

It must be noted at this time that since the force F_ϕ is applied in one plane the motion of the masses is also in one plane. However, for computational and analytical simplicity, it will be assumed that the force F_ϕ acts in two mutually perpendicular planes, in a manner similar to the unbalance force. Since the motion is assumed to be circular, the maximum amplitudes in the X or Y direction, will be equal to the absolute value of R_i. Therefore, the solution R_i is valid even when the applied force F_ϕ is in one plane only. Similarly the phase angles calculated above are also valid for the force F_ϕ.

The next section presents the results of a computer program, using the modified equations of motion for finding the amplitudes and phase angles of a two-mass rotor system. A listing of the program is given in the Appendix E.

Discussion of Plots

The plots in Figs. 12-37 illustrate the effect of a change in sensor location on the vibrational characteristics of the two-degree-of-freedom rotor system. These are plots of critical frequency vs. sensor location (defined in terms of α) and amplitude at critical frequency vs. sensor location. The different line types indicate different cases of mass and stiffness ratios. Additional

plots of amplitude vs. frequency and phase angle vs. frequency for the 2-mass Jeffcott model with a constant bearing damping value are given in Appendix G. Figure 11 shows an example plot of this type. The plots are made for the data:

mass ratios $(M_1/M_2) = 1 , 0.25$

stiffness ratios $(K_1/K_2) = 0.5 , 2$

amplification factors $(\sqrt{K_1 \times M_1}\,/C_1) = 10 , 0.5$

The damping of the shaft is assumed to be zero and the damping of the bearing is calculated assuming an amplification factor and considering the critical damping of the bearing mass. If the amplification factor is less there is more effective damping in the system and vice versa. The data for the two-mass rotor system is given in Table 1.

Positive α values indicate that the sensor is placed between a bearing location and midspan *i.e.,* the sensor is placed inboard while negative α values indicate that the sensor is located on the rotor shaft overhang *i.e.,* the sensor is placed outboard. Increasing α values indicate increasing distance of the sensor from the bearing location in either direction.

Figures 12-24 show sensor influence on rotor vibrational characteristics when an unbalance excitation of 6.78 Nmm is applied to the midspan mass, while Figs. 25-37 show sensor influence on rotor vibrational characteristics when a planar excitation of 88.96 N is applied to both the journal masses at the bearing locations.

It is to be kept in mind that the rotor is subject to either the unbalance force or the constant excitation force but never both the forces simultaneously, as the results would be very difficult to interpret and would be of limited use.

Figures 12-17 show the effect of sensor location on the first and third critical frequencies for amplification factors of 10 (Figs. 12-15) and 0.5 (Figs. 16-17) for different values of mass ra-

Table 1. Data for Simple Two Mass Jeffcott Model AMB Rotor System

ROTOR SYSTEM PROPERTY	SI UNITS	ENGLISH UNITS
Weight of Mass M_2	88.96 N	20.0 lb_f
Shaft length L	635 mm	25 in
Shaft diameter	25.4 mm	1 in
Shaft stiffness K_2	763.40 N/mm	4359.14 lb_f/in
Modulus of Elasticity E	1.99×10^5 N/mm^2	28.9×10^6 lb_f/in^2
Critical damping of the system C_{cr}	5.26 Ns/mm	30.054 lb_f sec /in
Shaft damping C_2	0.0 Ns/mm	0.0 lb_f sec /in
Eccentricity a	0.0762 mm	0.003 in
Constant Excitation F_ϕ	177.93 N	40 lb_f

tios and stiffness ratios and the application of unbalance force excitation. Figures 18-23 show the effect of sensor location on the amplitudes at the first and third critical frequencies for amplification factors of 10 (Figs. 18-21) and 0.5 (Figs. 22-23) for different values of mass and stiffness ratios with the application of unbalance force excitation.

Figures 25-30 show sensor influence on critical frequencies for amplification factors of 10 (Figs. 25-28) and 0.5 (Figs. 29-30) for different values of mass ratios and stiffness ratios and the application of an excitation force in one plane. Figures 31-36 show sensor influence on amplitudes at the critical frequencies for amplification factors of 10 (Figs. 31-34) and 0.5 (Figs. 35-36) for different values of mass ratios and stiffness ratios and the application of planar excitation at the bearing locations.

Figures 24 and 37 show the influence of mass ratio on the peak amplitudes at critical frequency for an amplification factor of 0.5 and the application of unbalance force excitation (Fig. 24) and planar excitation (Fig. 37).

Results of the Modified Jeffcott Model

From the results of the test run of the modified Jeffcott model the following observations were made.

1. The first critical frequency increases as the sensor is moved from the outboard location in the direction of inboard location. This is illustrated by Figs. 12, 13, 16, 17 for unbalance excitation and by Figs. 25, 26, 29 and 30 for planar excitation. The third critical frequency decreases as the sensor is moved from the outboard location towards the inboard location. This is illustrated by Figs. 14 and 15 for unbalance excitation and by Figs. 27 and 28 for planar excitation. This effect of sensor location on the critical fre-

quencies has been noted and explained by Keesee (1989). However a significant new phenomena not recorded by Keesee is observed from these plots. The increasing first mode critical frequency and the decreasing third mode critical frequency coincide when a particular inboard sensor location is reached and the first mode transforms into the third mode as the sensor is moved further inboard. The particular inboard sensor location at which the first mode and third mode critical frequencies coincide depends on the amplification factor, the mass ratio and the stiffness ratio of the rotor system.

2. The amplitude at first mode critical frequency decreases as the sensor is moved from the outboard location in the direction of inboard location as illustrated by Figs. 18 and 19 for unbalance excitation and by Figs. 26 and 27 for planar excitation. This can be explained by a study of the first mode shape shown in Fig. 10. As the sensor is moved inboard it senses a greater deflection and this leads to an increase in the effective stiffness of the bearing, thus raising the first critical frequency. The amplitude at third mode critical frequency increases as the sensor is moved from the outboard location towards the inboard location until a particular inboard sensor location is reached. For this particular sensor location a peak amplitude is recorded and as the sensor is moved further inboard the amplitude starts decreasing as illustrated by Figs. 20 and 21 for unbalance excitation and by Figs. 27 and 28 for planar excitation. This phenomena can be explained by a study of the third mode shape shown in Fig. 10. As the sensor is moved from the outboard location towards the inboard location the sensor senses smaller and smaller shaft deflection values until a particular inboard sensor location where a minimum shaft deflection is found. For this particular sensor location the stiffness and damping forces at the bearing location are reduced to a negligible value and the rotor system essentially exhibits free-free vibration with large amplitudes. As the sensor is moved further inboard the sensor detects increasing shaft deflection values and therefore the amplitude starts decreasing. For cases where the first and third mode critical frequencies coincide however, the amplitude characteristics of the rotor system are a combination of the first and third

mode amplitude characteristics. This is illustrated by Figs. 22 and 23 for unbalance excitation and by Figs. 35 and 36 for planar excitation. As long as the rotor system exhibits first mode vibration, amplitude behaviour is similar to that observed in the first mode. As the first and third mode critical frequencies come together a transition stage is observed with critical frequency behaviour similar to that observed in the first mode and amplitude behaviour similar to that observed in the third mode. As the sensor is moved further inboard the amplitude and frequency characteristics of the rotor system become similar to that observed in the third mode.

3. The particular inboard sensor location at which the first and third mode critical frequencies coincide depends primarily on the the amplification factor of the rotor system. As the amplification factor is decreased *i.e.,* the bearing damping is increased, the first and third mode critical frequencies coincide at an inboard sensor location nearer the bearing. This can be seen when Fig. 12 is compared to Fig. 16 or Fig. 13 is compared to Fig. 17. Other relevant cases can be similarly compared for verification. Mass and stiffness ratios however, also affect the sensor location at which the first and third modes come together. As the mass ratio is increased *i.e.,* the mass at the journal location is increased relative to the mass at midspan, the first and third mode critical frequencies coincide at an inboard sensor location nearer the bearing. This is shown by Figs. 16, 17, 29 and 30. Stiffness ratio has an indirect effect upon this phenomena. A higher stiffness ratio *i.e.,* greater bearing stiffness relative to shaft stiffness, makes the critical frequencies and amplitudes more sensitive to changes in the sensor location. Again this is noted and explained by Keesee (1989). Consequently the rate of increase of the first critical frequency and the rate of decrease of the third critical frequency, with inboard movement of the sensor, increases and the first and third modes come together for a sensor location nearer the bearing. This behaviour is illustrated by Figs. 12-15 and by Figs. 25-28.

4. The particular inboard sensor location for which a peak amplitude is recorded in the third mode depends significantly on the mass ratio of the rotor system. As the mass ratio is

increased, the peak amplitude occurs for inboard sensor locations nearer the bearing. This is illustrated by Figs. 20, 21 and 24 for unbalance excitation and by Figs. 33, 34 and 37 for planar excitation. The reason for this behavior is due to the fact that the rotor system exhibits free-free vibration when this peak amplitude is observed. The bearing damping and stiffness values become negligible. Due to this, the deflection along the rotor longitudinal axis will depend only on the mass distribution of the rotor system and not on the bearing stiffness and damping. A higher mass ratio means greater mass at the bearing location and therefore less deflection in free-free vibration at the bearing location than at midpan. Due to this, the point of minimum shaft deflection occurs nearer to the bearing location and a sensor placed at this point will produce peak amplitudes of vibration in the rotor system.

5. The vibrational characteristics of the two-mass rotor system do not vary when a planar excitation force in one plane is used instead of a rotating unbalance. The critical frequency values, for both the first mode and the third mode, are almost the same for the unbalance force case and the planar force case. This can be seen by comparing Figs. 12-17 with Figs. 25-30.

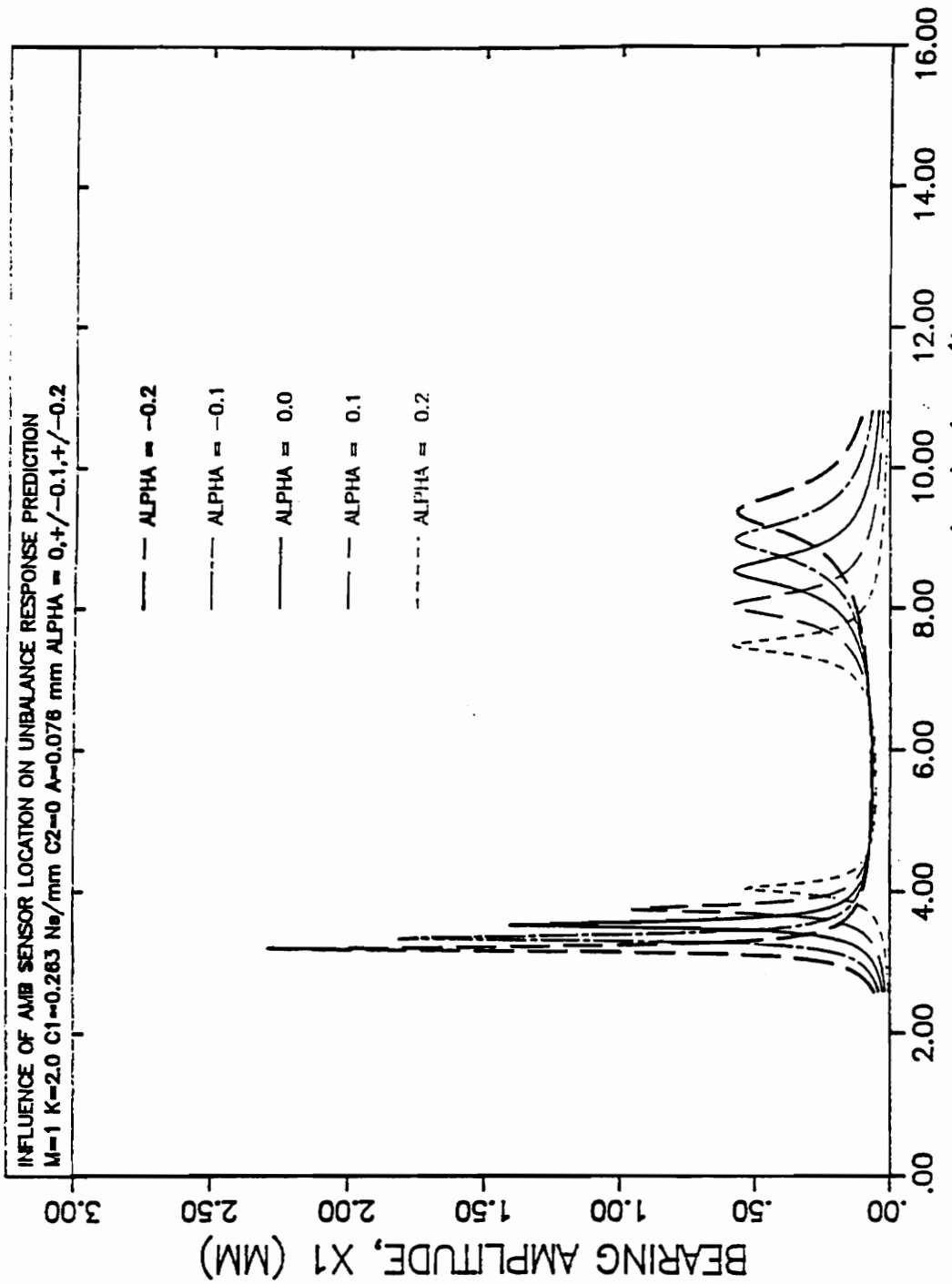

Figure 11.
Sensor Influence on Bearing Amplitude, Unbalance Excitation, M = 1, K = 2.

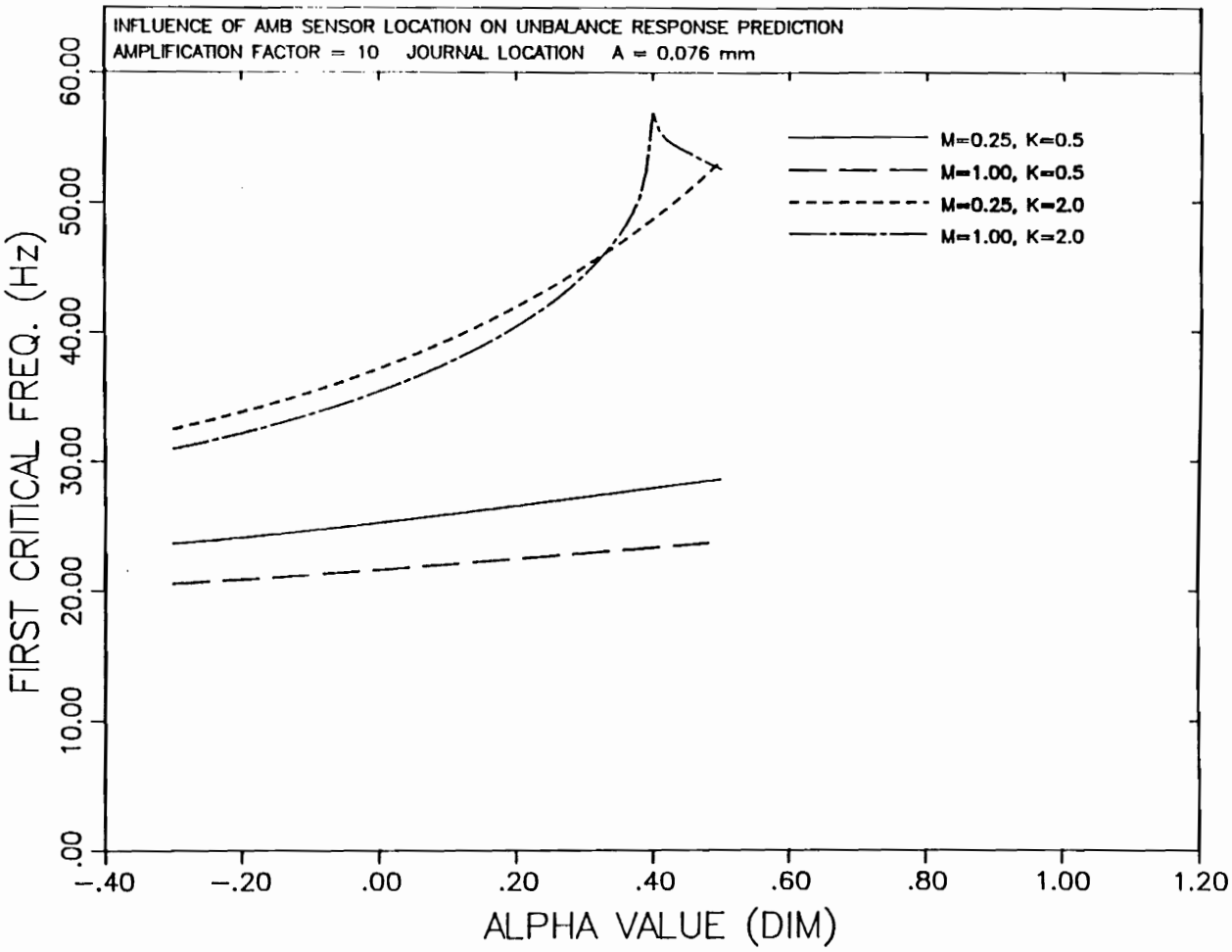

Figure 12.

Sensor Influence on First Critical Frequency, Unbalance Excitation, Journal Location, Amplification factor = 10

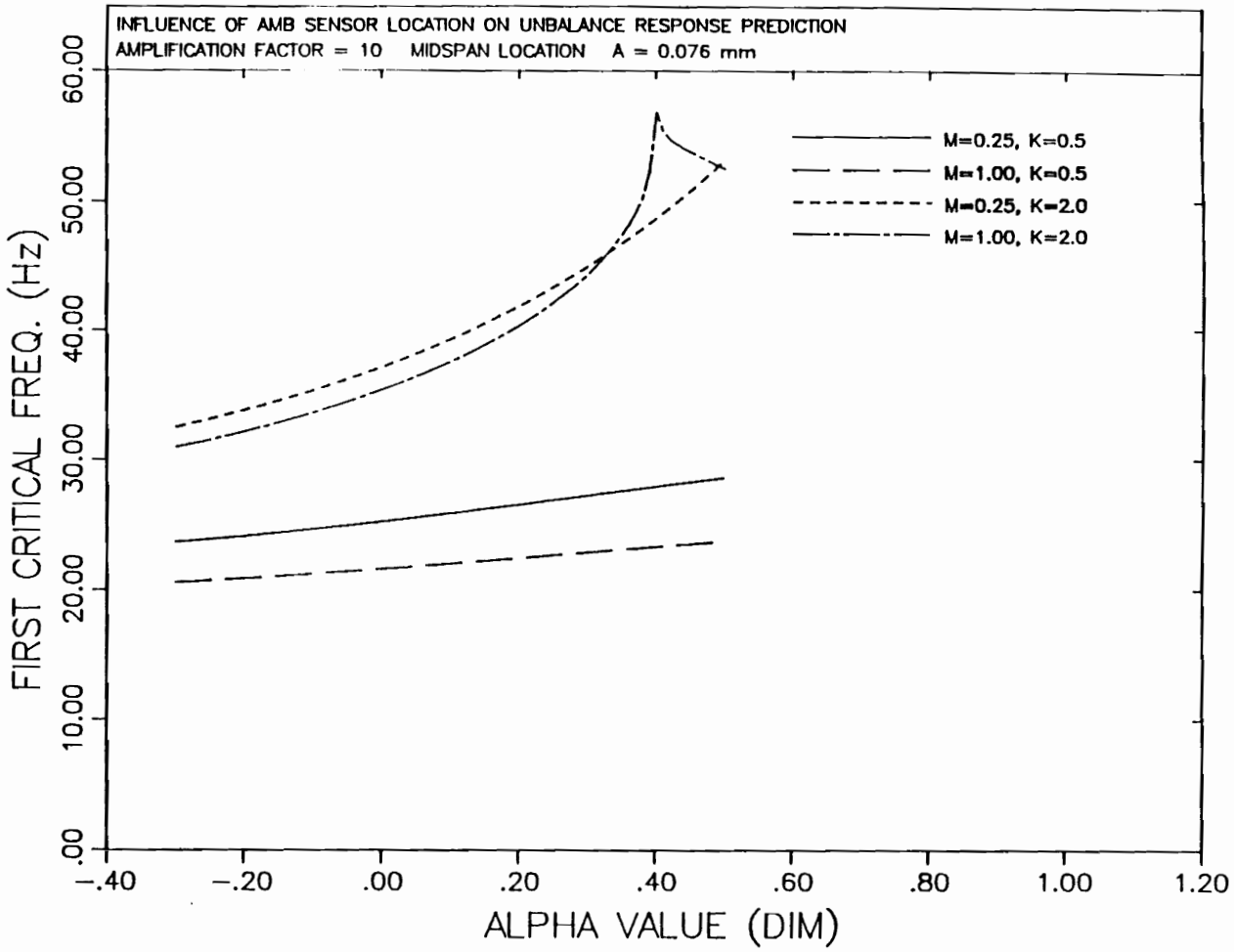

Figure 13.

Sensor Influence on First Critical Frequency, Unbalance Excitation, Midspan Location, Amplification factor = 10

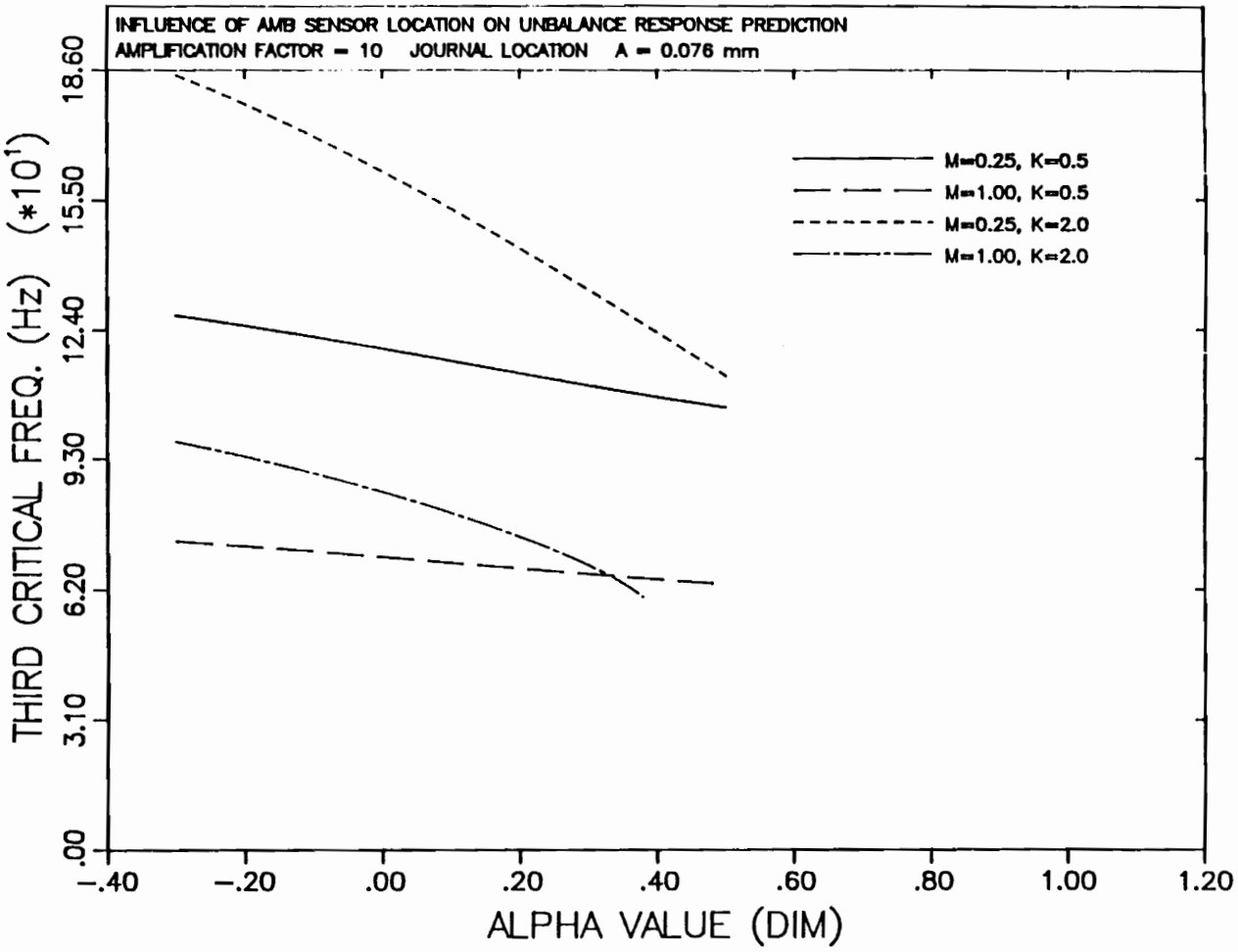

Figure 14.

Sensor Influence on Third Critical Frequency, Unbalance Excitation, Journal Location, Amplification factor = 10

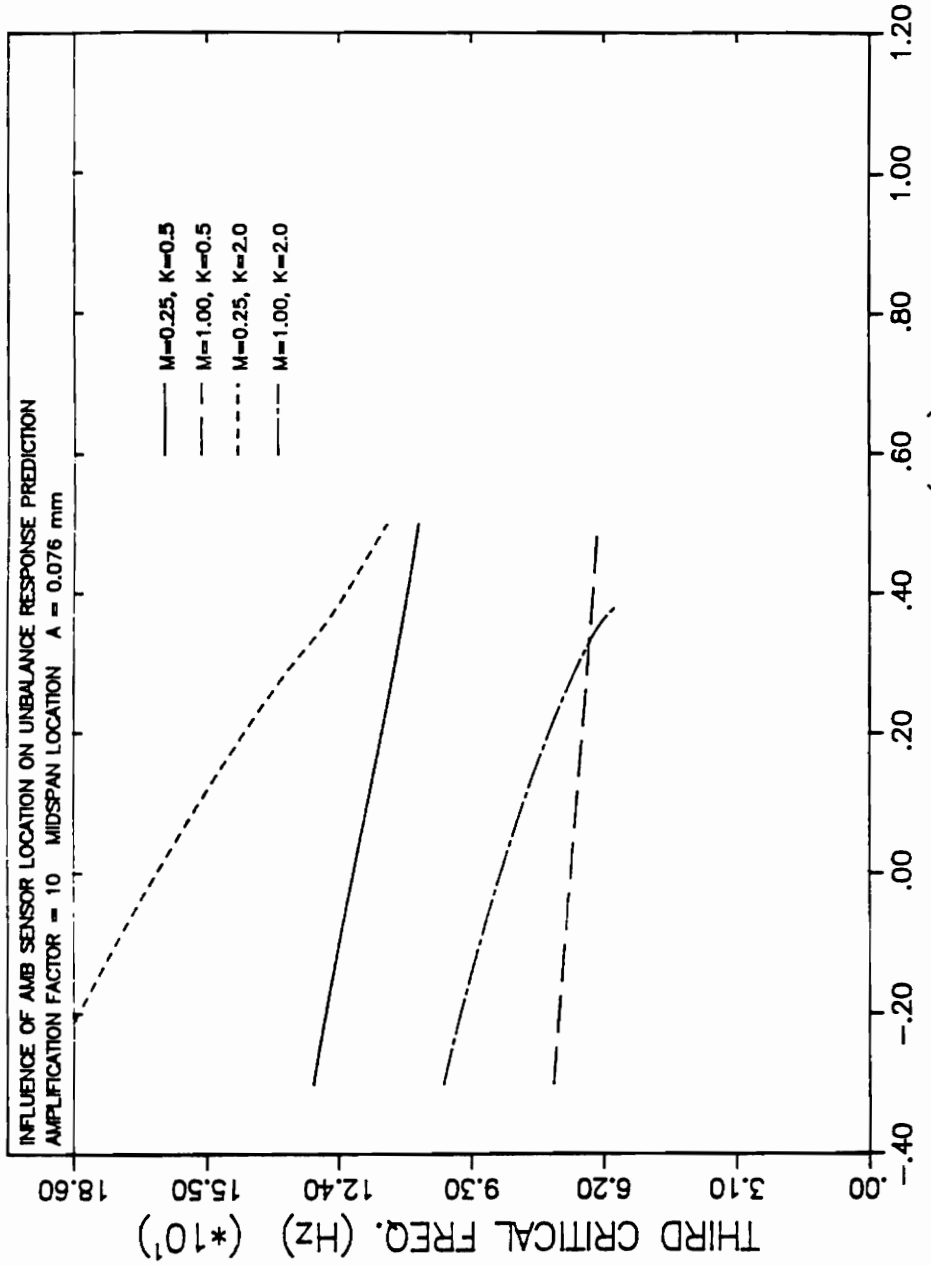

Figure 15.
Sensor Influence on Third Critical Frequency, Unbalance Excitation, Midspan Location, Amplification factor = 10

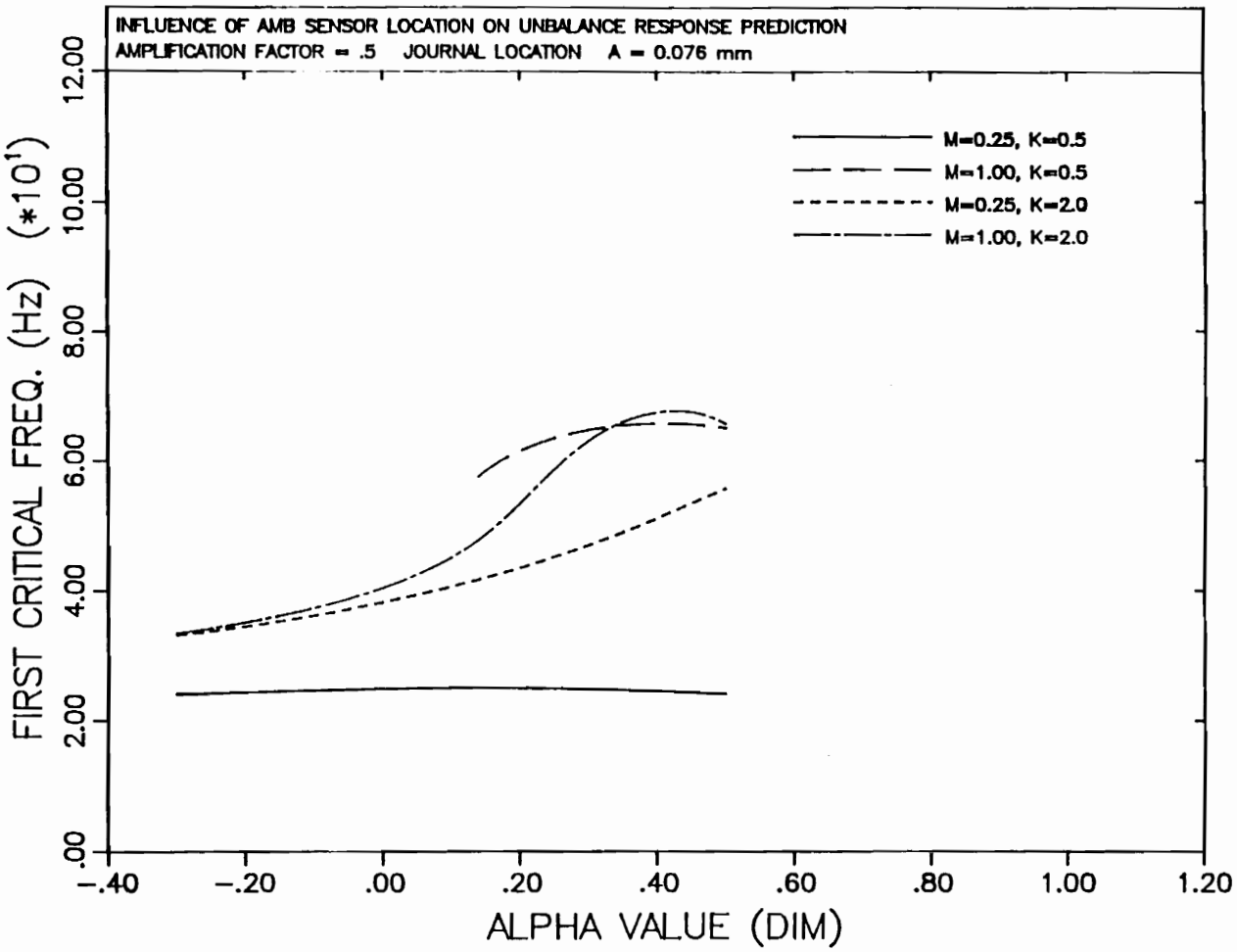

Figure 16.

Sensor Influence on First Critical Frequency, Unbalance Excitation, Journal Location, Amplification factor = 0.5

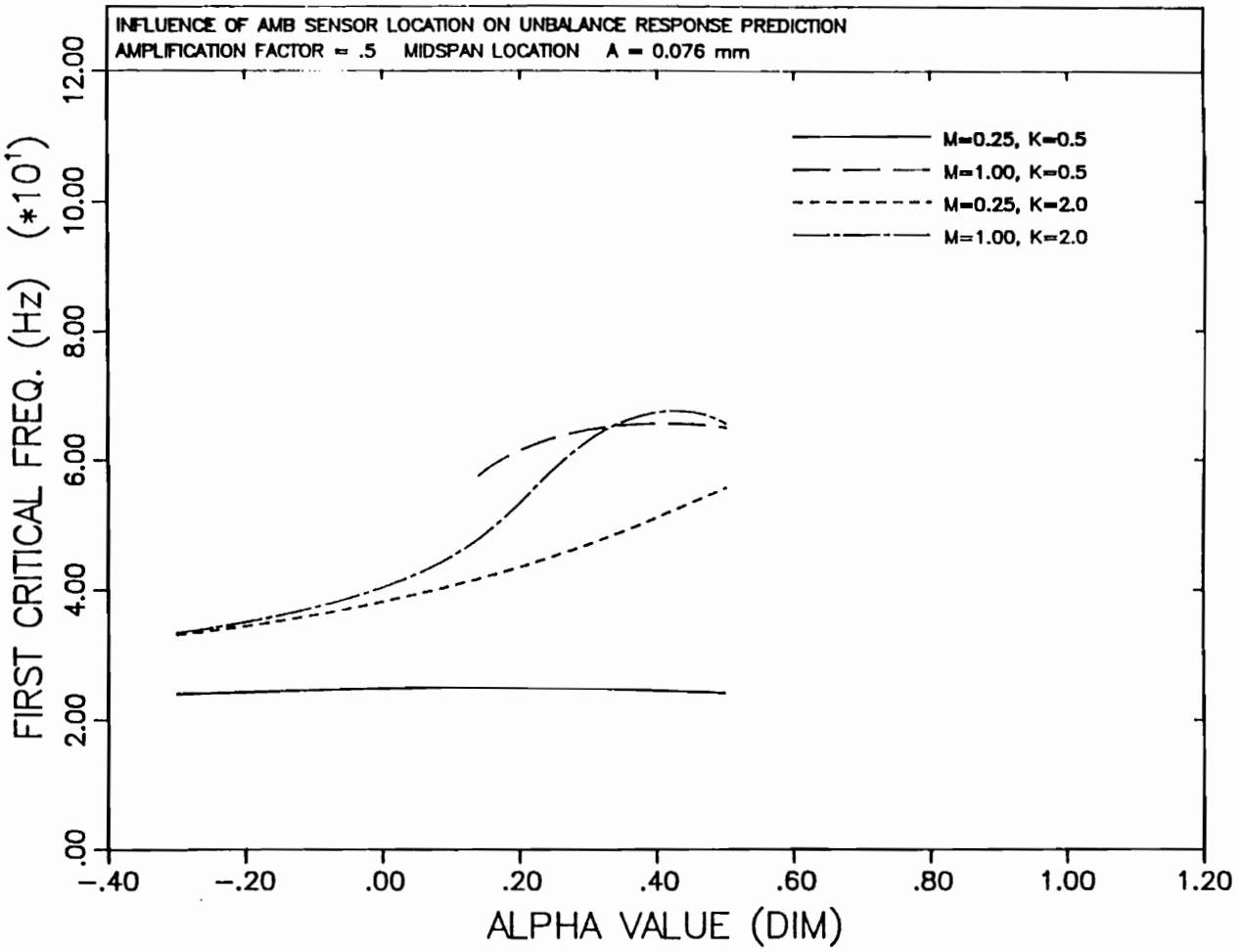

Figure 17.

Sensor Influence on First Critical Frequency, Unbalance Excitation, Midspan Location, Amplification factor = 0.5

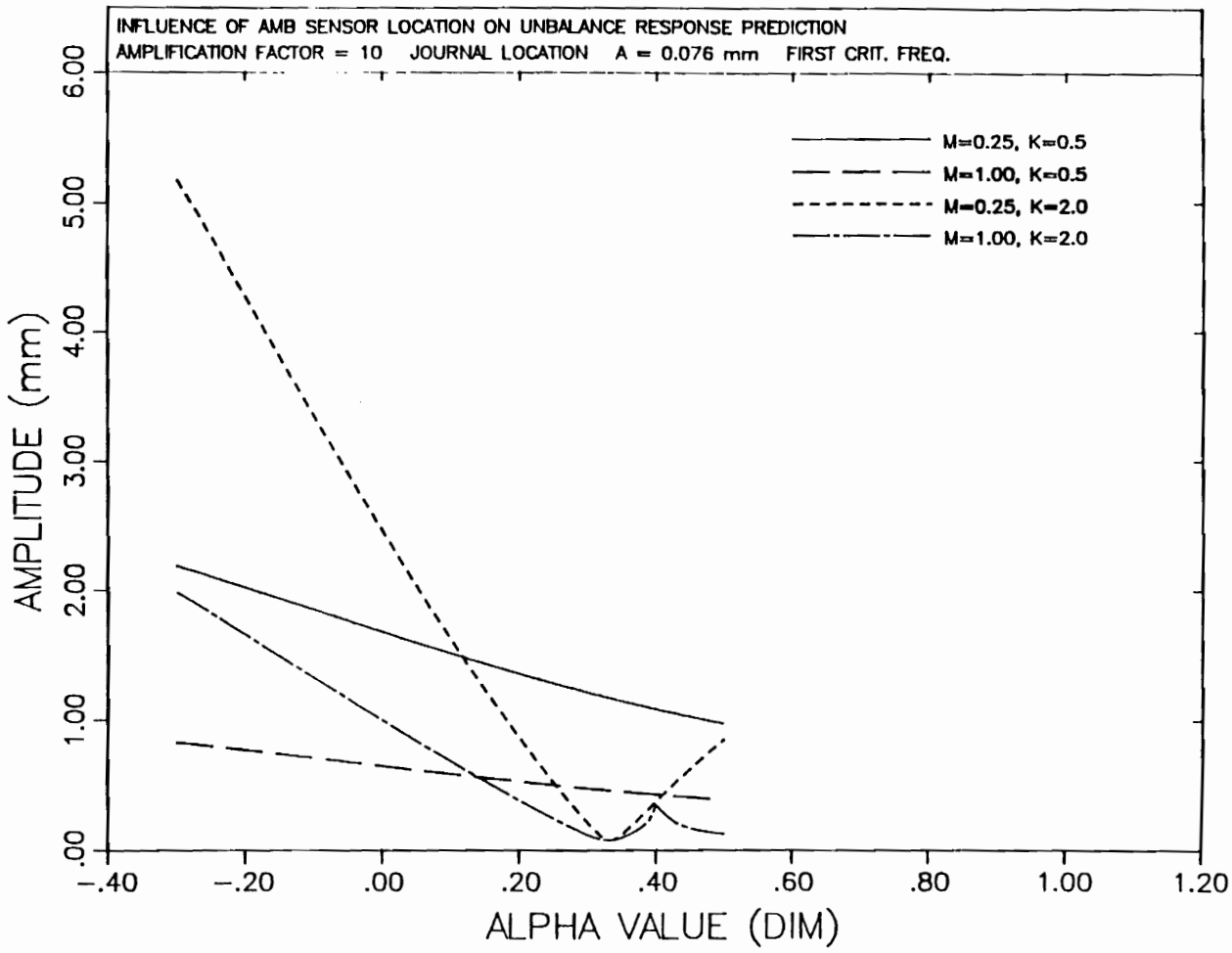

Figure 18.

Sensor Influence on Journal Amplitude, Unbalance Excitation, First Critical Frequency, Amplification factor = 10

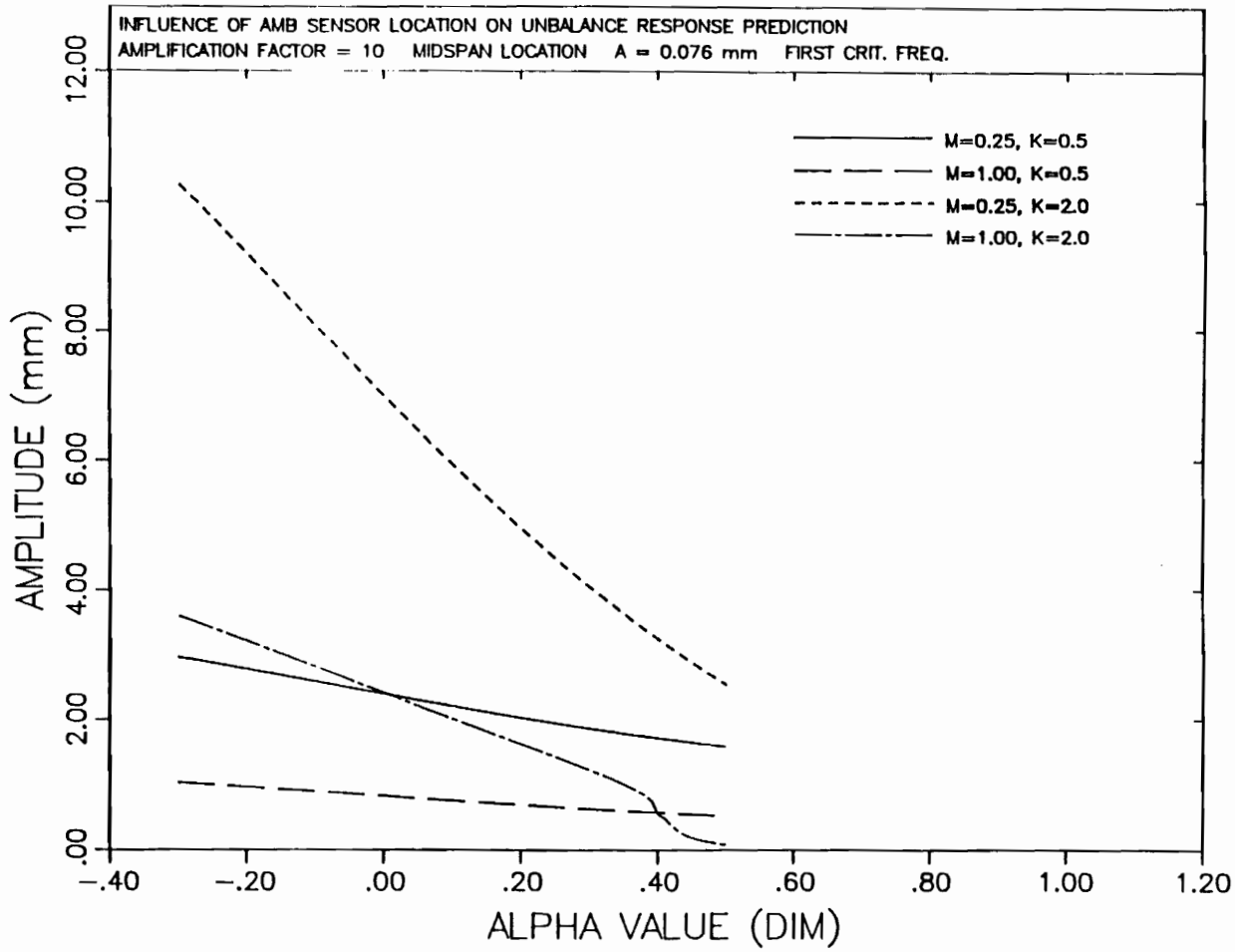

Figure 19.

Sensor Influence on Midspan Amplitude, Unbalance Excitation, First Critical Frequency, Amplification factor = 10

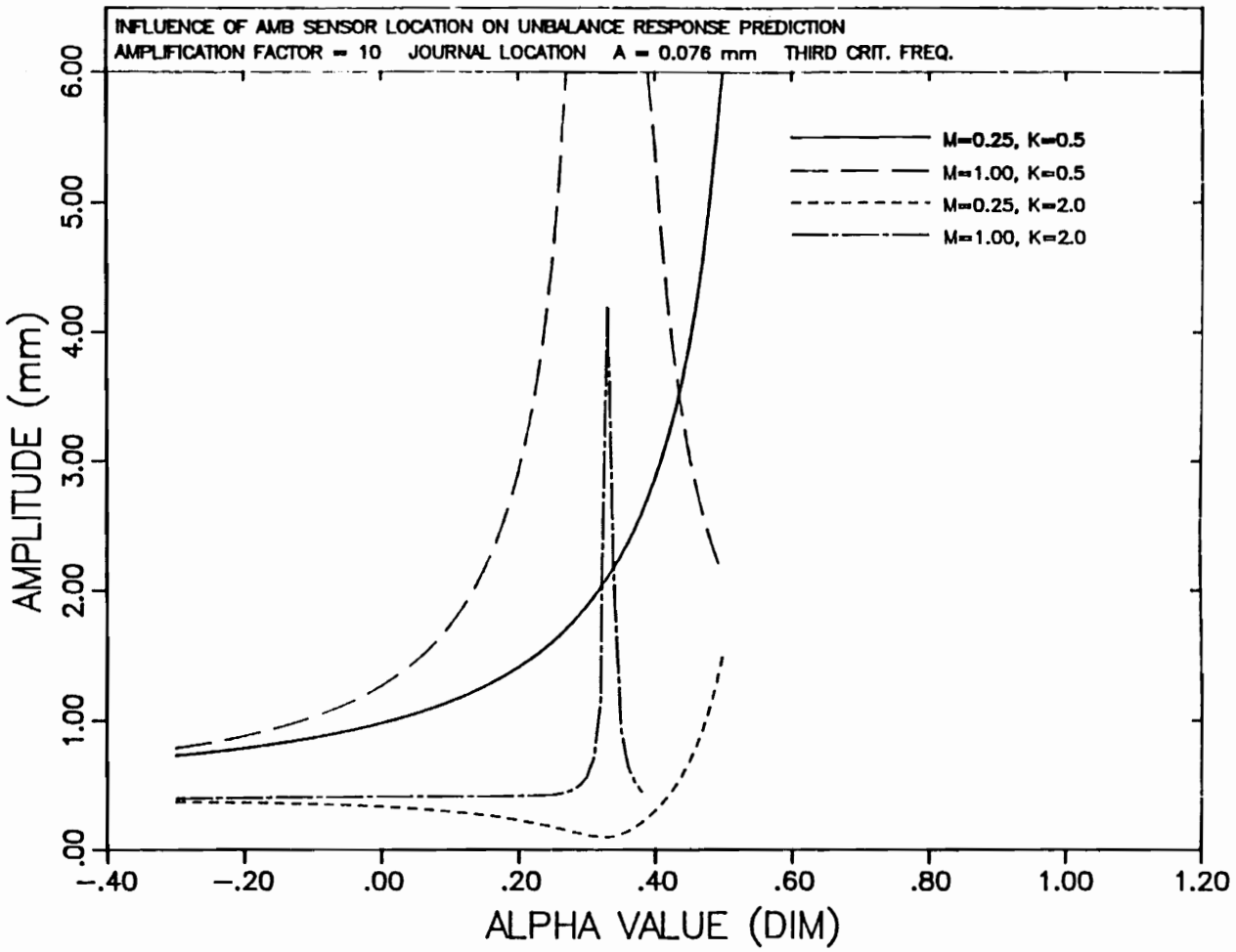

Figure 20.

Sensor Influence on Journal Amplitude, Unbalance Excitation, Third Critical Frequency, Amplification factor = 10

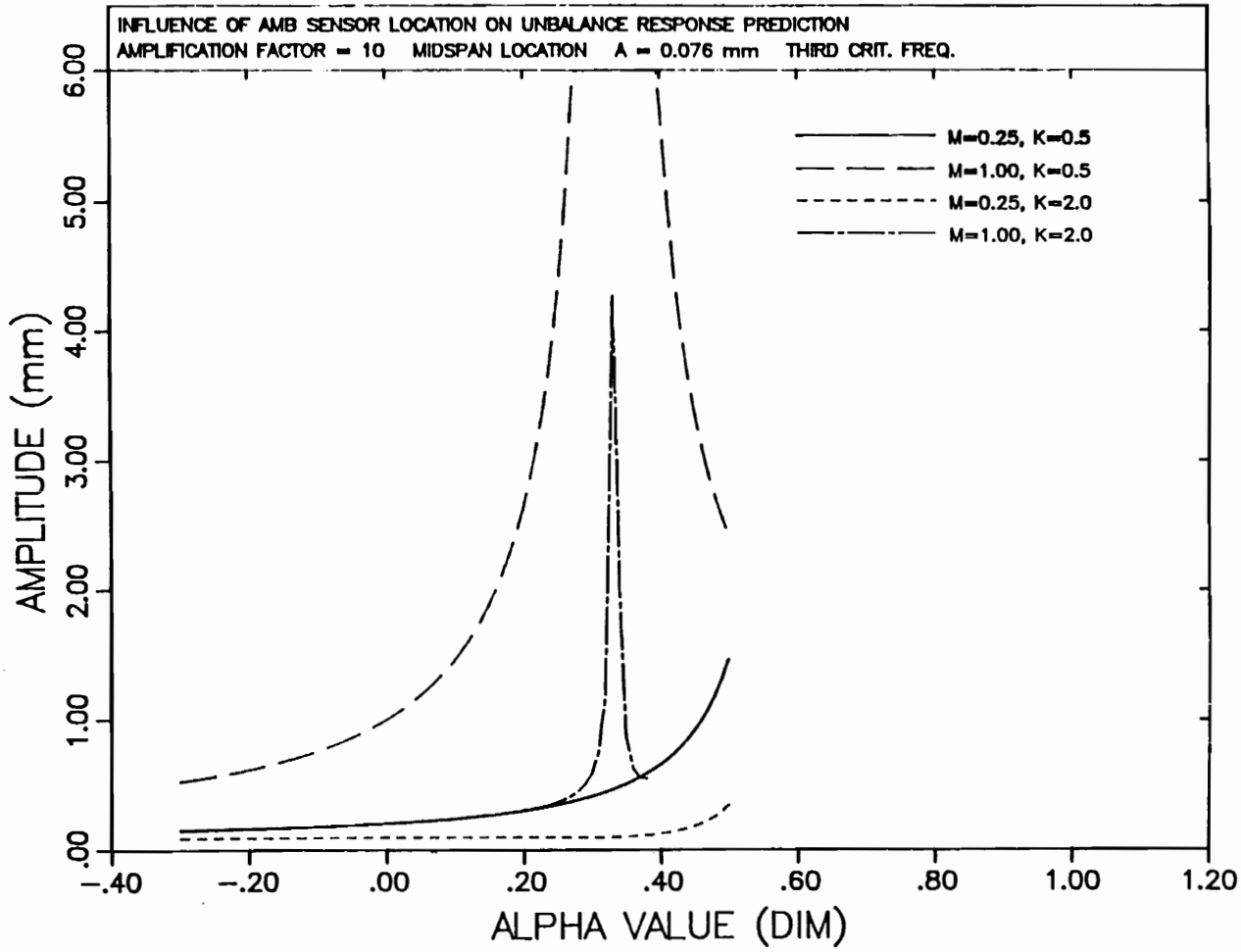

Figure 21.

Sensor Influence on Midspan Amplitude, Unbalance Excitation, Third Critical Frequency, Amplification factor = 10

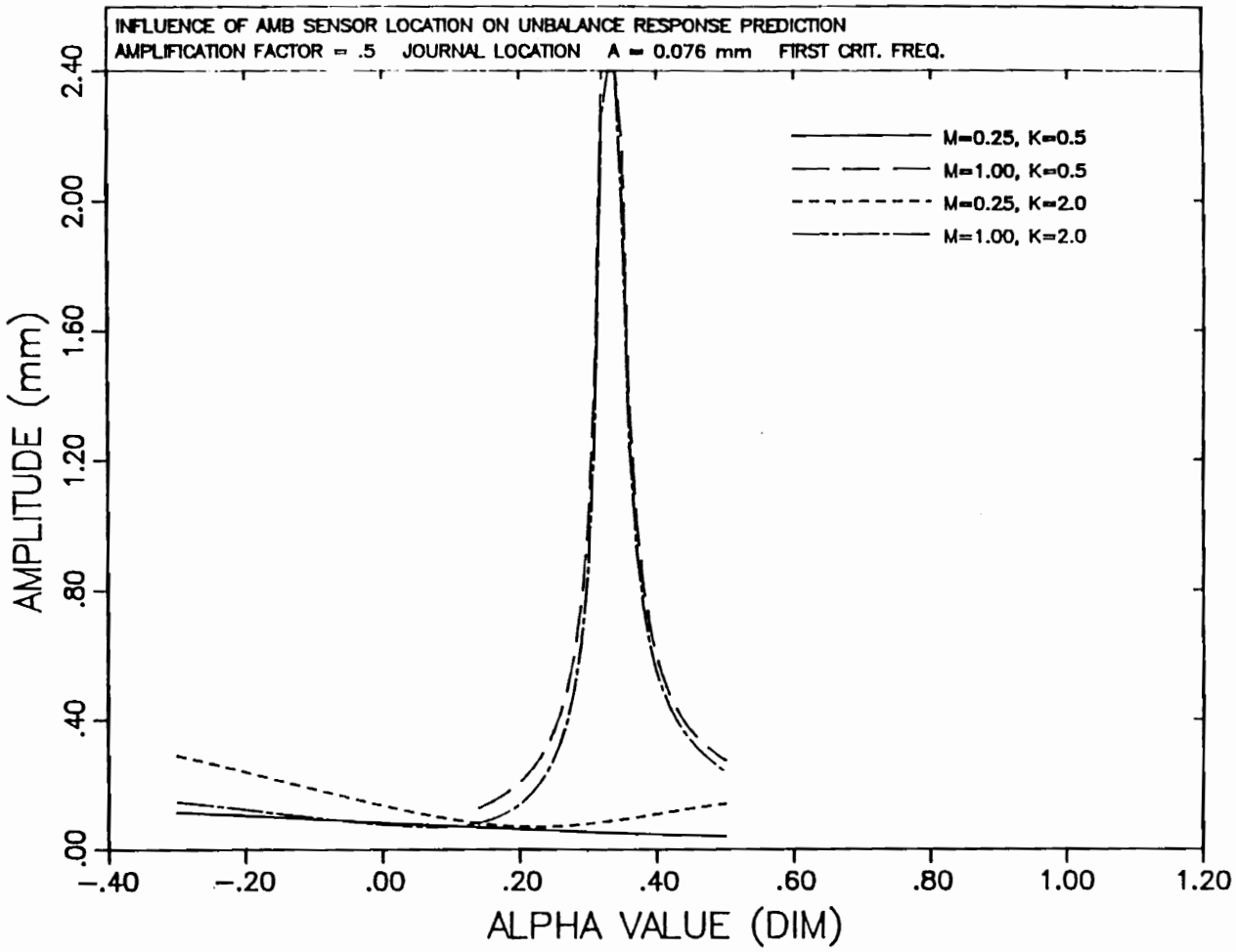

Figure 22.

Sensor Influence on Journal Amplitude, Unbalance Excitation, First Critical Frequency, Amplification factor = 0.5

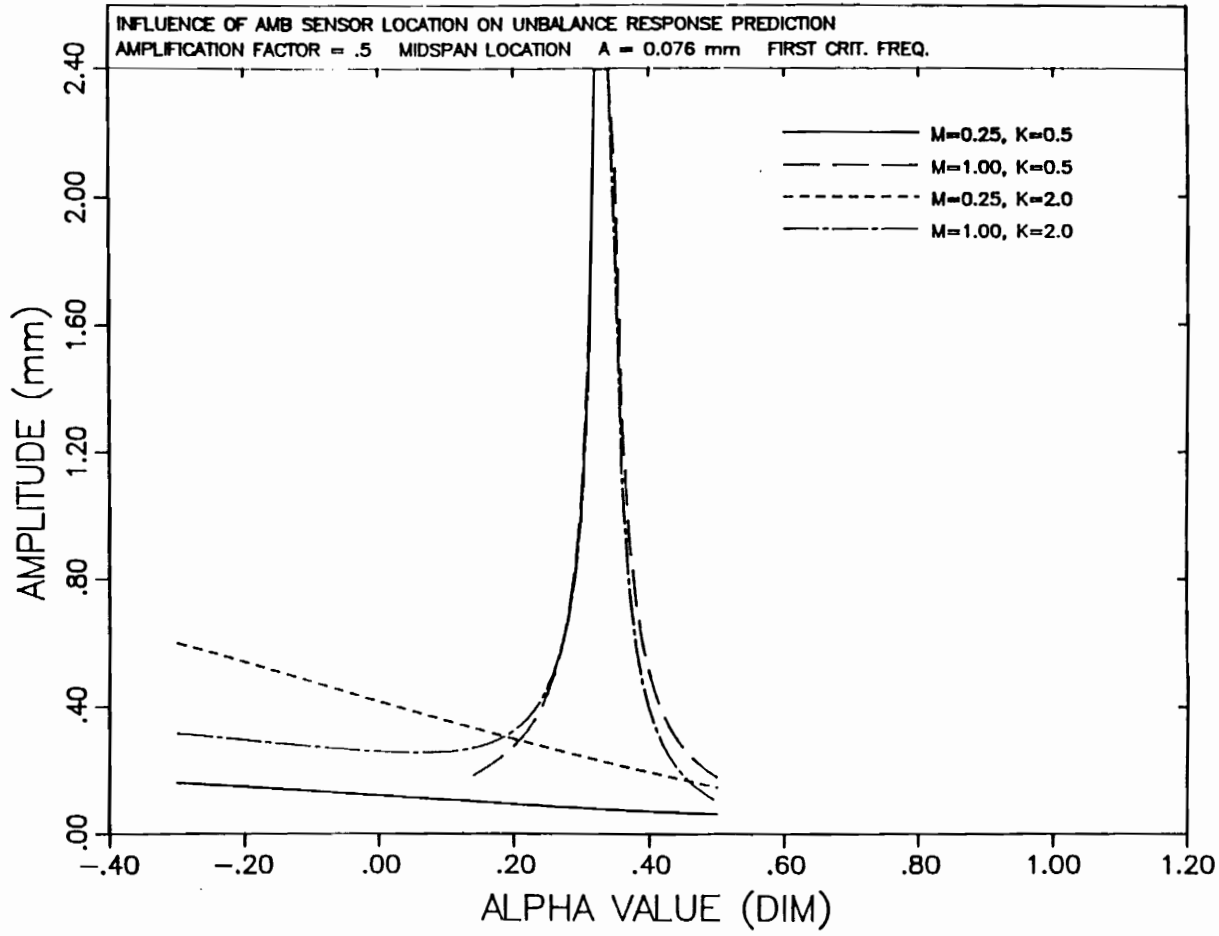

Figure 23.
Sensor Influence on Midspan Amplitude, Unbalance Excitation, First Critical Frequency, Amplification factor = 0.5

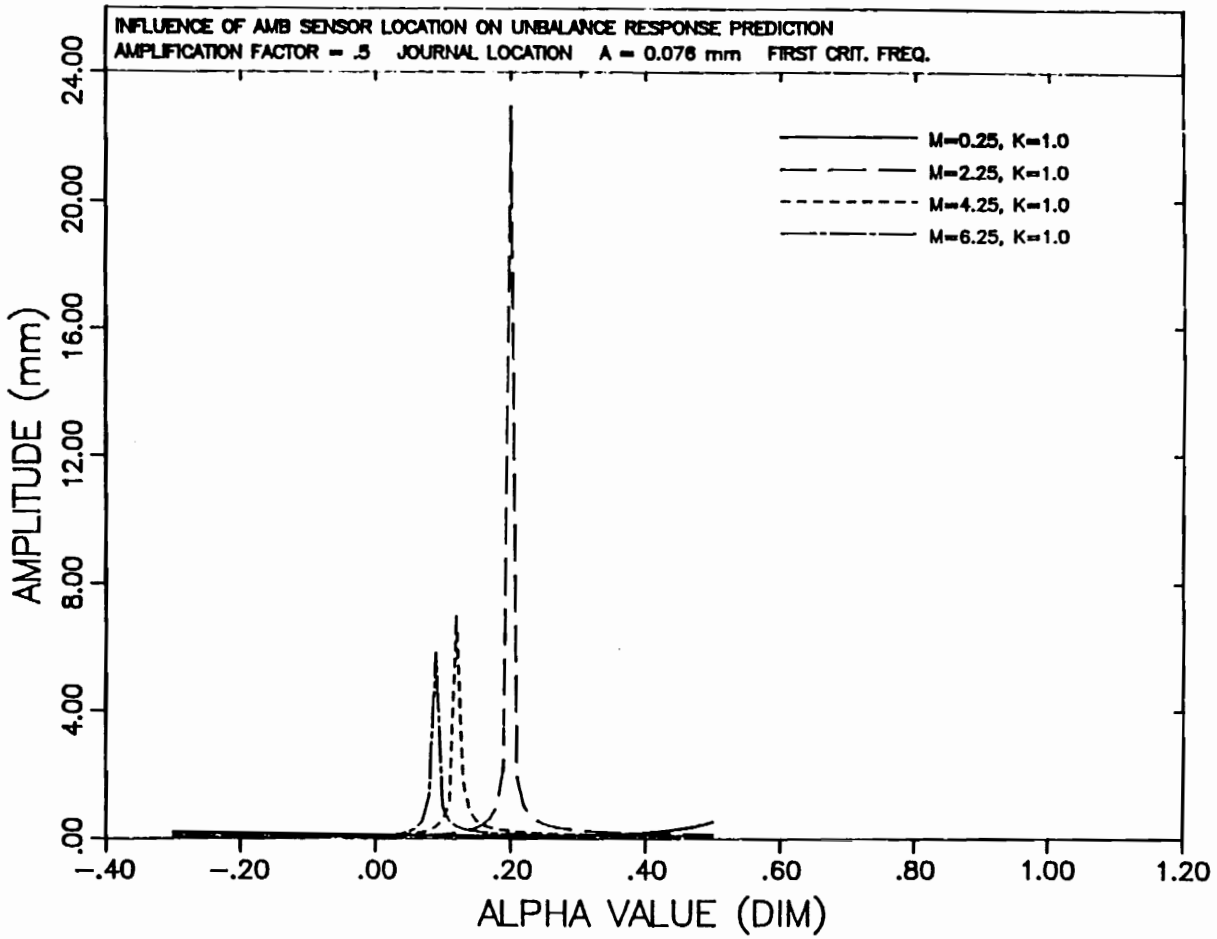

Figure 24.

Influence of Mass Ratio on Peak Amplitudes, Unbalance Excitation, Journal Location, Amplification factor = 0.5

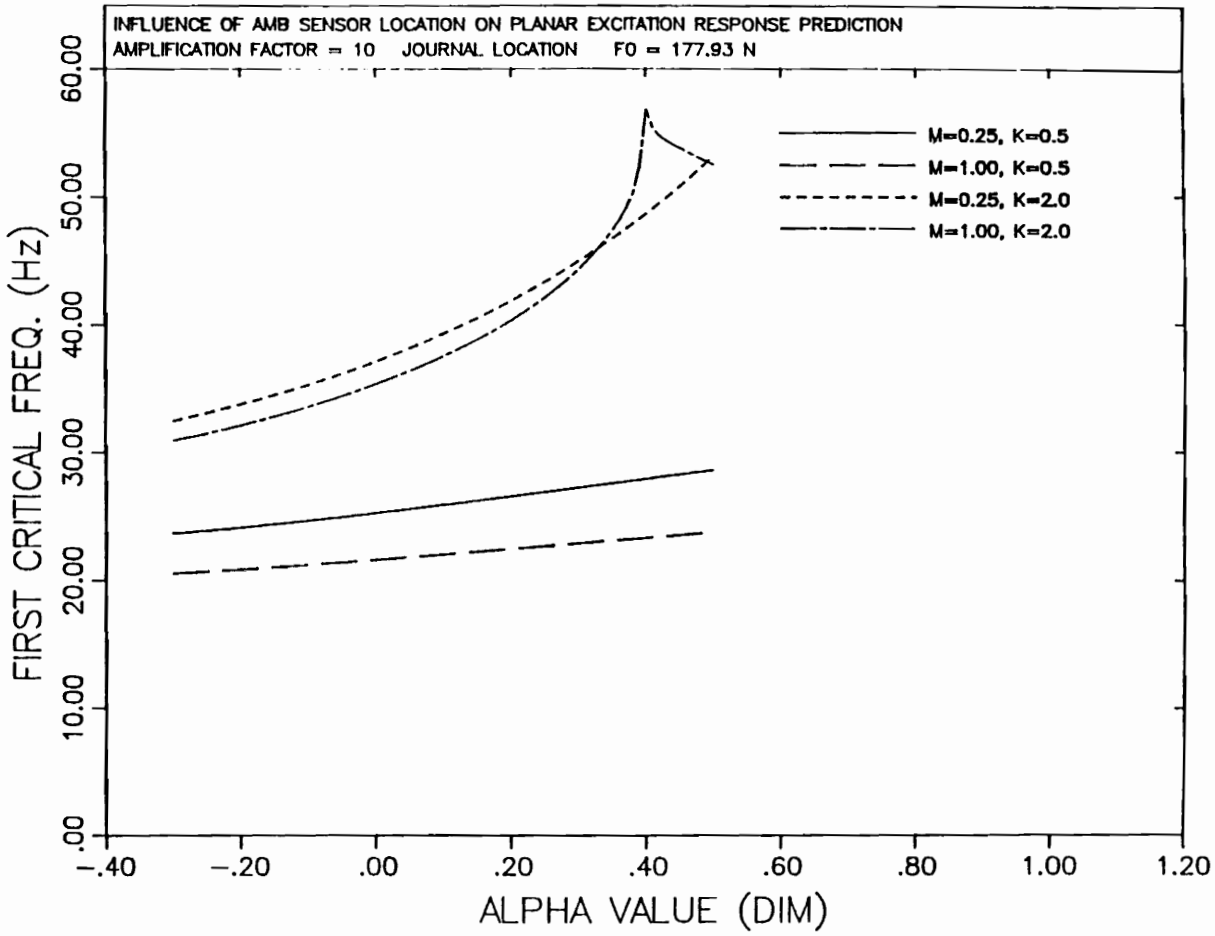

Figure 25.

Sensor Influence on First Critical Frequency, Planar Excitation, Journal Location, Amplification factor = 10

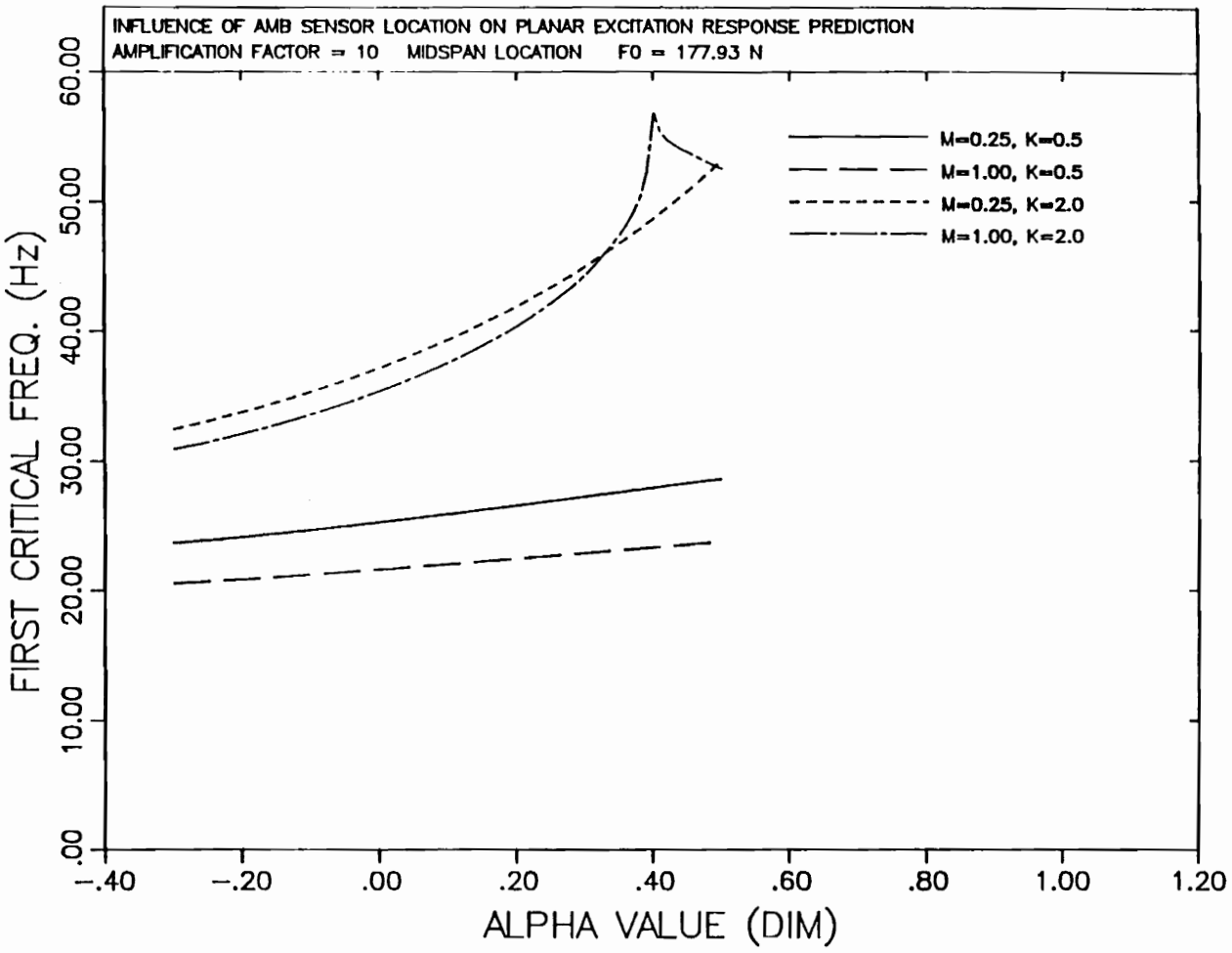

Figure 26.

Sensor Influence on First Critical Frequency, Planar Excitation, Midspan Location, Amplification factor = 10

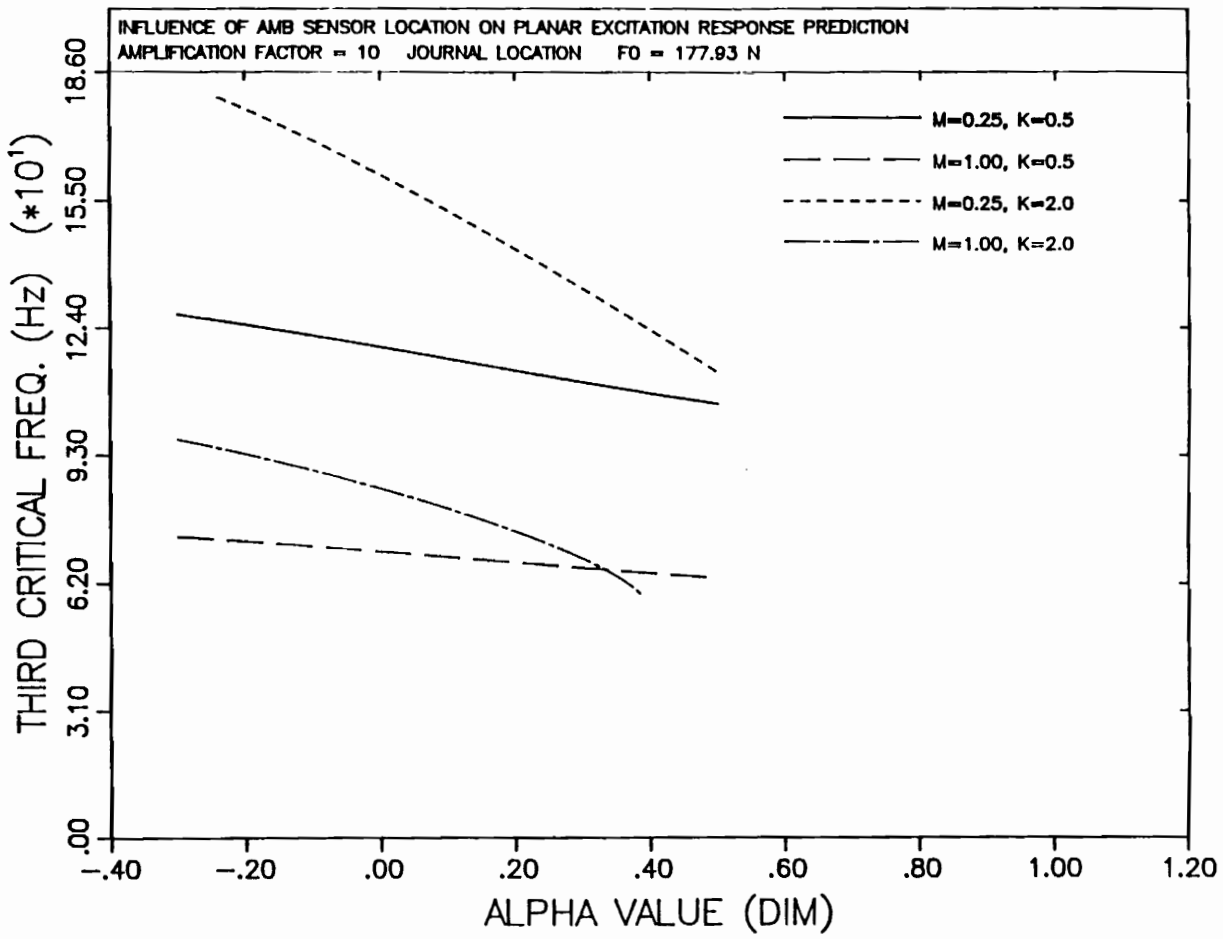

Figure 27.
Sensor Influence on Third Critical Frequency, Planar Excitation, Journal Location, Amplification factor = 10

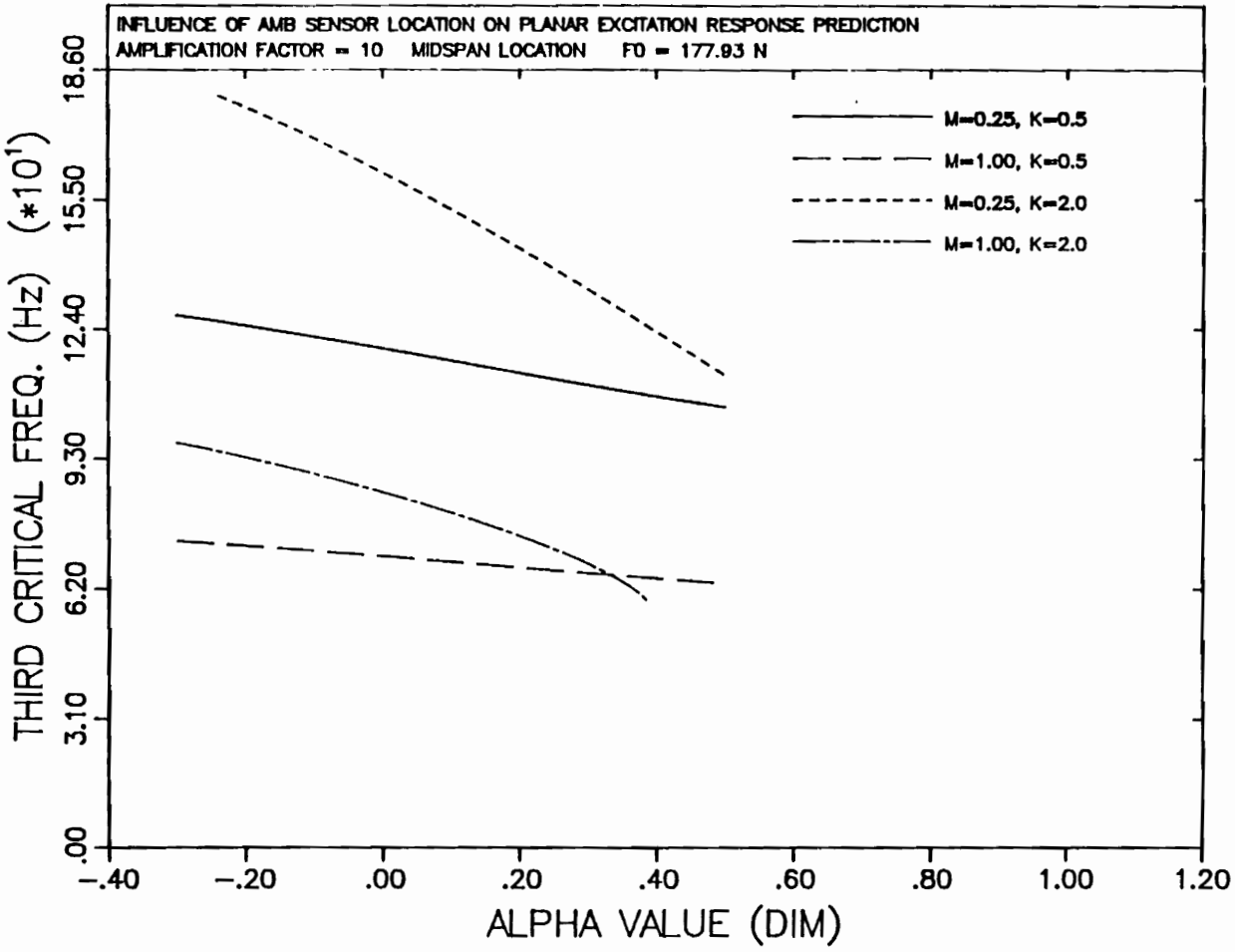

Figure 28.

Sensor Influence on Third Critical Frequency, Planar Excitation, Midspan Location, Amplification factor = 10

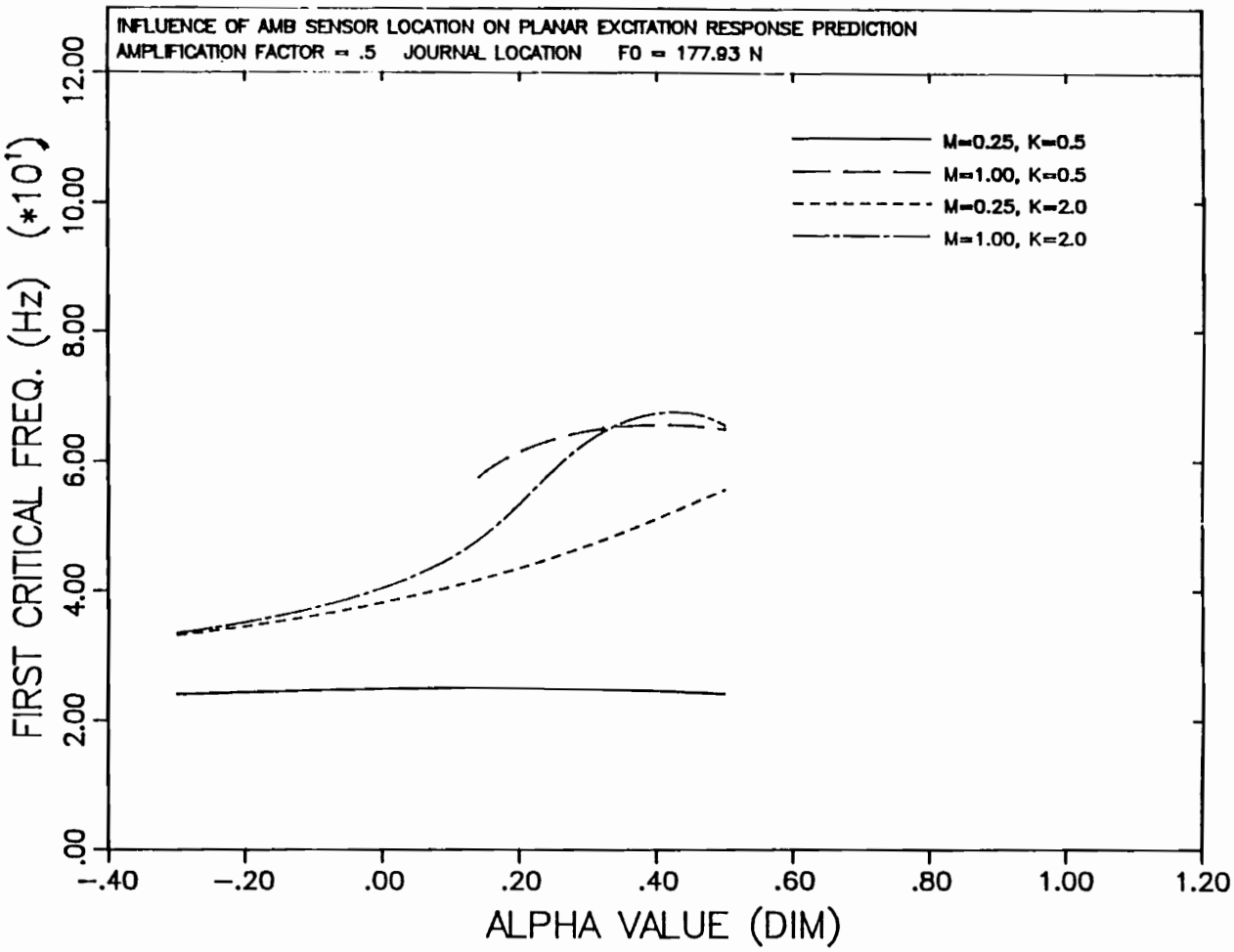

Figure 29.

Sensor Influence on First Critical Frequency, Planar Excitation, Journal Location, Amplification factor = 0.5

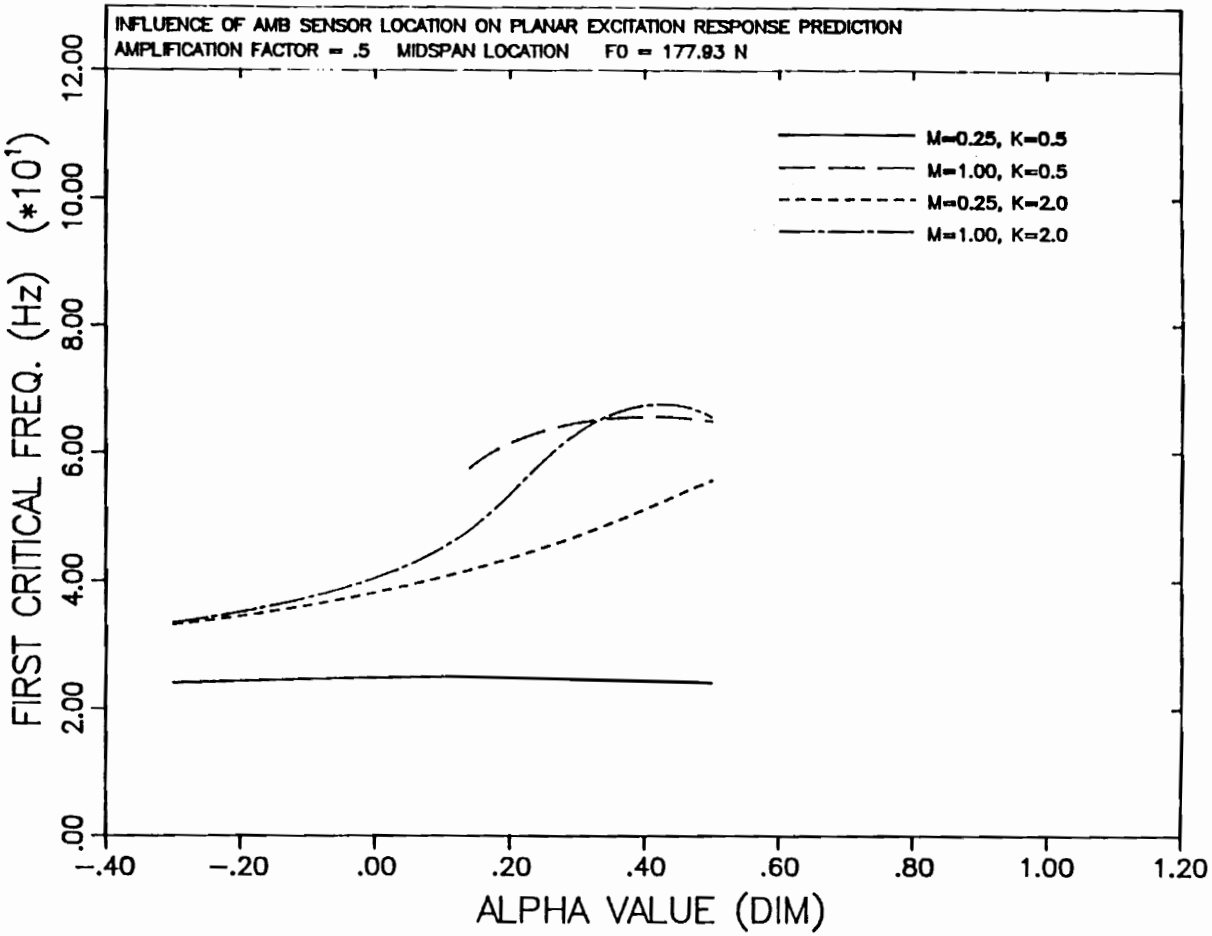

Figure 30.
Sensor Influence on First Critical Frequency, Planar Excitation, Midspan Location, Amplification factor = 0.5

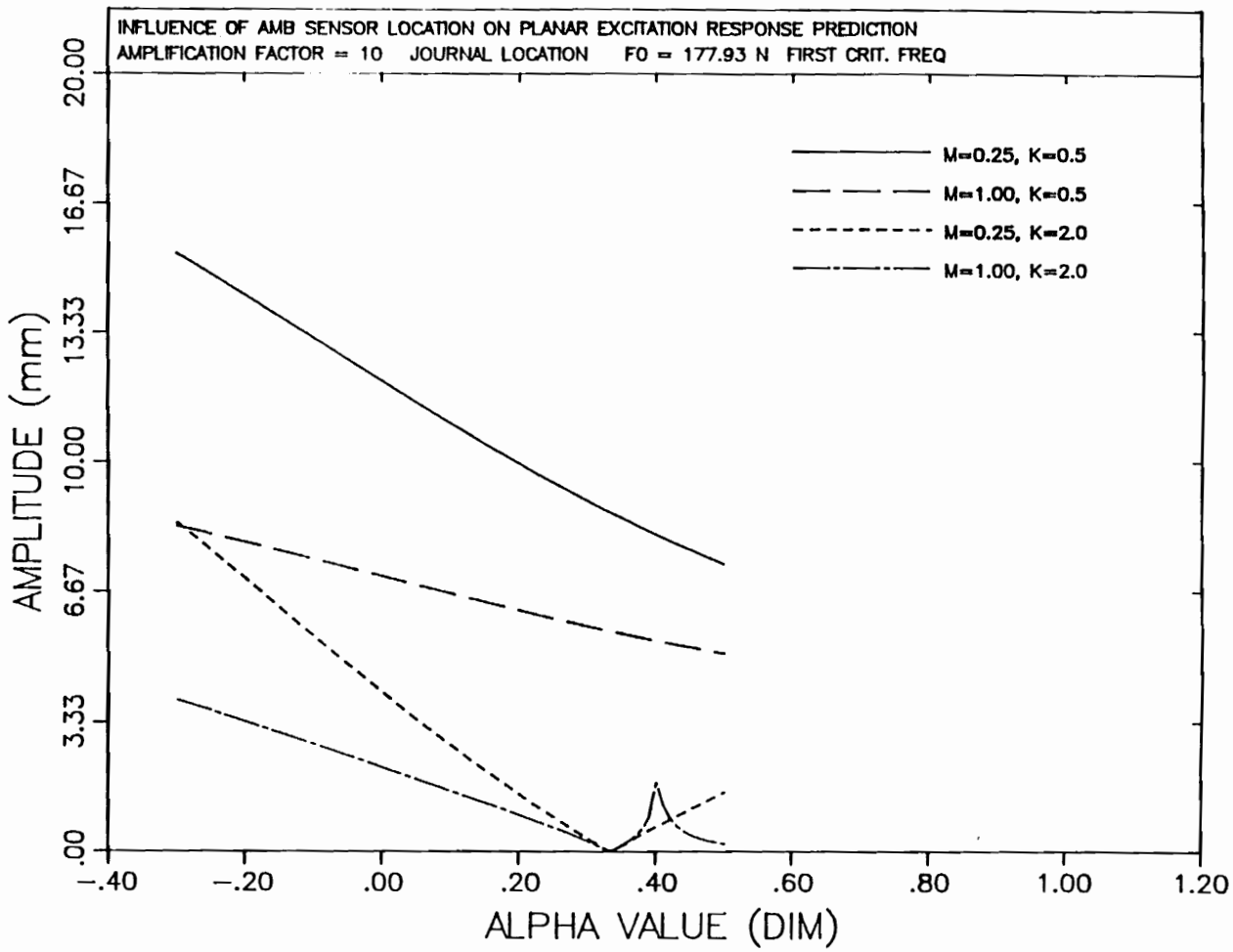

Figure 31.

Sensor Influence on Journal Amplitude, Planar Excitation, First Critical Frequency, Amplification factor = 10

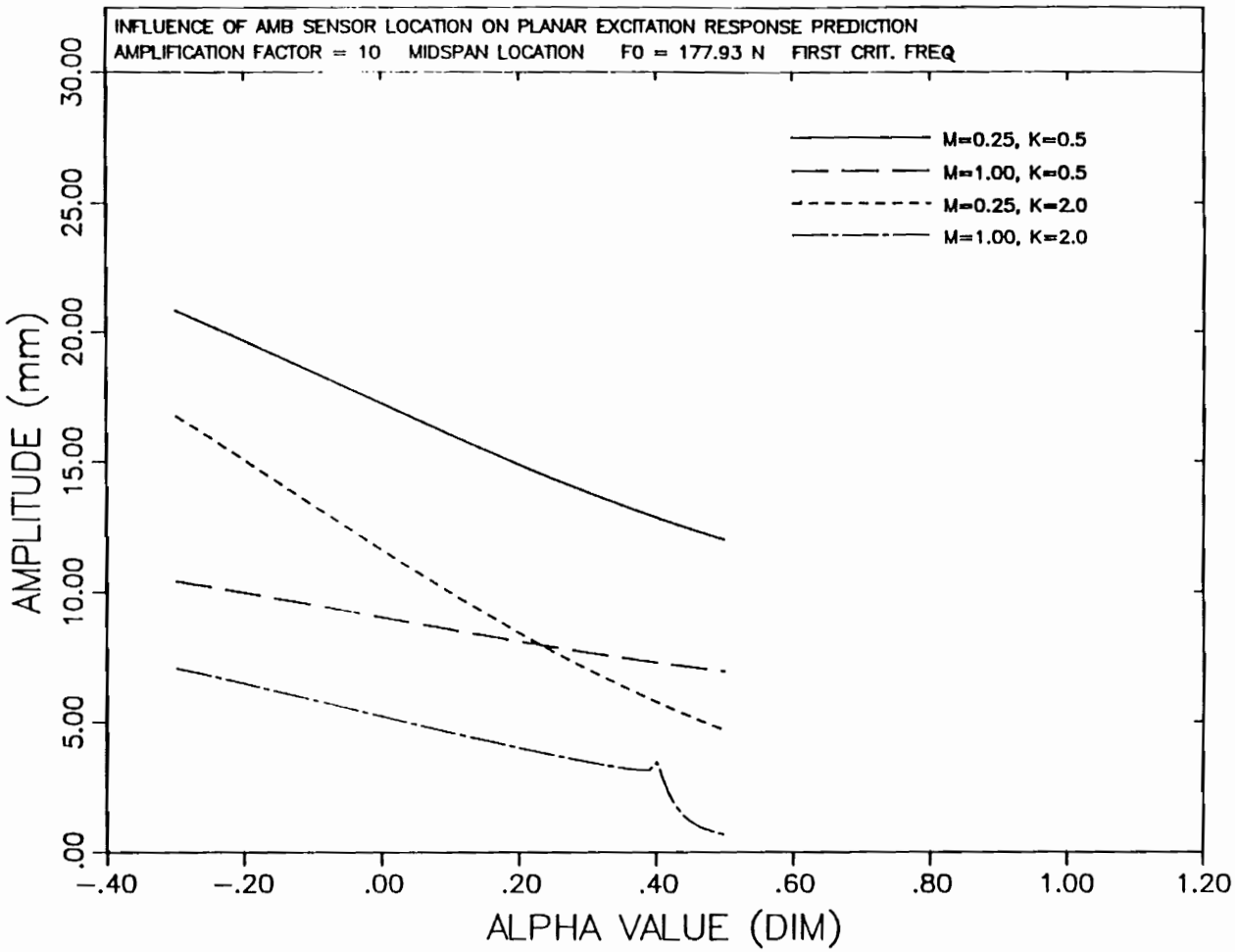

Figure 32.

Sensor Influence on Midspan Amplitude, Planar Excitation, First Critical Frequency, Amplification factor = 10

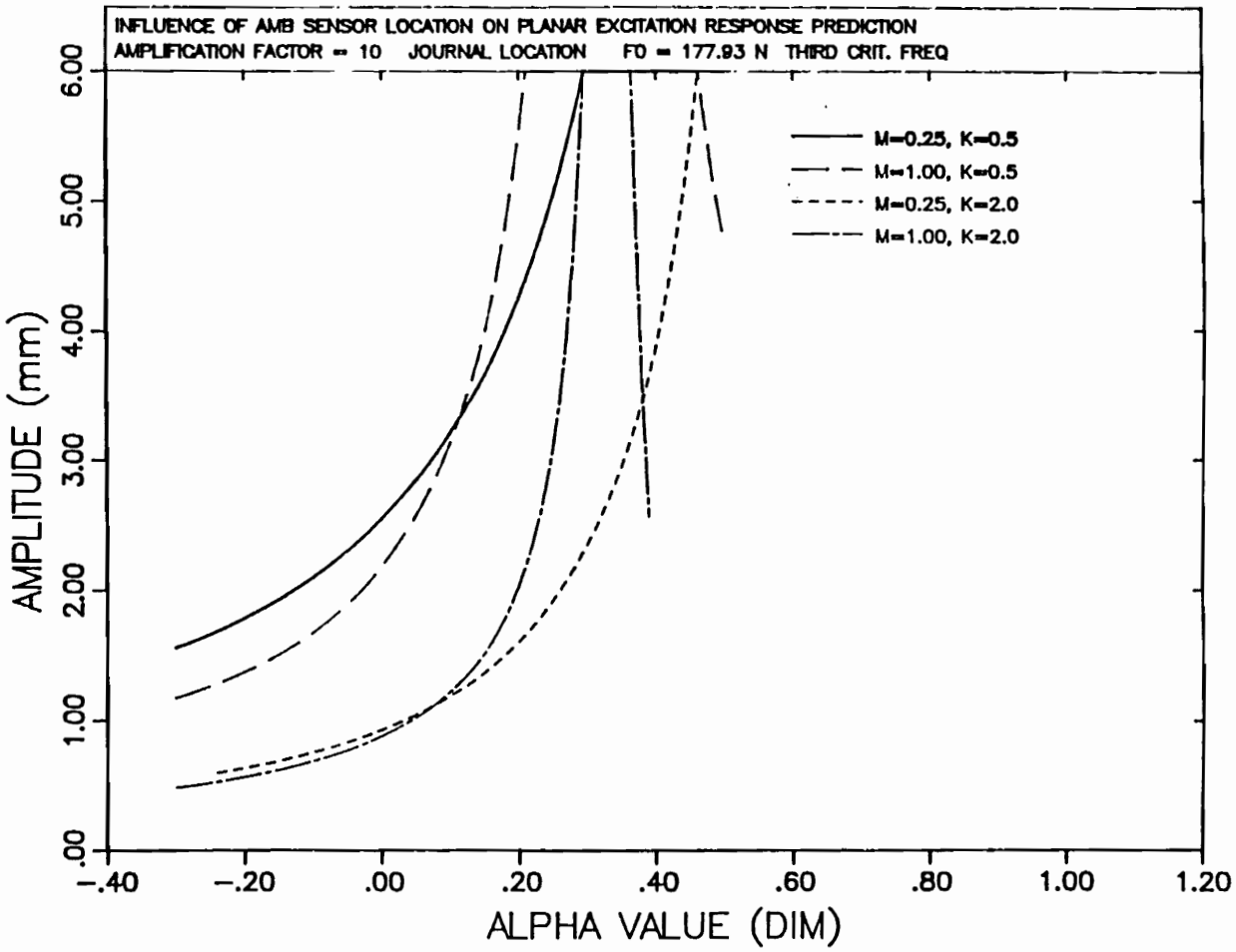

Figure 33.

Sensor Influence on Journal Amplitude, Planar Excitation, Third Critical Frequency, Amplification factor = 10

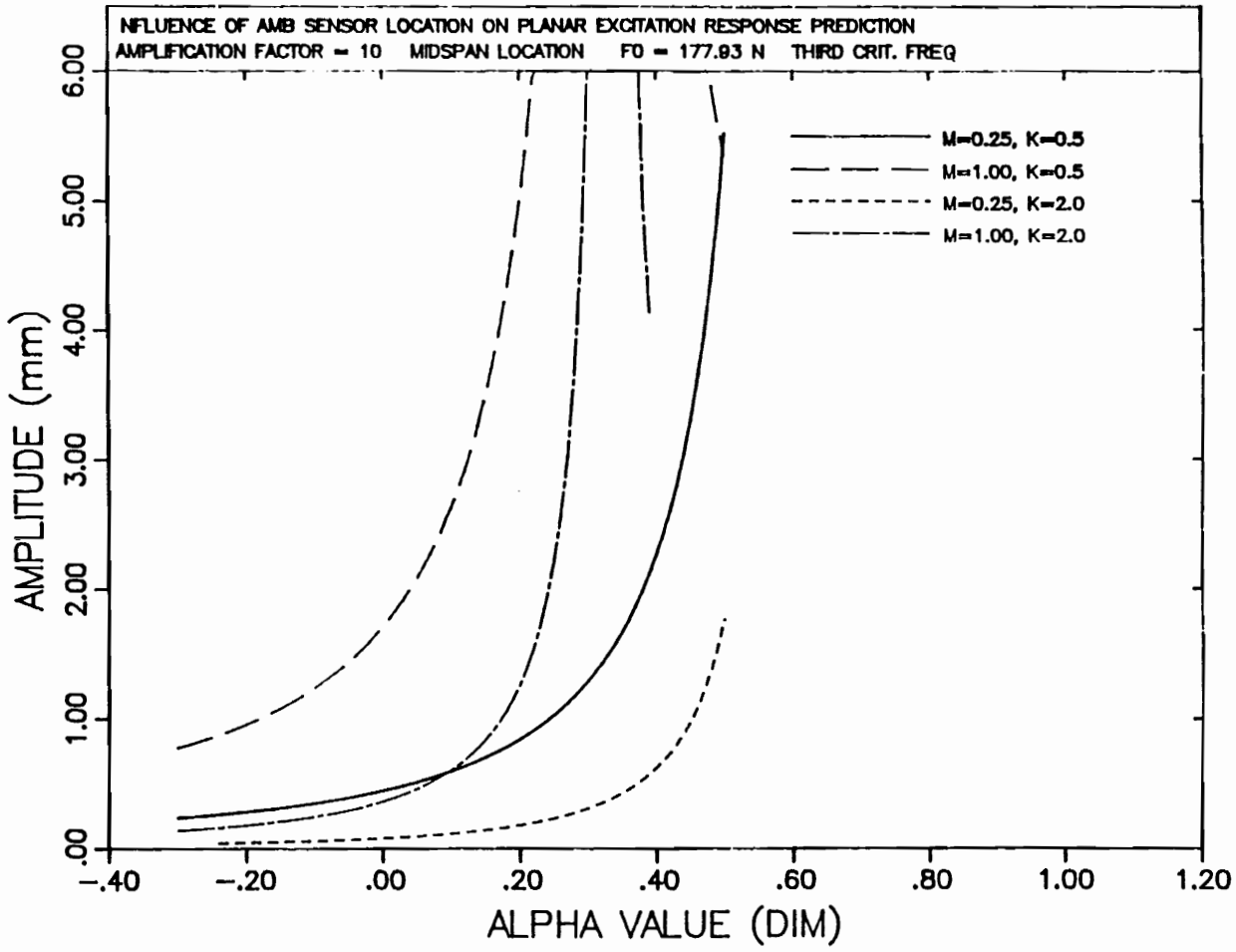

Figure 34.

Sensor Influence on Midspan Amplitude, Planar Excitation, Third Critical Frequency, Amplification factor = 10

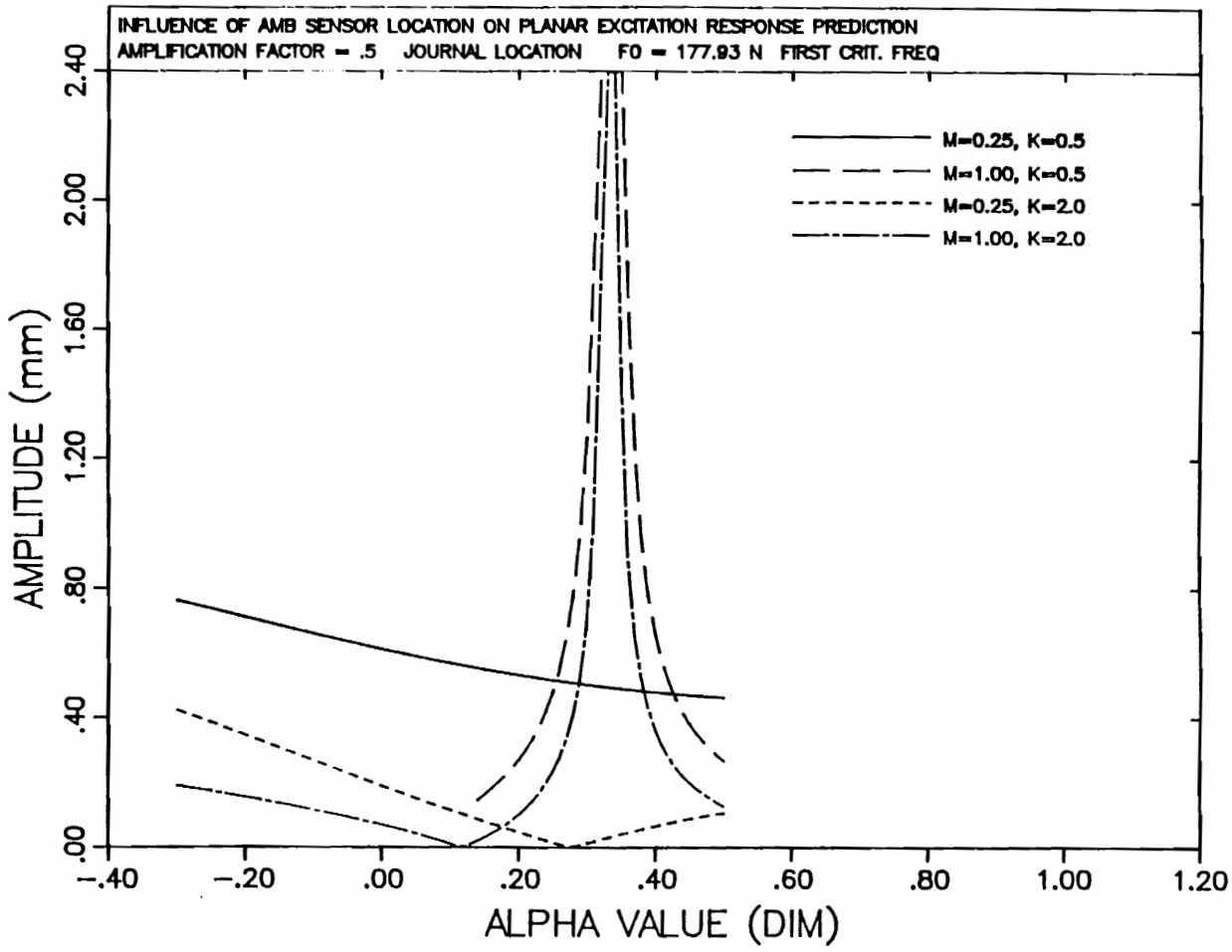

Figure 35.
Sensor Influence on Journal Amplitude, Planar Excitation, First Critical Frequency, Amplification factor = 0.5

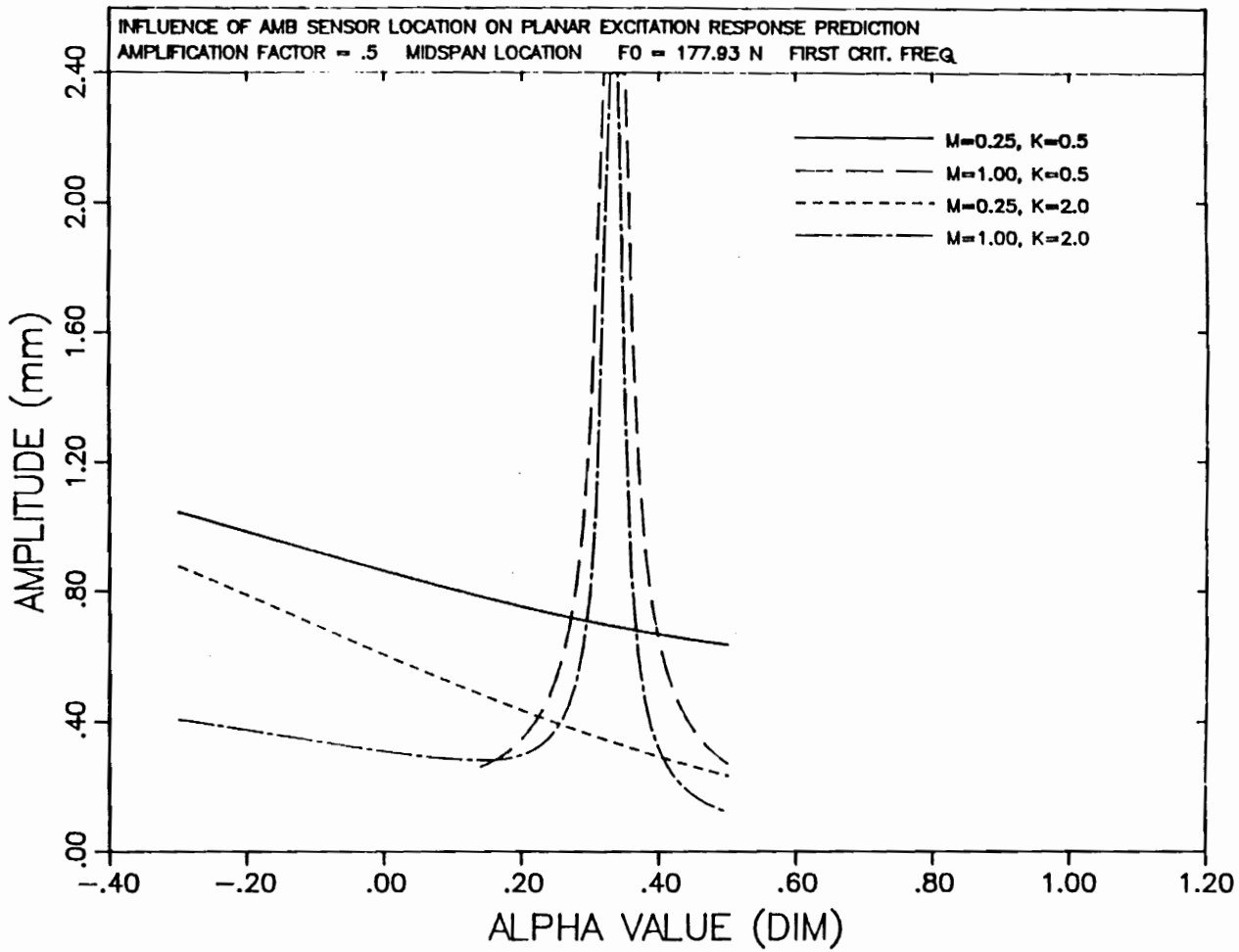

Figure 36.

Sensor Influence on Midspan Amplitude, Planar Excitation, First Critical Frequency, Amplification factor = 0.5

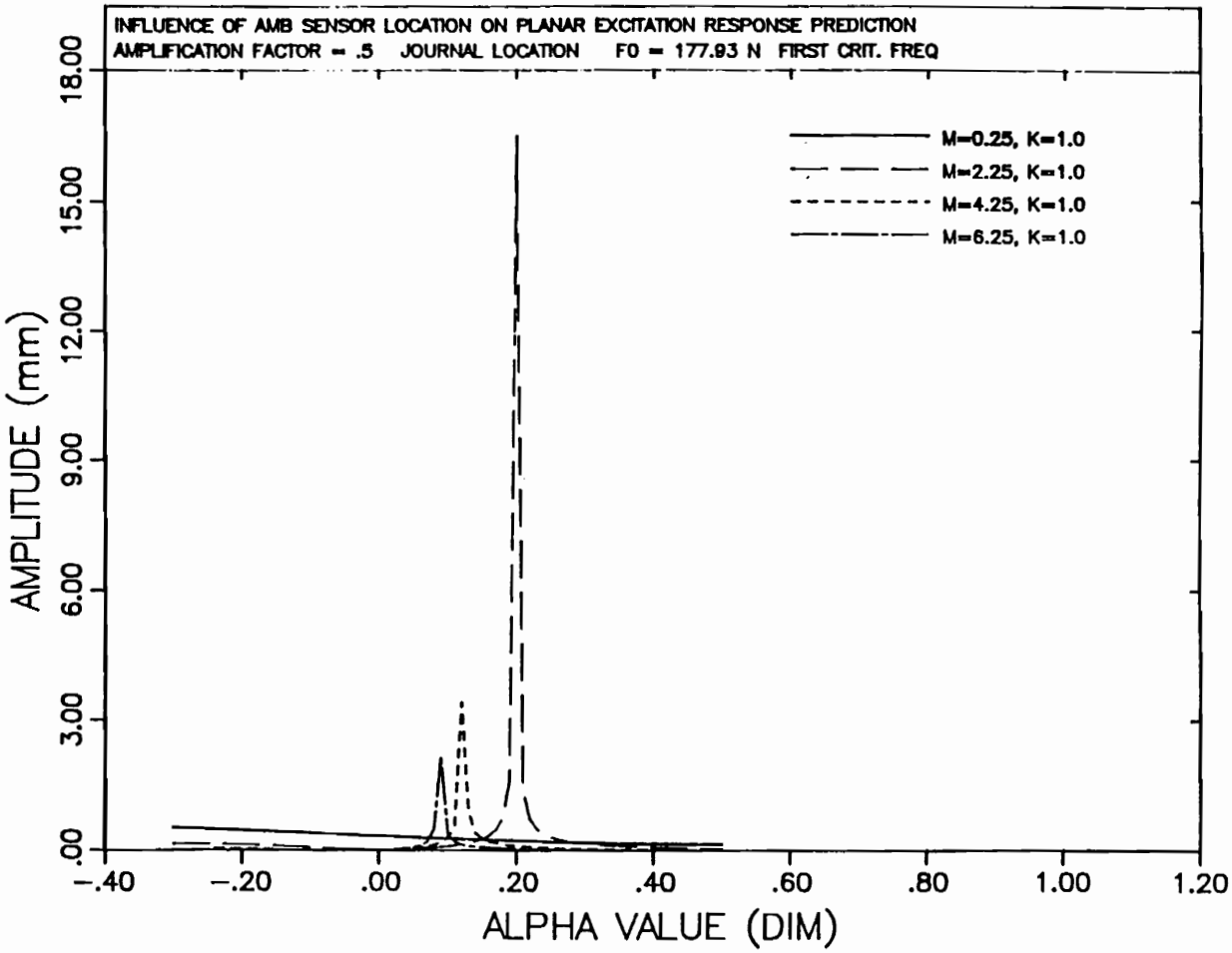

Figure 37.
Influence of Mass Ratio on Peak Amplitudes, Planar Excitation, Journal Location, Amplification factor = 0.5

Chapter 3

THE MODIFIED TRANSFER MATRIX METHOD

The first analytical study of flexible rotors using the transfer matrix method is presented by Myklestad (1944) and Prohl (1945). The rotor is divided into several discrete masses called stations and these masses are joined by massless flexible shafts. The response of the system is computed from a set of equations, formulated by using influence coefficients. These equations are solved and a final sweep is made to obtain the solution. J. W. Lund (1965) has analyzed the equations involved in the transfer matrix method for the case of elliptic response of the rotor system and has written a program using these equations to study the vibrational characteristics of rotor systems. The program has been subsequently simplified to analyze circular synchronous response of rotor systems. This thesis describes the modification of this simplified transfer matrix program. The current modification is required to model the non-colocation of sensors in active magnetic bearings.

To understand the classical transfer matrix method, consider a typical rotor section element assumed to be composed of a point mass and a massless elastic shaft to its right. This is illustrated by Fig. 38.

Consider the forces acting on the mass to formulate the equations required for equilibrium. Referring to Fig. 39

$$V^R_{xic} = V^L_{x\,i-1\,c} + (m_i\omega^2 - K_i)x_{ic} - C_i\omega x_{is} + FXC_i + a_{x_i}m_i\omega^2 \quad [3.1]$$

$$V^R_{xis} = V^L_{x\,i-1\,s} + C_i\omega x_{ic} + (m_i\omega^2 - K_i)x_{is} + FXS_i - a_{y_i}m_i\omega^2 \quad [3.2]$$

$$M^R_{yic} = M^L_{y\,i-1\,c} + (I_p - I_T)\omega^2\,\theta^L_{xic} \quad [3.3]$$

$$M^R_{yis} = M^L_{y\,i-1\,s} + (I_p - I_T)\omega^2\,\theta^L_{xis} \quad [3.4]$$

$$\theta^R_{xic} = \theta^L_{xic} \quad [3.5]$$

$$\theta^R_{xis} = \theta^L_{xis} \quad [3.6]$$

$$x^R_{ic} = x^L_{ic} \quad [3.7]$$

$$x^R_{is} = x^L_{is} \quad [3.8]$$

The above equations represent only the forces acting in the X direction. However, since it has been assumed that the motion of the shaft is circular, there is no necessity to formulate the equations of motion in the Y direction. The deflection in the Y direction can be easily obtained from the deflection in the X direction, using the relationships $x_s = y_c$ and $x_c = -y_s$, derived from basic principles of coordinate geometry. Additionally, it may be noted that for applying a simple harmonic excitation force in one plane, only one of FXC or FXS can be non-zero. If both FXC and FXS are non-zero the applied force is a sum of two simple harmonic forces in one plane.

These equations can be presented in matrix form and the matrices are called transfer matrices. The matrix form for Eqs. [3.1 ... 3.8] is as follows.

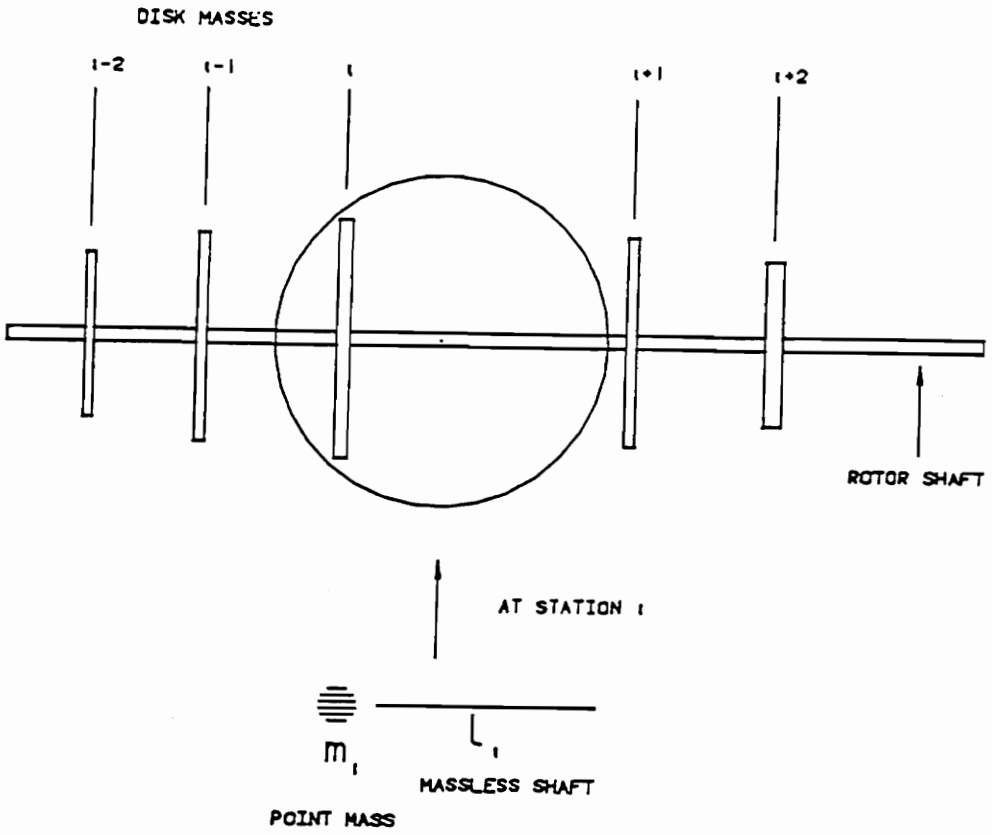

Figure 38. Typical Rotor Section Element

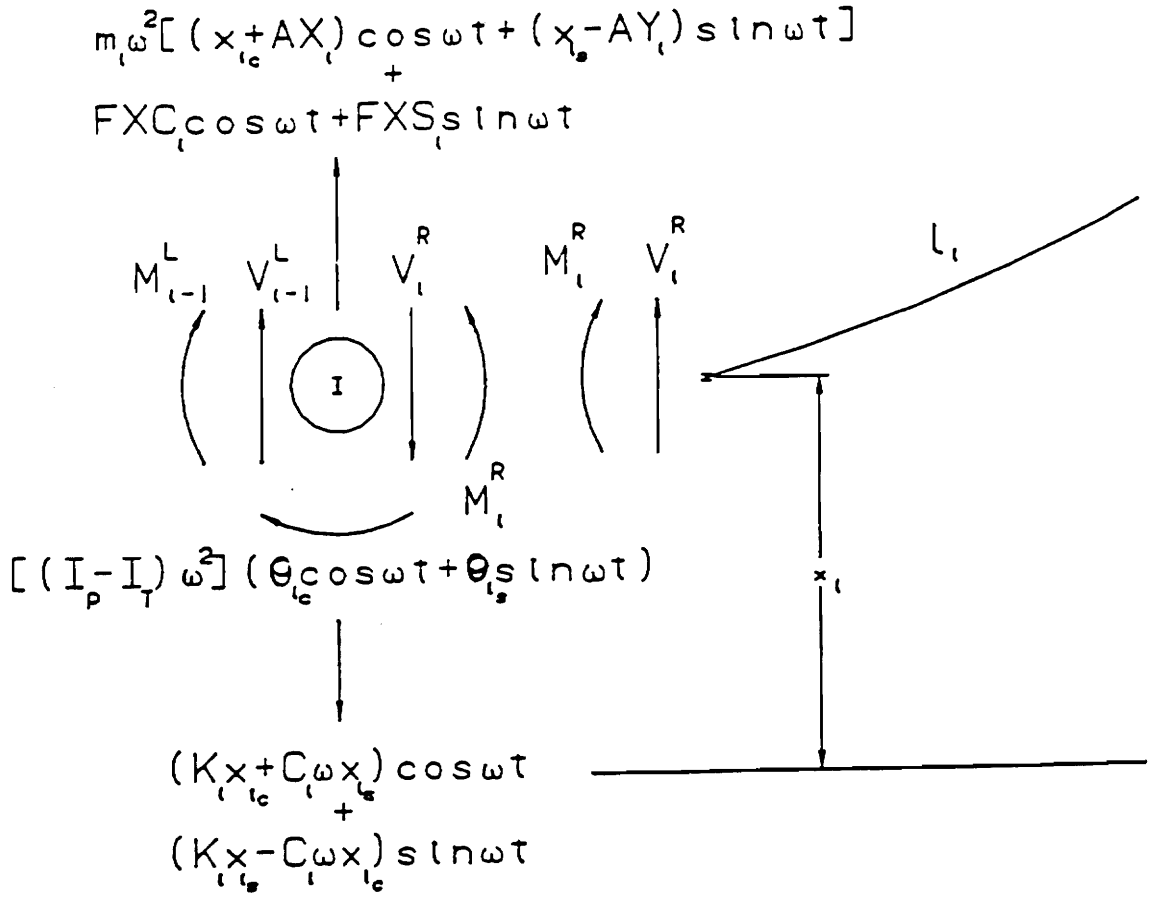

Figure 39. Forces Acting on the Point Mass

$$\begin{bmatrix} V_{xic} \\ V_{xis} \\ M_{yic} \\ M_{yis} \\ \theta_{xic} \\ \theta_{xis} \\ x_{ic} \\ x_{is} \\ 1 \end{bmatrix}_i^R = \begin{bmatrix} 1 & 0 & 0 & 0 & 0 & 0 & m_i\omega^2 - K_i & -C_i\omega & a_{x_i}m_i\omega^2 + FXC_i \\ 0 & 1 & 0 & 0 & 0 & 0 & C_i\omega & m_i\omega^2 - K_i & -a_{y_i}m_i\omega^2 + FXS_i \\ 0 & 0 & 1 & 0 & (I_p - I_T)\omega^2 & 0 & 0 & 0 & 0 \\ 0 & 0 & 0 & 1 & 0 & (I_p - I_T)\omega^2 & 0 & 0 & 0 \\ 0 & 0 & 0 & 0 & 1 & 0 & 0 & 0 & 0 \\ 0 & 0 & 0 & 0 & 0 & 1 & 0 & 0 & 0 \\ 0 & 0 & 0 & 0 & 0 & 0 & 1 & 0 & 0 \\ 0 & 0 & 0 & 0 & 0 & 0 & 0 & 1 & 0 \\ 0 & 0 & 0 & 0 & 0 & 0 & 0 & 0 & 1 \end{bmatrix} \begin{bmatrix} V_{xic} \\ V_{xis} \\ M_{yic} \\ M_{yis} \\ \theta_{xic} \\ \theta_{xis} \\ x_{ic} \\ x_{is} \\ 1 \end{bmatrix}_i^L$$

[3.9]

The coefficient matrix in Eq. [3.9] is called the "point" matrix. Now consider the equations for the massless elastic shaft of station i. From Fig. 40

$$V^L_{x\,i+1c} = V^R_{xic} \qquad [3.10]$$

$$V^L_{x\,i+1s} = V^R_{xis} \qquad [3.11]$$

$$M^L_{y\,i+1c} = M^R_{yic} + l_i.V^R_{xic} \qquad [3.12]$$

$$M^L_{y\,i+1s} = M^R_{yis} + l_i.V^R_{xis} \qquad [3.13]$$

$$\theta^L_{x\,i+1c} = \theta^R_{xic} + \frac{l_i^2}{2EI} V^R_{xic} + \frac{l_i}{EI} M^R_{yic} \qquad [3.14]$$

$$\theta^L_{x\,i+1s} = \theta^R_{xis} + \frac{l_i^2}{2EI} V^R_{xis} + \frac{l_i}{EI} M^R_{yis} \qquad [3.15]$$

$$x^L_{i+1c} = x^R_{ic} + l_i.\theta^R_{xic} + \left(\frac{l_i^3}{6EI} - GN_i\right)V^R_{xic} + \frac{l_i^2}{2EI} M^R_{yic} \qquad [3.16]$$

$$x^L_{i+1s} = x^R_{is} + l_i.\theta^R_{xis} + \left(\frac{l_i^3}{6EI} - GN_i\right)V^R_{xis} + \frac{l_i^2}{2EI} M^R_{yis} \qquad [3.17]$$

Presenting these equations in matrix form

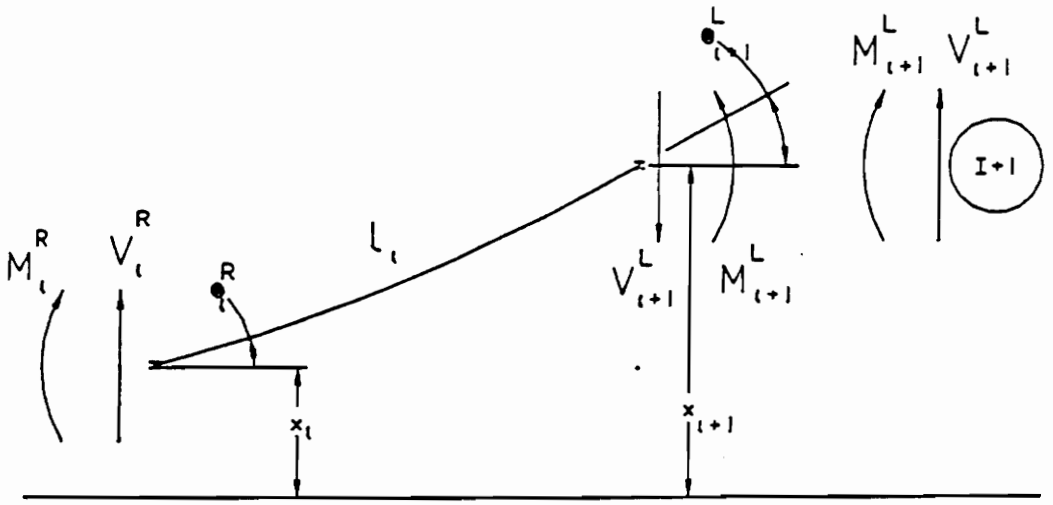

Figure 40. Forces Acting on the Massless Elastic Shaft

$$\begin{bmatrix} V_{xlc} \\ V_{xls} \\ M_{yic} \\ M_{yis} \\ \theta_{xlc} \\ \theta_{xls} \\ x_{ic} \\ x_{is} \\ 1 \end{bmatrix}_{i+1}^{L} = \begin{bmatrix} 1 & 0 & 0 & 0 & 0 & 0 & 0 & 0 & 0 \\ 0 & 1 & 0 & 0 & 0 & 0 & 0 & 0 & 0 \\ l_i & 0 & 1 & 0 & 0 & 0 & 0 & 0 & 0 \\ 0 & l_i & 0 & 1 & 0 & 0 & 0 & 0 & 0 \\ l_i^2/2EI & 0 & l_i/EI & 0 & 1 & 0 & 0 & 0 & 0 \\ 0 & l_i^2/2EI & 0 & l_i/EI & 0 & 1 & 0 & 0 & 0 \\ l_i^3/6EI - GN_i & 0 & l_i^2/2EI & 0 & l_i & 0 & 1 & 0 & 0 \\ 0 & l_i^3/6EI - GN_i & 0 & l_i^2/2EI & 0 & l_i & 0 & 1 & 0 \\ 0 & 0 & 0 & 0 & 0 & 0 & 0 & 0 & 1 \end{bmatrix} \begin{bmatrix} V_{xlc} \\ V_{xls} \\ M_{yic} \\ M_{yis} \\ \theta_{xlc} \\ \theta_{xls} \\ x_{ic} \\ x_{is} \\ 1 \end{bmatrix}_{i}^{R}$$

[3.18]

The coefficient matrix in the above eq. [3.18] is called the "field" matrix. As can be seen from this matrix, a correction to account for the shear deformation effect is also included. The terms of this correction factor are explained below

$$GN_i = \frac{l_i}{a_i . G_i . sf_i} \qquad [3.19]$$

a_i = area of section i

G_i = shear modulus of section i

$$sf_i = \frac{[(7. + .6\mu)(1. + dr_i^2)^2 + (20. + 12.\mu)dr_i^2]}{[6.(1. + \mu)(11. + dr_i^2)^2]} \qquad [3.20]$$

μ is poissons ratio = $E_i/2G_i - 1$

dr_i is the diameter ratio = inner diameter/outer diameter

Modification for Sensor Non-Colocation

Due to sensor non-colocation, at the station representing the bearing location, Eqs. [3.1] and [3.2] are modified as follows.

$$V_{xic}^{R} = V_{xic}^{L} + m_i\omega^2 x_{ic} - K_i x_{ic_{sen}} - C_i\omega x_{is_{sen}} + FXC_i + a_{x_i} m_i\omega^2 \qquad [3.21]$$

$$V_{xis}^{R} = V_{xis}^{L} + C_i\omega_{ic_{sen}} + m_i\omega^2 x_{is} - K_i x_{is_{sen}} + FXS_i - a_{y_i} m_i\omega^2 \qquad [3.22]$$

The bearing stiffness is multiplied by the deflection sensed at the sensor location instead of the actual deflection at the bearing.

Algorithm for Modification Due to Sensor Non-Colocation

The modification in the point matrix for the bearing station, due to the sensor non-colocation has already been discussed. However, a straight-forward sweep of the rotor is possible only in certain cases of sensor location. The possible cases of sensor position are illustrated in the probe configurations shown in Figs. 41-43. Upon examination of these figures, three cases of sensor location relative to the bearing location can be listed.

1. One sensor before the bearing

2. One sensor after the bearing

3. Two sensors, one each on either side of the bearing.

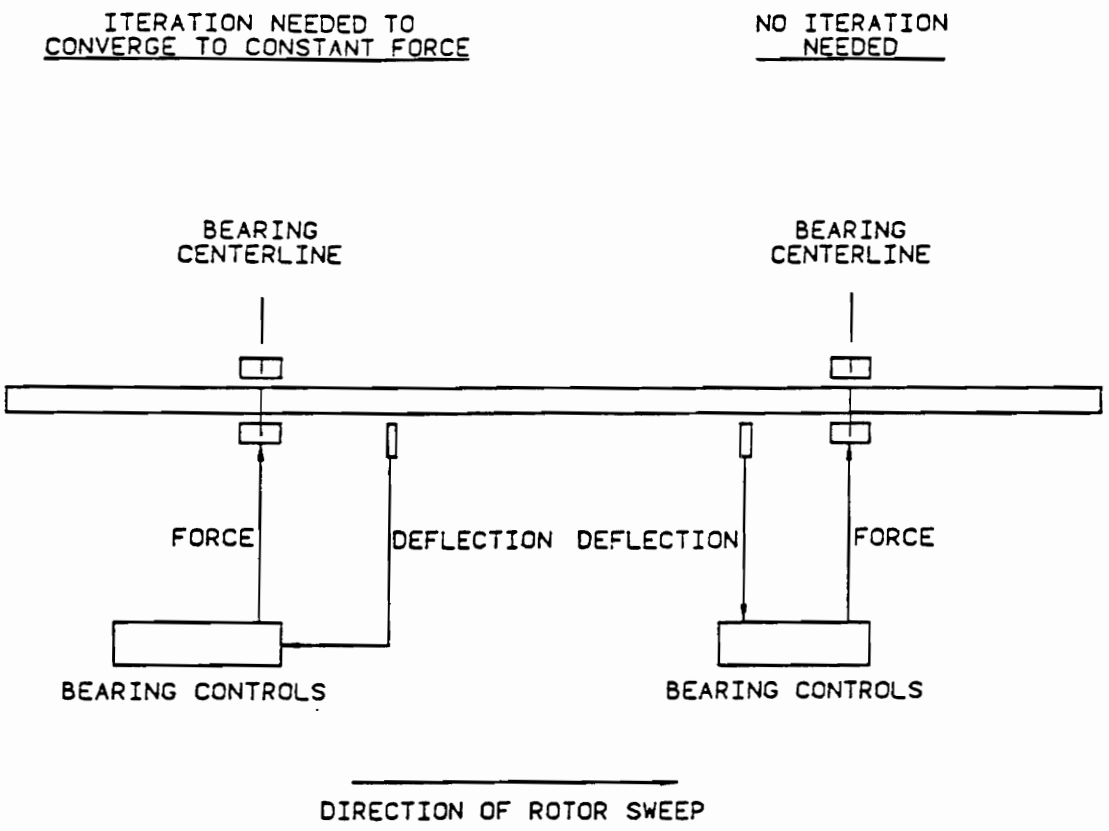

Figure 41. Inboard Sensors

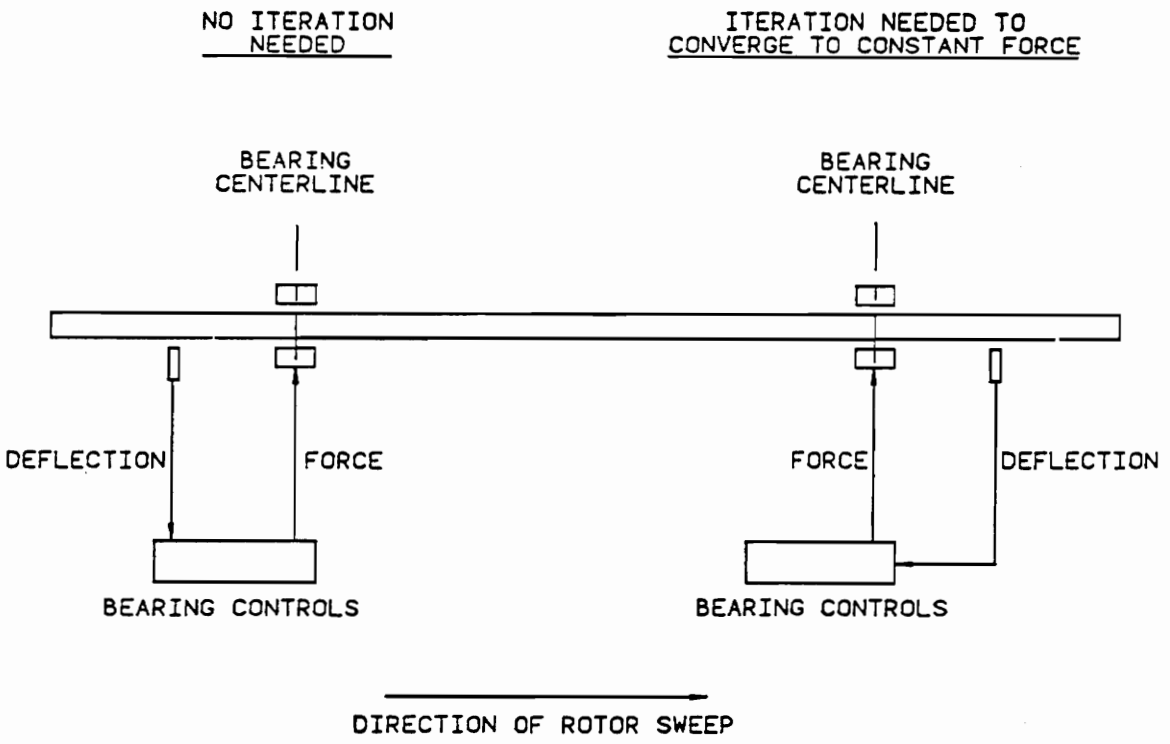

Figure 42. Outboard Sensors

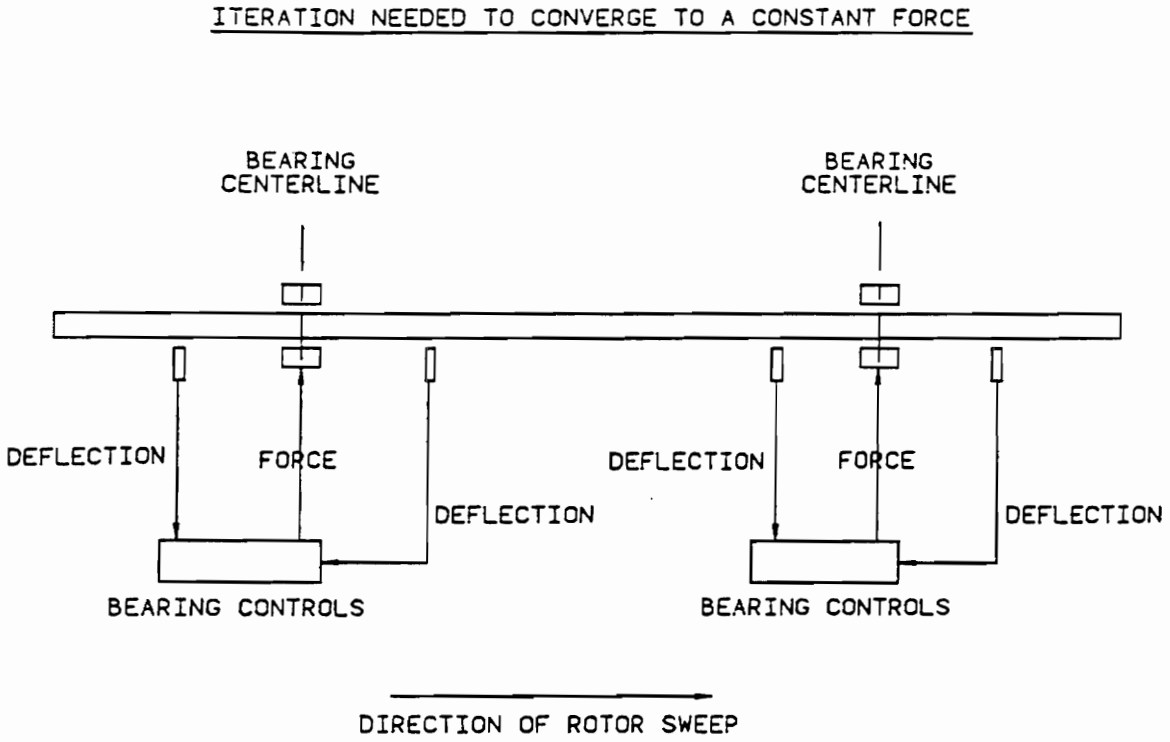

Figure 43. Sensors on Either Side of the Bearings

Case 1

For case 1, the sensor deflections are saved in the sweeping process and then used at the bearing station. This is illustrated in Fig. 41 by the second bearing location and in Fig. 42 by the first bearing location. The sweeping process is straightforward and no iteration scheme is required for the solution process.

Case 2

In this case, since the sensor comes after the bearing, the sensor deflections are not known when the sweeping process reaches the bearing. Thus the sensor deflections are assumed to be some arbitrary value. Generally, the deflections at the station before the bearing are used as these arbitrary values. The sweeping process is then continued until the sensor location is reached. Here a comparison is made between the assumed sensor deflection and the sensor deflection calculated by the sweeping process. If the two quantities agree to within a certain margin of error, the sweeping process is continued from the sensor station onwards. If the two quantities do not lie within the error margin, the program iterates back to the bearing location and uses the sensor deflections calculated by the current sweeping process. These sensor deflections are used as explained before, in the bearing station point matrix calculations and the sweep process is continued. This leads to a series of iterations between the bearing station and the sensor station and these iterations are continued until the sensor deflections used at the bearing station agree with the sensor deflections calculated at the sensor station by the sweeping process, *i.e.* convergence is obtained. This case is illustrated in Fig. 41 by the first bearing location and in Fig. 42 by the second bearing location.

Case 3

With two sensors, one each before and after the bearing, the case can be split up into two cases one resembling case one and the other resembling case two. This case is shown in Fig.

43. When the sensor before the bearing is reached, the sensor deflections are saved. These are used, the first time the bearing location is reached. The sweep process is then continued and the sensor after the bearing is dealt with in a manner similar to case two.

Discussion of the Convergence Process

The problem of converging to the correct values of sensor deflections is similar to the problem of finding the roots of a polynomial and thus, root-finding techniques are applied to predict the new values of sensor deflections using the previous sensor deflection values. The Taylor series convergence technique in two variables can be used to predict the roots two functions, both functions depending on two independent variables. Since there is cross-coupling between the stiffness and damping terms in equations [3.21] and [3.22] this method was considered the most suitable and was used. However, due to the very low magnitude derivatives involved in the convergence equations, the convergence process fails and leads to divergence from the correct solution.

When the cross-coupling of the stiffness and damping terms is ignored, and the Secant method of convergence is used to converge on the two sensor deflection components independently, the algorithm converges with diminishing oscillations. However, the number of iterations required were more than those required, when no convergence algorithm was used. Thus, simply using the sensor deflections obtained from the sweeping process, back at the bearing location, gives the fastest convergence. This can be verified by studying Table 2.

Table 2. Comparison of Different Convergence Schemes

2 MASS MODEL, UNBALANCE EXCITATION, M = 1, K = 2, ALPHA = 0.3 FREQ = 130 HZ, CONVERGENCE TO XC, TRUE SOLUTION = 7.649442						
No. of Iter.	Taylor's series Convergence	% Diff. from true Soln.	Secant method Convergence	% Diff. from true Soln.	Simple Iteration	% Diff. from true Soln.
1	3.500004	54.24	3.500004	54.24	3.500004	54.24
2	8.051951	-5.26	8.051951	-5.26	8.051951	-5.26
3	7.737319	-1.15	7.737319	-1.15	7.737319	-1.15
4	7.581234	0.89	7.930811	-3.68	7.628863	0.27
5	7.849375	-2.61	7.605373	0.576	7.648726	0.0094
6	3.625942	52.60	7.642738	0.088	7.650135	-0.0091
7	69.54724	-809.2	7.655252	-0.076	7.649398	0.00058
8	-959.629	12645.1	7.650030	-0.0077	7.649425	0.00022
9	15109.55	-197425	7.649057	0.0050	7.649445	-0.00004
10	-235777.3	3082381	7.649363	0.001	7.649442	0.0
11	3681287.0	-48124809	7.649458	-0.00021	7.649442	0.0
12	---	---	7.649447	-0.000065	7.649442	0.0
13	---	---	7.649434	0.0001	7.649442	0.0
14	---	---	7.649441	0.000013	7.649442	0.0
15	---	---	7.649443	-0.000013	7.649442	0.0
16	---	---	7.649442	0.0	7.649442	0.0
17	---	---	7.649441	0.000013	7.649442	0.0
18	---	---	7.649441	0.000013	7.649442	0.0
19	---	---	7.649442	0.0	7.649442	0.0

Modification to Separate Gyroscopic Forces and Transverse Forces Acting at the Point Mass Stations

The gyroscopic forces and transverse forces are due to the inertial effects of the rotating and whirling disk masses. When the rotor is subjected to an external vibrational force assuming no unbalance to be present, the gyroscopic force at the point masses will depend only on the rotor spinning speed and not on the frequency of excitation. Considering the rotor spinning frequency to be "s", Eqs. [3.3] and [3.4] are modified as follows

$$M_{yic}^{R} = M_{yic}^{L} + \omega(sI_p - \omega I_T)\theta_{xic} \qquad [3.23]$$

$$M_{yis}^{R} = M_{yis}^{L} + \omega(sI_p - \omega I_T)\theta_{xis} \qquad [3.24]$$

Here ω is the frequency of excitation.

Obtaining the Solution with the Transfer Matrix Method

The shear and bending moments are obtained on the right end of the rotor by assuming first, a unit deflection at the left end of the rotor and then, by assuming a unit slope at the left end. The shear and bending moments on the right end are obtained by consecutively using the point and field matrices, starting from the left end station and sweeping all the stations until the right end is reached. Finally the shear and bending moments on the right end due to the application of the unbalance or the constant excitation force are obtained. This gives a series of algebraic equations which can be solved by matrix inversion to obtain the actual slopes and deflections on the left end of the rotor.

One more sweep is made using the true slopes and deflections on the left end and the unbalance or the constant excitation forces, to obtain the final solution of amplitudes and phase angles along the rotor axis.

Appendix F gives the input parameters needed to run the modified transfer matrix analysis code and provides guidelines to study the output files obtained by running this code.

Comparison of the Results of the two-Mass Rotor System, for the Jeffcott Model and the Transfer Matrix Method

The results of the two-mass rotor system (data shown in Table 1) as obtained by the Jeffcott Model program have already been shown and discussed in Chapter 2. The same rotor system data is adapted for use with the modified transfer matrix method program and the input data files are shown in Appendices A and B. The results obtained from the modified transfer matrix method program are compared with the results obtained from the modified Jeffcott model program to validate the correctness of the modifications. The modified Jeffcott model is important but because of its simplicity, its results are of limited use. Also it does not model a complex rotor system composed of many disk masses and possibly different shaft cross-sections along the rotor length. Hence, it is the transfer matrix method that is more useful for application purposes. The Jeffcott model serves for the purpose of comparison only.

Tables 3-6 give the comparison between the two programs. As can be seen from the tables, there is a fairly close agreement between the results obtained from the two programs. The agreement in the critical frequency values is much better than that between amplitude values and amplitude values agree better than phase angle values. This is because, the critical frequencies of a rotor system depends mostly on its mass and stiffness properties, both of which

Table 3. Results of the 2-Mass Rotor System, for the Jeffcott Model and the Transfer Matrix Model, Bearing Damping 0.263 Nsec/mm

FIRST MODE, UNBALANCE EXCITATION, M = 1, K = 2, BEARING/(MIDSPAN)			
	Jeffcott Code	Transfer matrix Code	% Difference
α = -0.2 Critical Frequency Amplitude Phase Angle	 32.167 / (32.167) 2.285 / (4.425) 103.48 / (102.57)	 32.167 / (32.167) 2.302 / (4.482) 86 / (85.1)	 0 / (0) -0.74 / (-1.29) 16.89 / (17.03)
α = 0.0 Critical Frequency Amplitude Phase Angle	 35.333 / (35.333) 1.408 / (3.401) 90.214 / (88.398)	 35.333 / (35.333) 1.408 / (3.402) 91.6 / (89.8)	 0 / (0) 0 / (-0.03) -1.54 / (-1.59)
α = 0.2 Critical Frequency Amplitude Phase Angle	 40.333 / (40.333) 0.539 / (2.281) 92.571 / (86.391)	 40.167 / (40.000) 0.571 / (2.310) 104.1 / (81.8)	 0.41 / (0.83) -5.94 / (-1.27) -12.45 / (5.31)

Table 4. Results of the 2-Mass Rotor System, for the Jeffcott Model and the Transfer Matrix Model, Bearing Damping 0.263 Nsec/mm

THIRD MODE, UNBALANCE EXCITATION, M = 1, K = 2, BEARING/(MIDSPAN)			
	Jeffcott Code	Transfer matrix Code	% Difference
α = -0.2 Critical Frequency Amplitude Phase Angle	93.834 / (94.834) 0.569 / (0.216) 267.15 / (133.11)	93.500 / (94.500) 0.569 / (0.217) 265.5 / (131.9)	0.36 / (0.35) 0 / (-0.46) 0.62 / (0.91)
α = 0.0 Critical Frequency Amplitude Phase Angle	85.167 / (85.834) 0.584 / (0.275) 266.16 / (127.23)	85.167 / (85.833) 0.583 / (0.275) 266.8 / (127.7)	0 / (0) 0.17 / (0) -0.24 / (-0.37)
α = 0.2 Critical Frequency Amplitude Phase Angle	74.667 / (74.834) 0.588 / (0.405) 275.91 / (122.35)	75.167 / (75.333) 0.587 / (0.396) 275.3 / (121.7)	-0.67 / (-0.67) 0.17 / (2.22) 0.22 / (0.53)

Table 5. Results of the 2-Mass Rotor System, for the Jeffcott Model and the Transfer Matrix Model, Bearing Damping 0.263 Nsec/mm

FIRST MODE, PLANAR EXCITATION, M = 1, K = 2, BEARING/(MIDSPAN)			
	Jeffcott Code	Transfer matrix Code	% Difference
α = -0.2 Critical Frequency Amplitude Phase Angle	32.167 / (32.167) 4.577 / (8.896) 104.24 / (104.24)	32.167 / (32.167) 5.410 / (10.522) 86.8 / (86.8)	0 / (0) -18.20 / (-18.28) 16.73 / (16.73)
α = 0.0 Critical Frequency Amplitude Phase Angle	35.333 / (35.333) 3.045 / (7.352) 90.214 / (90.214)	35.333 / (35.333) 3.262 / (7.882) 91.6 / (91.6)	0 / (0) -7.13 / (-7.21) -1.54 / (-1.54)
α = 0.2 Critical Frequency Amplitude Phase Angle	40.333 / (40.333) 1.335 / (5.643) 88.527 / (88.527)	40.000 / (40.000) 1.420 / (5.709) 83.9 / (83.9)	0.83 / (0.83) -6.37 / (-1.17) 5.23 / (5.23)

Table 6. Results of the 2-Mass Rotor System, for the Jeffcott Model and the Transfer Matrix Model, Bearing Damping 0.263 Nsec/mm

THIRD MODE, PLANAR EXCITATION, M = 1, K = 2, BEARING/(MIDSPAN)			
	Jeffcott Code	Transfer matrix Code	% Difference
α = -0.2 Critical Frequency Amplitude Phase Angle	93.834 / (93.500) 0.814 / (0.261) 89.377 / (262.55)	93.500 / (93.167) 0.864 / (0.280) 87.70 / (260.9)	0.36 / (0.36) -6.14 / (-7.28) -4.61 / (0.63)
α = 0.0 Critical Frequency Amplitude Phase Angle	85.334 / (85.167) 1.261 / (0.524) 91.007 / (266.16)	85.167 / (85.000) 1.363 / (0.569) 86.70 / (261.9)	0.2 / (0.2) -8.09 / (-8.59) 4.73 / (1.6)
α = 0.2 Critical Frequency Amplitude Phase Angle	74.667 / (74.667) 2.882 / (1.783) 88.456 / (268.45)	75.000 / (75.000) 3.299 / (2.011) 79.50 / (259.5)	-0.45 / (-0.45) -14.47 / (-12.79) 10.12 / (3.34)

are accounted for in a similar manner in the two programs. The amplitude and phase angle values show greater disagreement due to the fact that the Jeffcott code assumes a sine-wave shape for the mode shapes and this assumption is only an approximation of the actual mode shape. It can be seen from the tables, that the Jeffcott code underestimates amplitude values in most cases. Also, amplitude values show a higher disagreement when a planar constant magnitude force excitation is applied instead of an unbalance force excitation.

The Eight-Stage Centrifugal Compressor Rotor System Model

The data of an eight-stage centrifugal compressor rotor is used with the transfer matrix code to observe the effects of changing sensor positions on the vibrational characteristics of an actual rotor system. This rotor system is illustrated in Fig. 44 and its design parameters are given in Table 7. A complete description of the geometric parameters of this rotor is given in Appendices C and D (Courtesy of Keesee, 1989).

The program is run with all the four cases of sensor positions, namely sensor colocation, inboard sensors, outboard sensors and two sensors on each side of the bearing. α values of -0.18, 0 and 0.18 are used.

Discussion of the Plots

The plots in Figs. 45-58 illustrate the effect of a change in the sensor location on the vibrational characteristics of the eight stage centrifugal compressor rotor system.

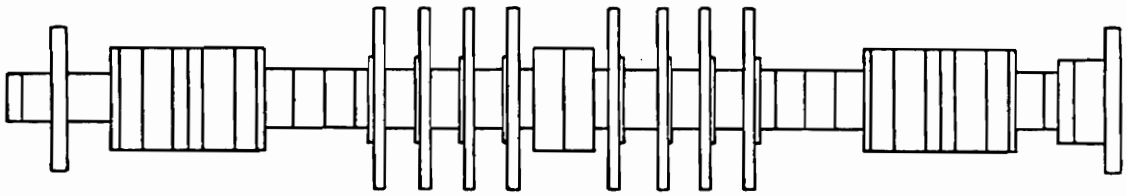

Figure 44. The Eight-Stage Centrifugal Compressor Rotor System

Table 7. Data for Eight-Stage Centrifugal Rotor System Model

ROTOR SYSTEM PROPERTY	SI UNITS	ENGLISH UNITS
Total rotor length	1879.6 mm	74.0 in
Distance to bearing 1 centerline	304.8 mm	12.0 in
Distance to sensor at bearing 1:		
Outboard sensor	190.5 mm	7.5 in
Inboard sensor	419.1 mm	16.5 in
Distance to bearing 2 centerline	1574.8 mm	62.0 in
Distance to sensor at bearing 2:		
Inboard sensor	1460.5 mm	57.5 in
Outboard sensor	1689.1 mm	66.5 in
Mid-span diameter	177.8 mm	7.0 in
Journal diameter	177.8 mm	7.0 in
Journal length	254.0 mm	10.0 in
Total rotor weight	2.95 KN	663.2 lb_f
Reaction at bearing 1	1.41 KN	317.0 lb_f
Reaction at bearing 2	1.54 KN	346.2 lb_f
Amplification factor of the Jeffcott model of the rotor system:		
Journal location	0.48	

Figures 45-47 show the influence of sensor position on amplitudes and critical speeds when an unbalance force is applied at midspan. Each plot shows the amplitude for a different location, namely, first bearing, midspan and second bearing. This compressor rotor is then simulated as a two-mass model with a mass ratio of 1.326 and a stiffness ratio of 3.773. The results obtained by solving this two-mass model with the modified Jeffcott model are illustrated in Figs. 48-50. These figures can be compared with Figs. 45-47 to verify the trends observed in the results.

Figures 52-54 illustrate the influence of sensor position on amplitudes and critical speeds when a constant magnitude force is applied at each of the two bearing locations. Three locations, first bearing, midspan and second bearing are considered. Figures 55 and 56 show the results obtained by solving a two-mass model of the compressor rotor with the modified Jeffcott method. These figures can be compared with Figs. 52-54 to verify the trend of behavior of the rotor system.

Figures 51 and 57 show the first mode shape of the rotor system when an unbalance force or a constant excitation force is applied. The mode shapes are useful to understand the behavior of the rotor system for a given sensor location.

Figure 58 (Keesee, 1989) shows the undamped critical speed map of the compressor rotor system for the first four modes. This figure shows the direction of change in the undamped critical speeds with different sensor locations.

Results Obtained from the Eight-Stage Compressor Rotor System

The results obtained from the eight-stage compressor rotor system are summarized below.

1. The first-mode critical frequency increases as the sensor is moved from the outboard location towards the inboard location. This is shown in Figs. 45-47 for unbalance excitation and in Figs. 51-53 for planar excitation. This is in agreement with the results obtained from the two-mass rotor system. However, no third-mode critical frequency is observed. The rotor system exhibits higher amplitudes as the sensors are moved in the inboard direction. It can be concluded from these observations that the first and third modes for the compressor rotor system must coincide just beyond the inboard sensor location considered *i.e.*, for an α value slightly greater than 0.18. Since the critical frequency behaviour with inboard sensors is similar to that observed in the first mode while the amplitude behaviour is similar to that observed in the third mode, the rotor system is exhibiting a mode shape that is in the transition stage from the first mode to the third mode. These mode shapes are illustrated in Figs. 56 and 57. The influence of sensor location on undamped critical speeds of the eight-stage compressor rotor system has been recorded by Keesee and is shown in Fig. 58 (Keesee, 1989).

2. To verify this behaviour, an approximate two-mass model of the compressor rotor system is run with the Jeffcott program. The results obtained with this approximate model are shown in Figs. 48-50, 54 and 55, and show agreement with the results obtained by the transfer matrix program with the compressor rotor system data as input. As discussed in Chapter 2, a combination of low amplification factor, high stiffness ratio and high mass ratio leads to the first mode critical frequency coinciding with the third mode critical frequency for some particular inboard sensor location and the first mode gradually changing into the third mode as the sensors are moved further inboard. The amplification factor of the approximate two-mass Jeffcott model for the eight-stage compressor rotor

system is 0.48 (Refer to Table 7), the stiffness ratio is 3.773 and the mass ratio is 1.326. These damping, stiffness and mass parameters determine the critical frequency and amplitude characteristics of the rotor system.

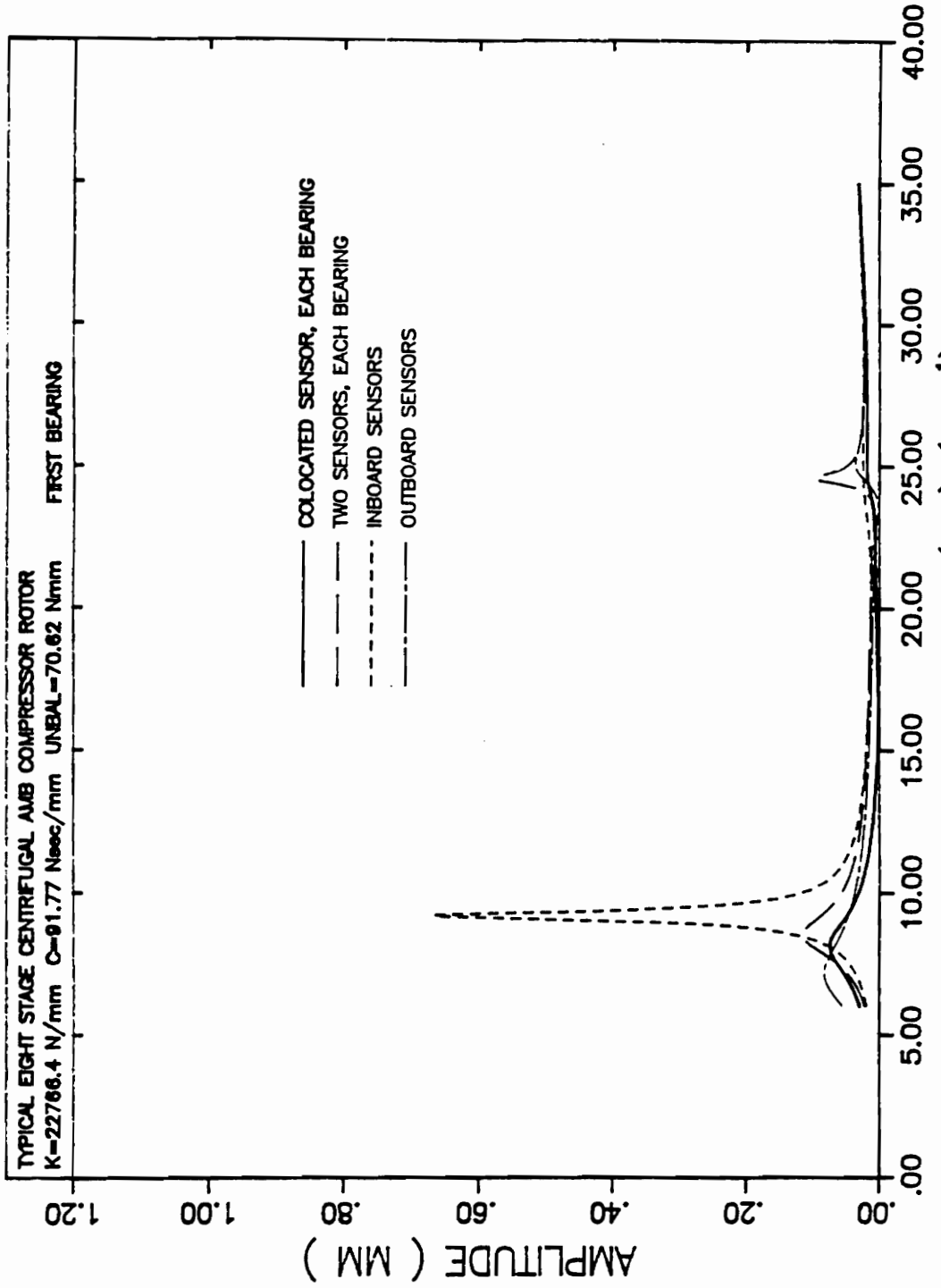

Figure 45.
Sensor Influence on Amplitude, Eight-Stage Compressor Rotor, Unbalance Excitation, First bearing

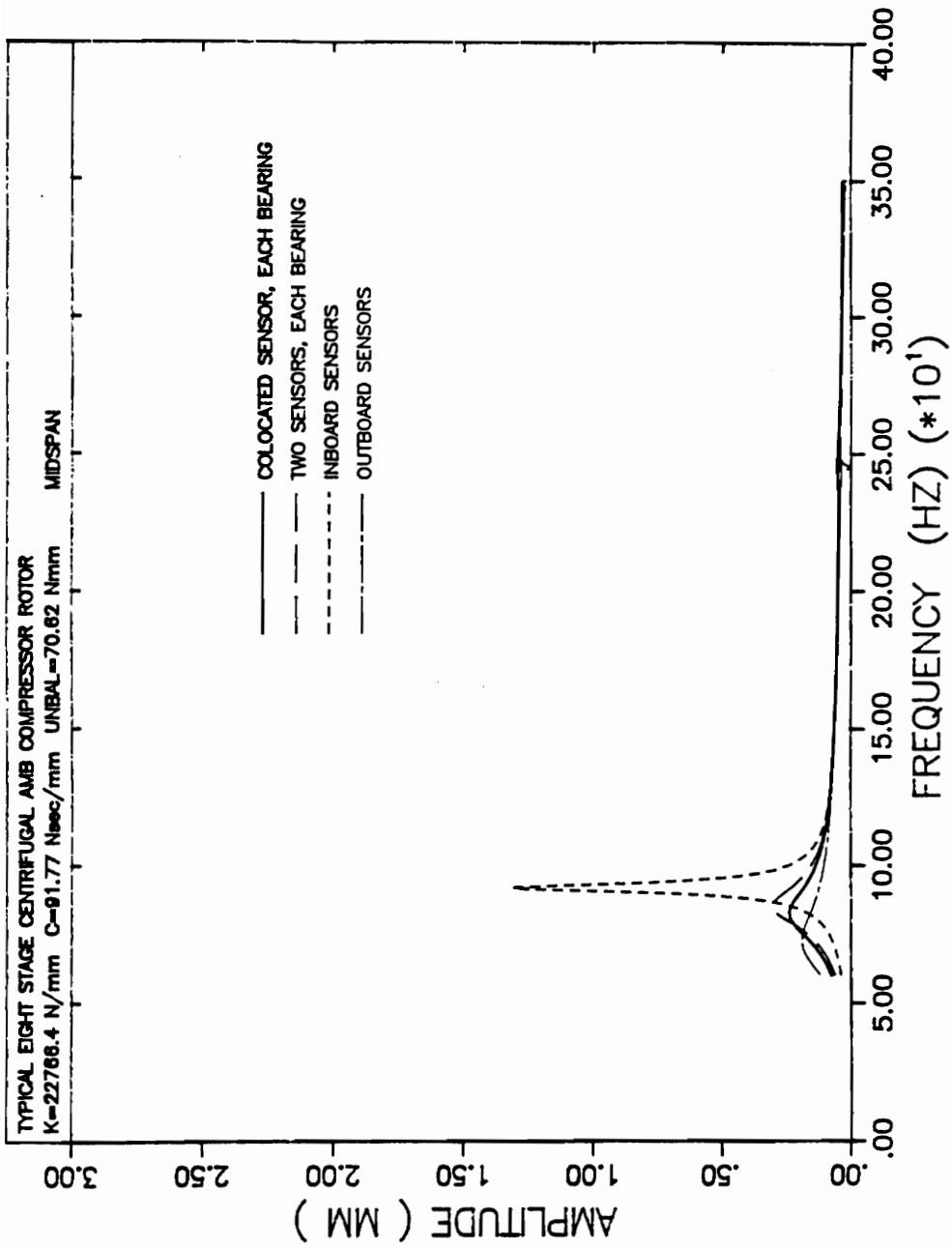

Figure 46.
Sensor Influence on Amplitude, Eight-Stage Compressor Rotor, Unbalance Excitation, Midspan

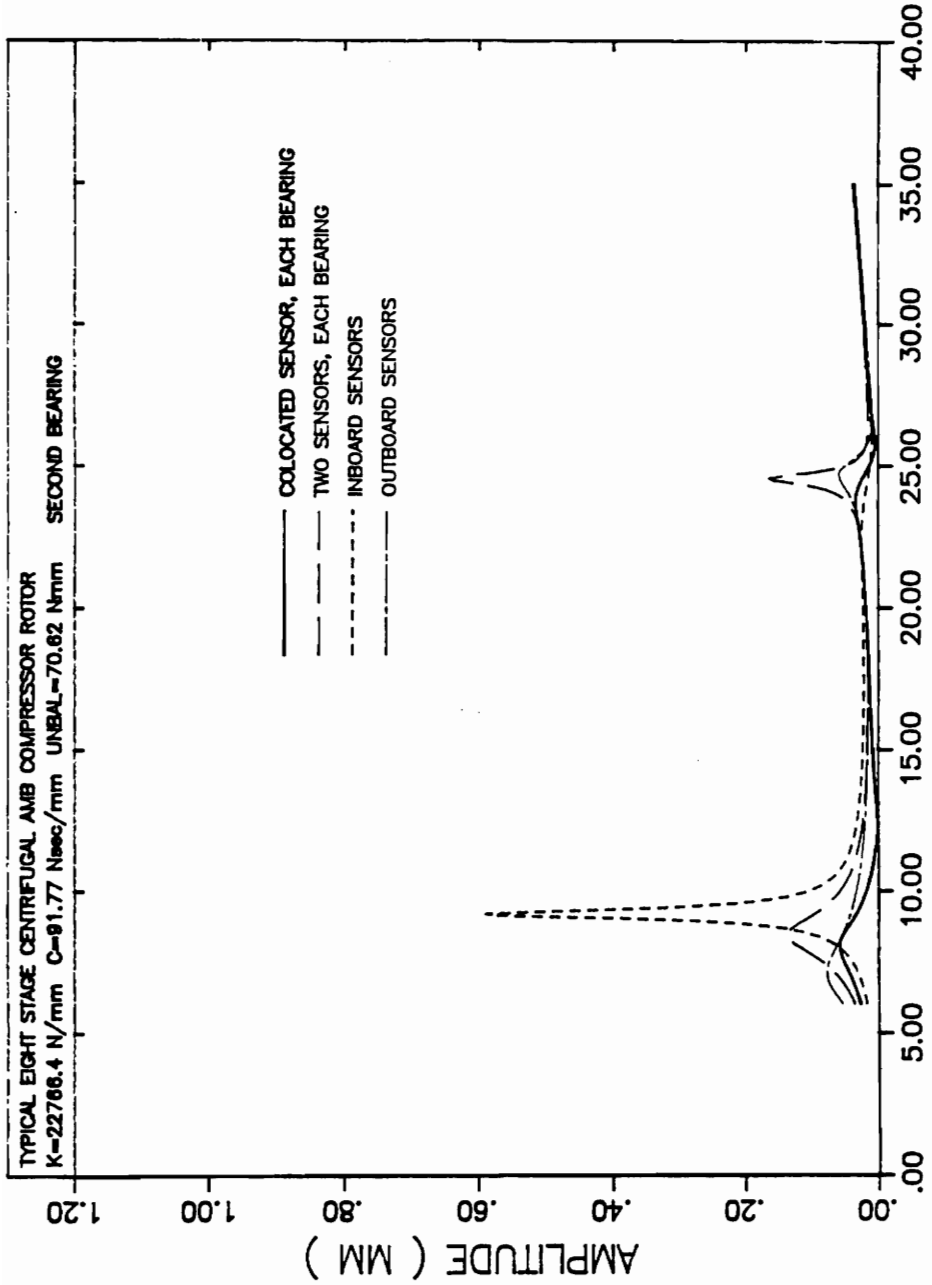

Figure 47.
Sensor Influence on Amplitude, Eight-Stage Compressor Rotor, Unbalance Excitation, Second bearing

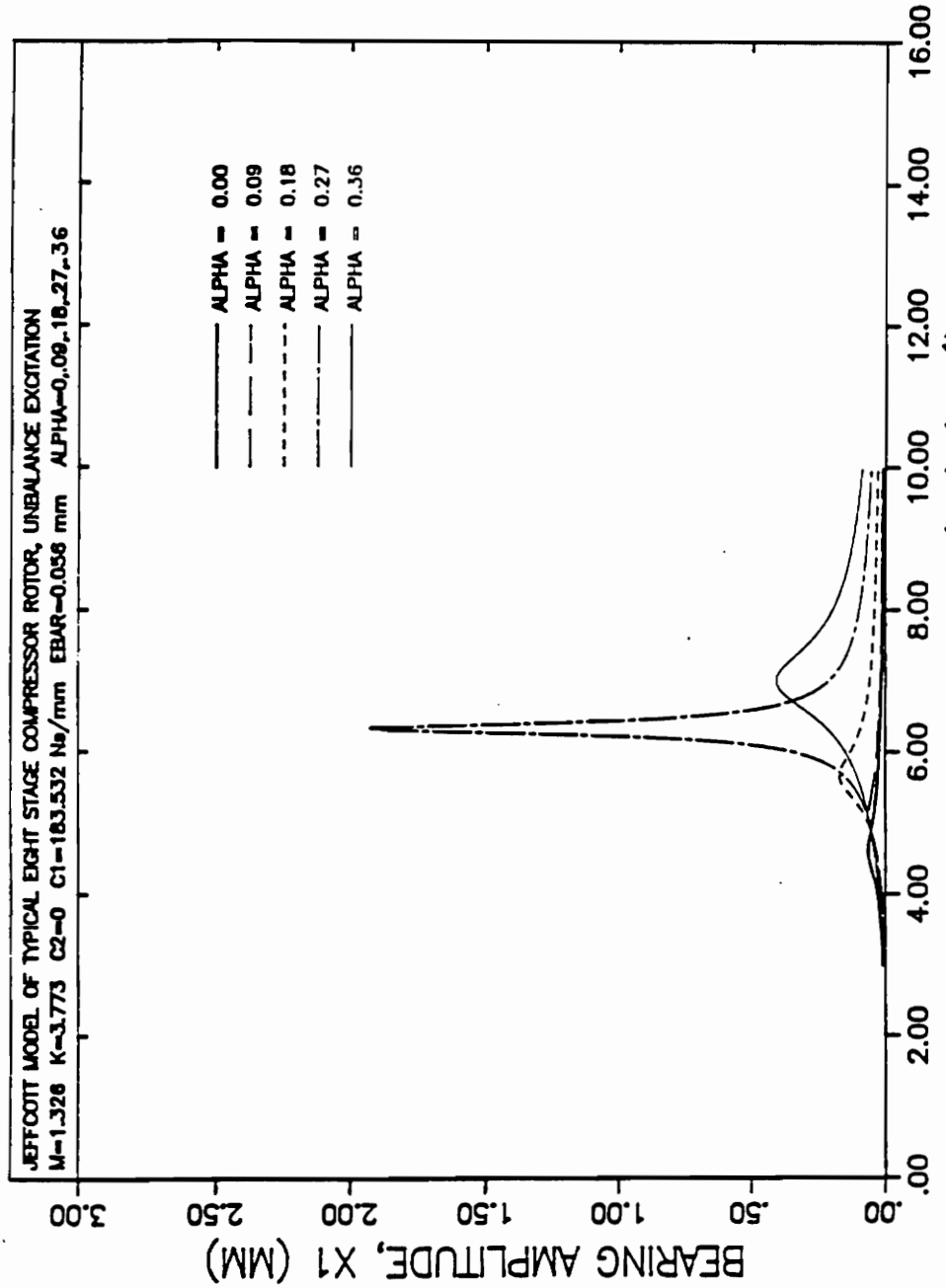

Figure 48.
Jeffcott Approximation of the Compressor Rotor, Unbalance Excitation, M = 1.326, K = 3.773, Inboard Sensors, Bearing

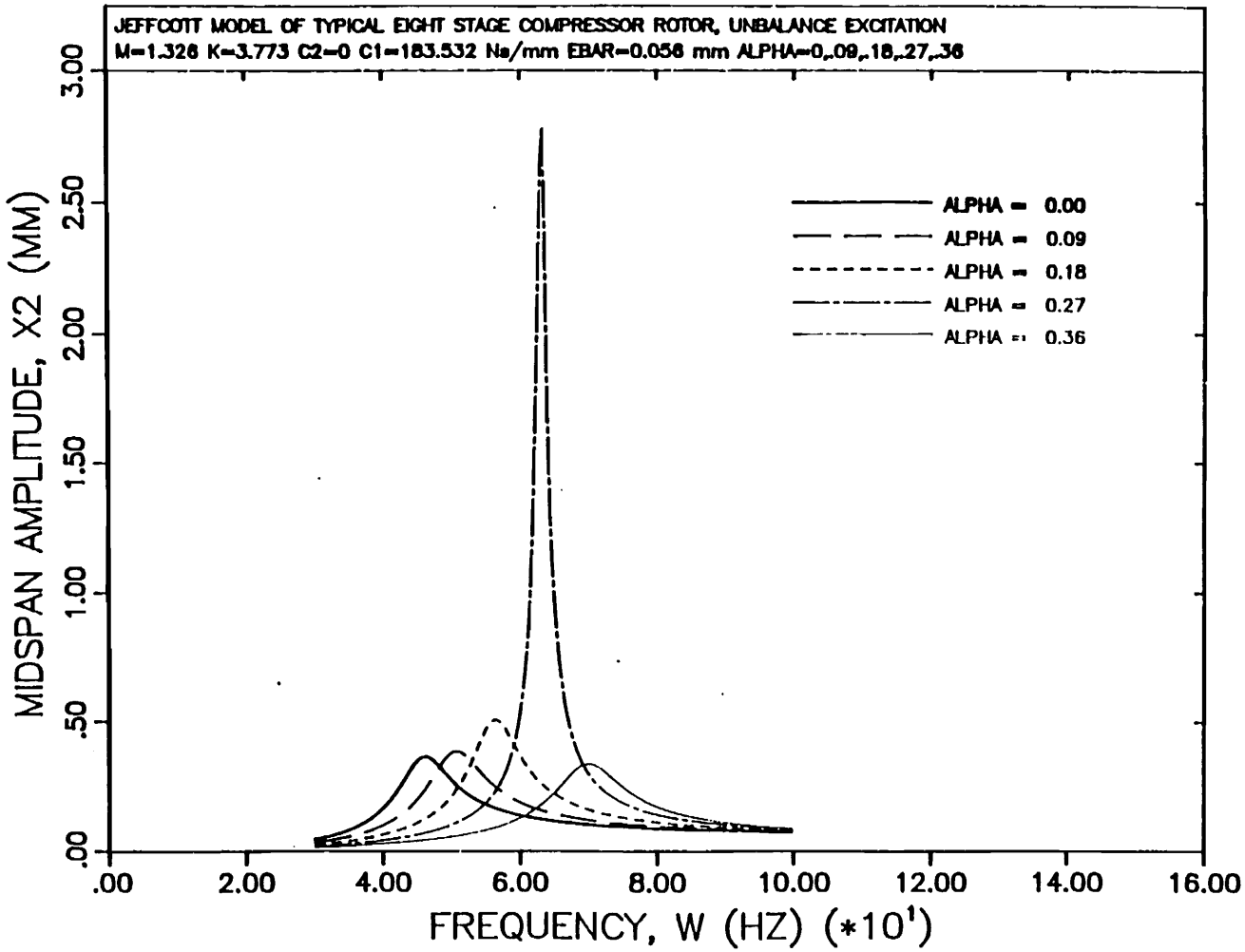

Figure 49.
Jeffcott Approximation of the Compressor Rotor, Unbalance Excitation, M = 1.326, K = 3.773, Inboard Sensors, Midspan

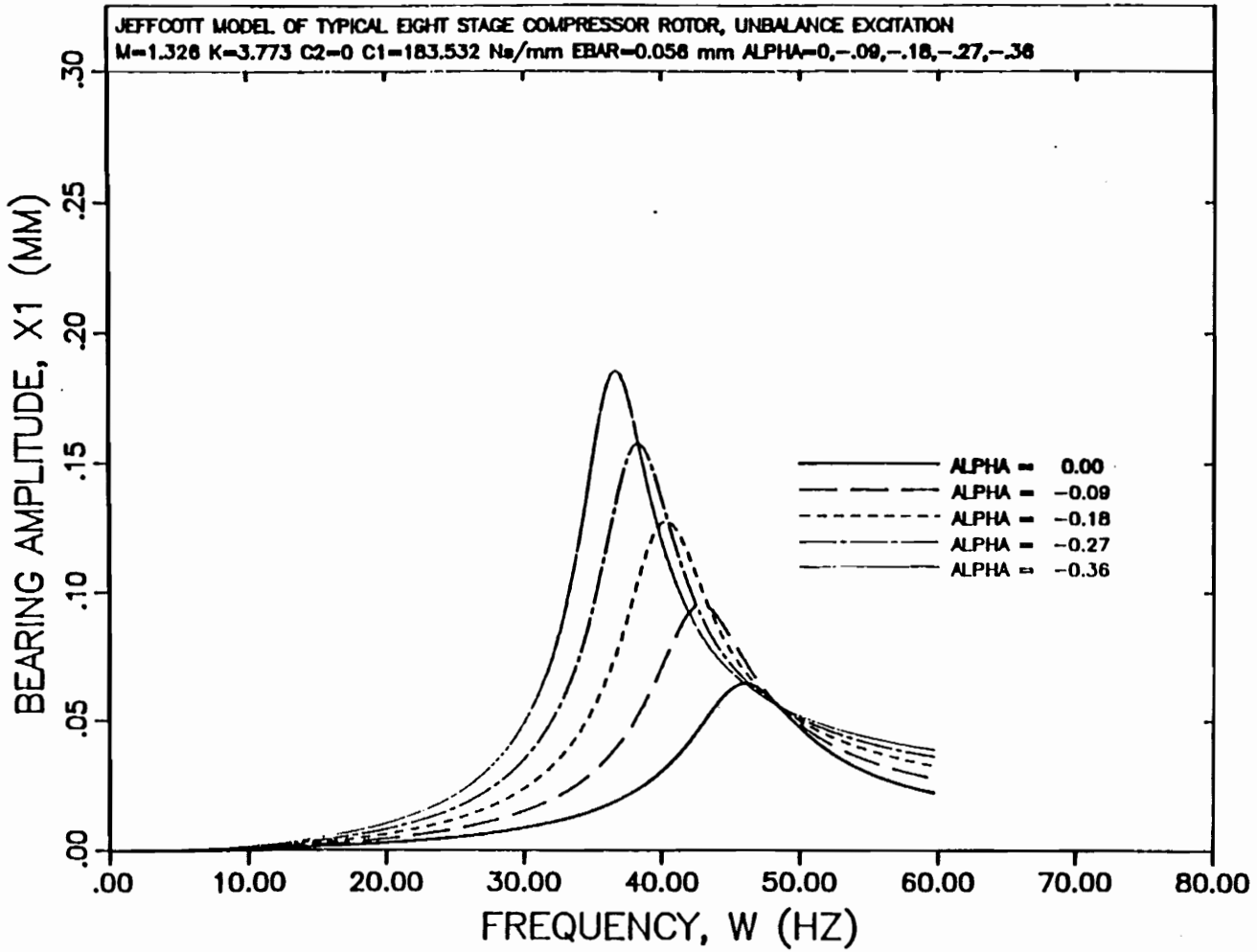

Figure 50.
Jeffcott Approximation of the Compressor Rotor, Unbalance Excitation, M = 1.326, K = 3.773, Outboard Sensors, Bearing

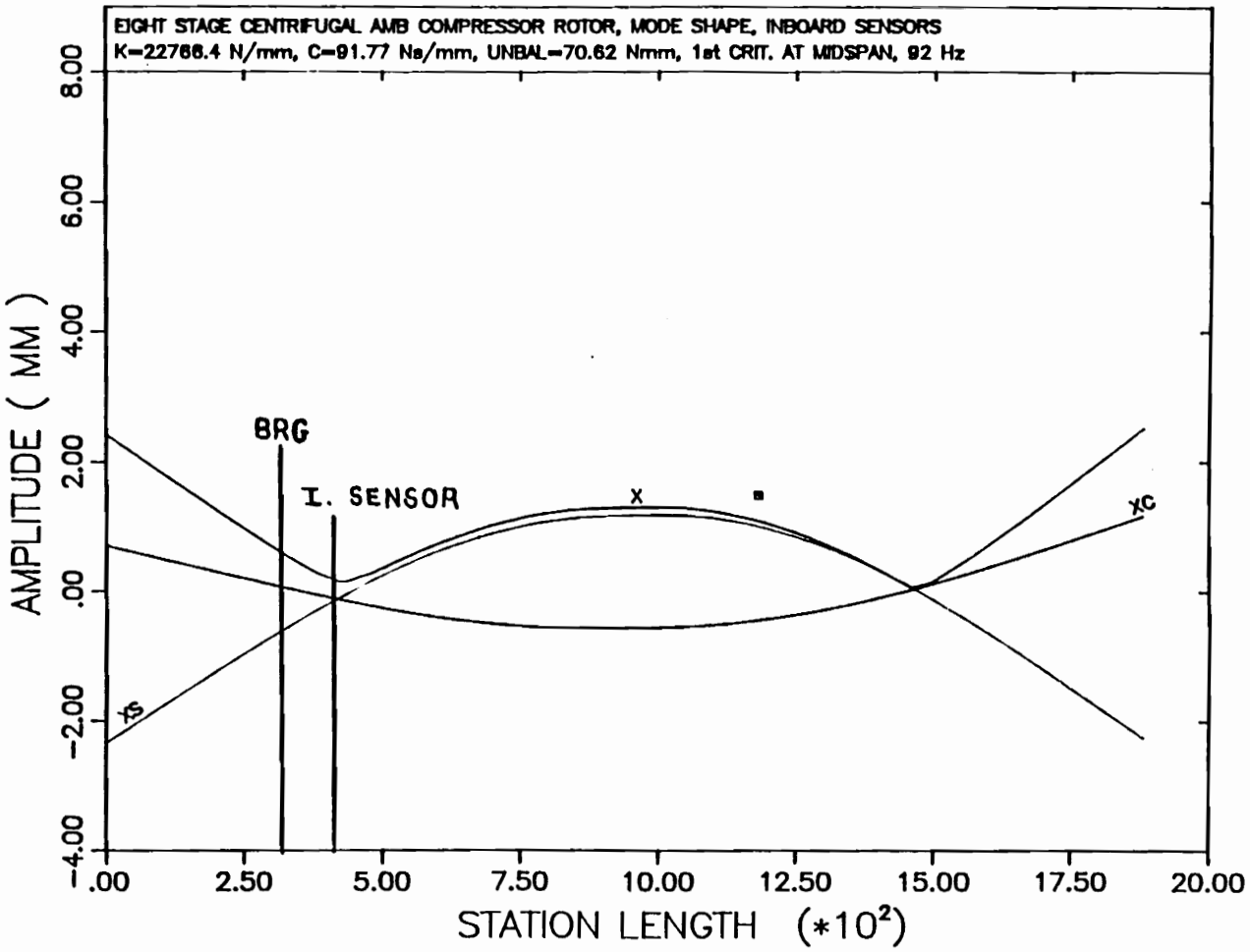

Figure 51.

Sensor Influence on Mode Shapes, Eight-Stage Compressor Rotor, Unbalance Excitation, First Mode

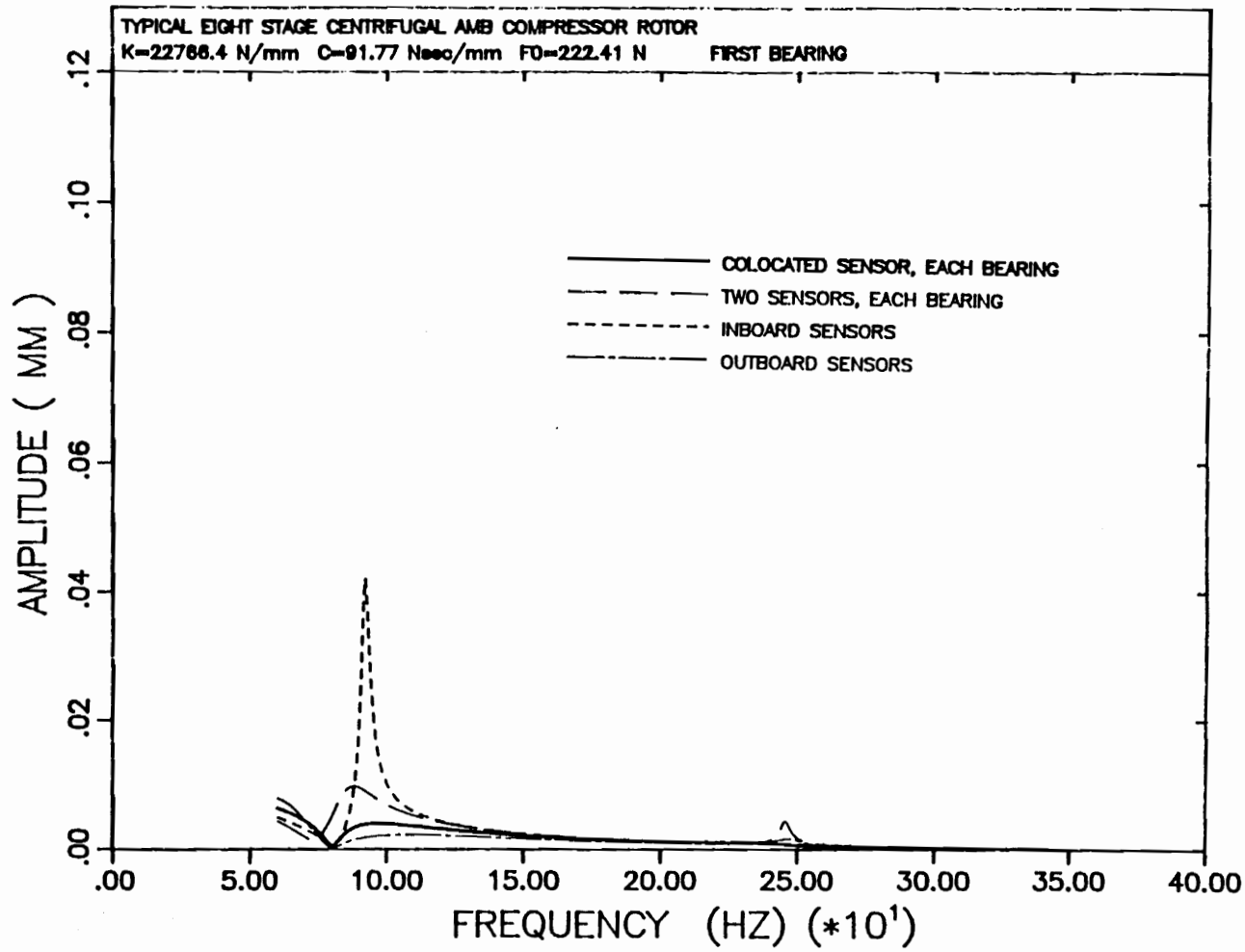

Figure 52.
Sensor Influence on Amplitude, Eight-Stage Compressor Rotor, Planar Excitation, First bearing

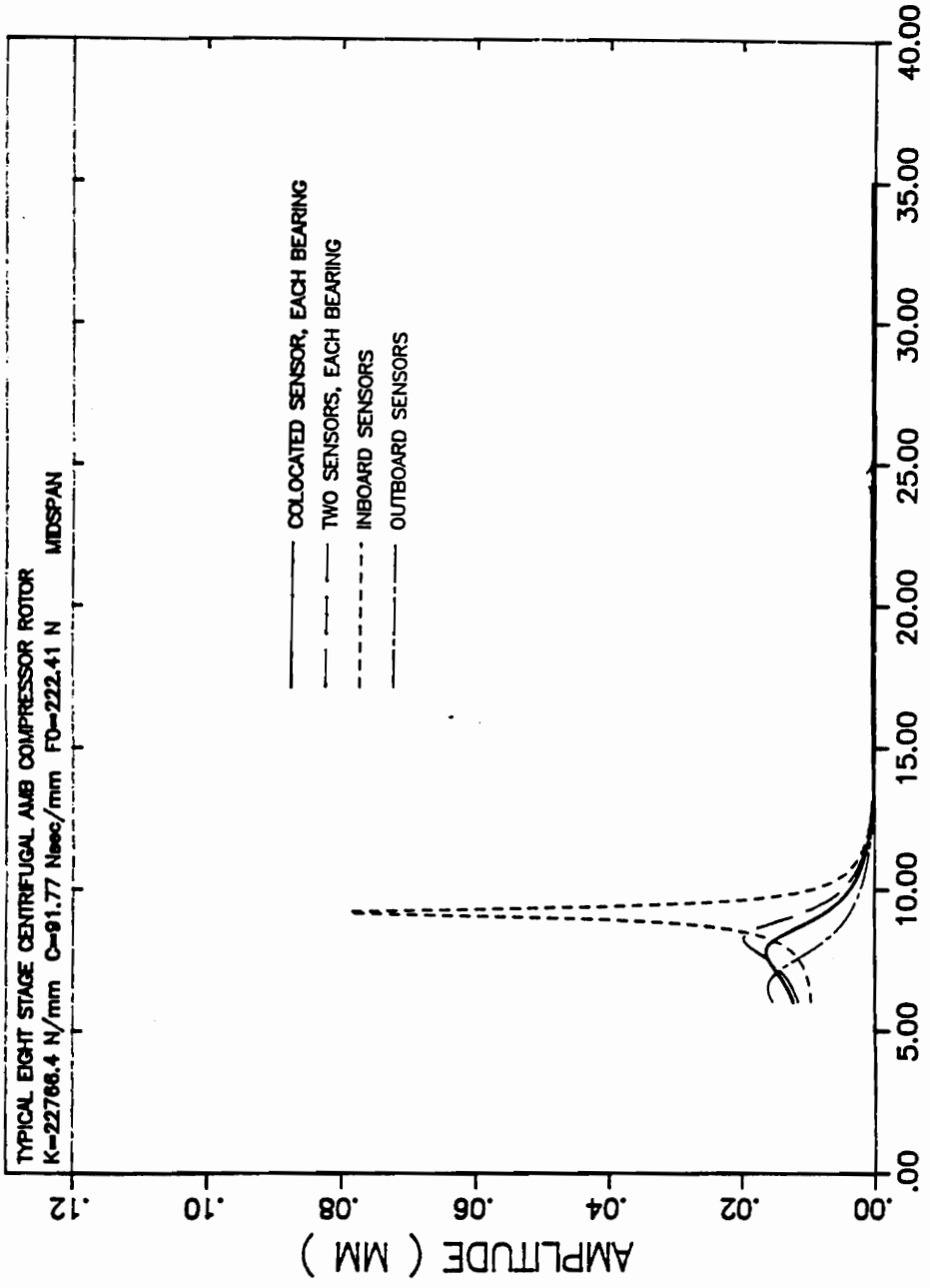

Figure 53.
Sensor Influence on Amplitude, Eight-Stage Compressor Rotor, Planar Excitation, Midspan

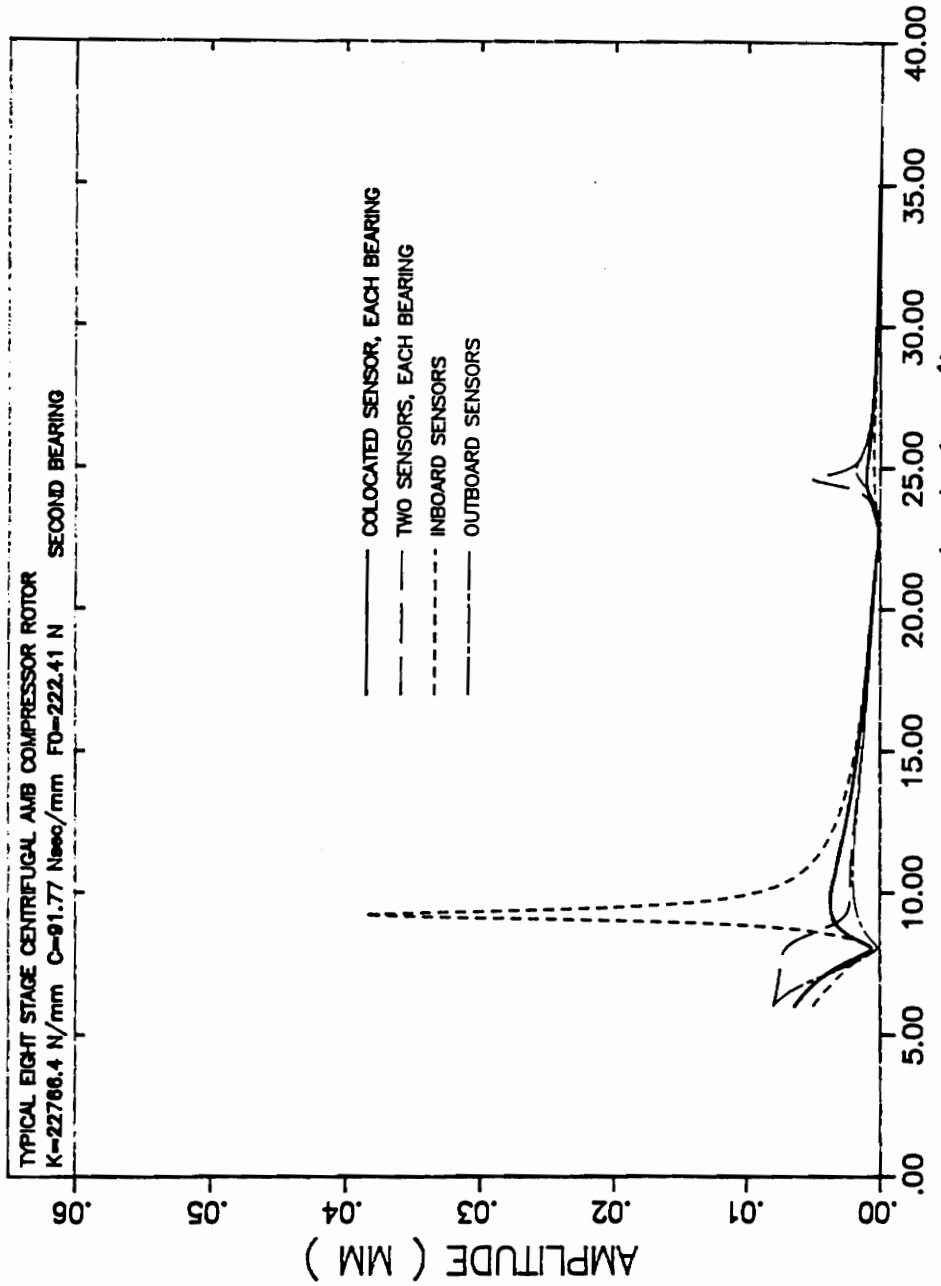

Figure 54.
Sensor Influence on Amplitude, Eight-Stage Compressor Rotor, Planar Excitation, Second bearing

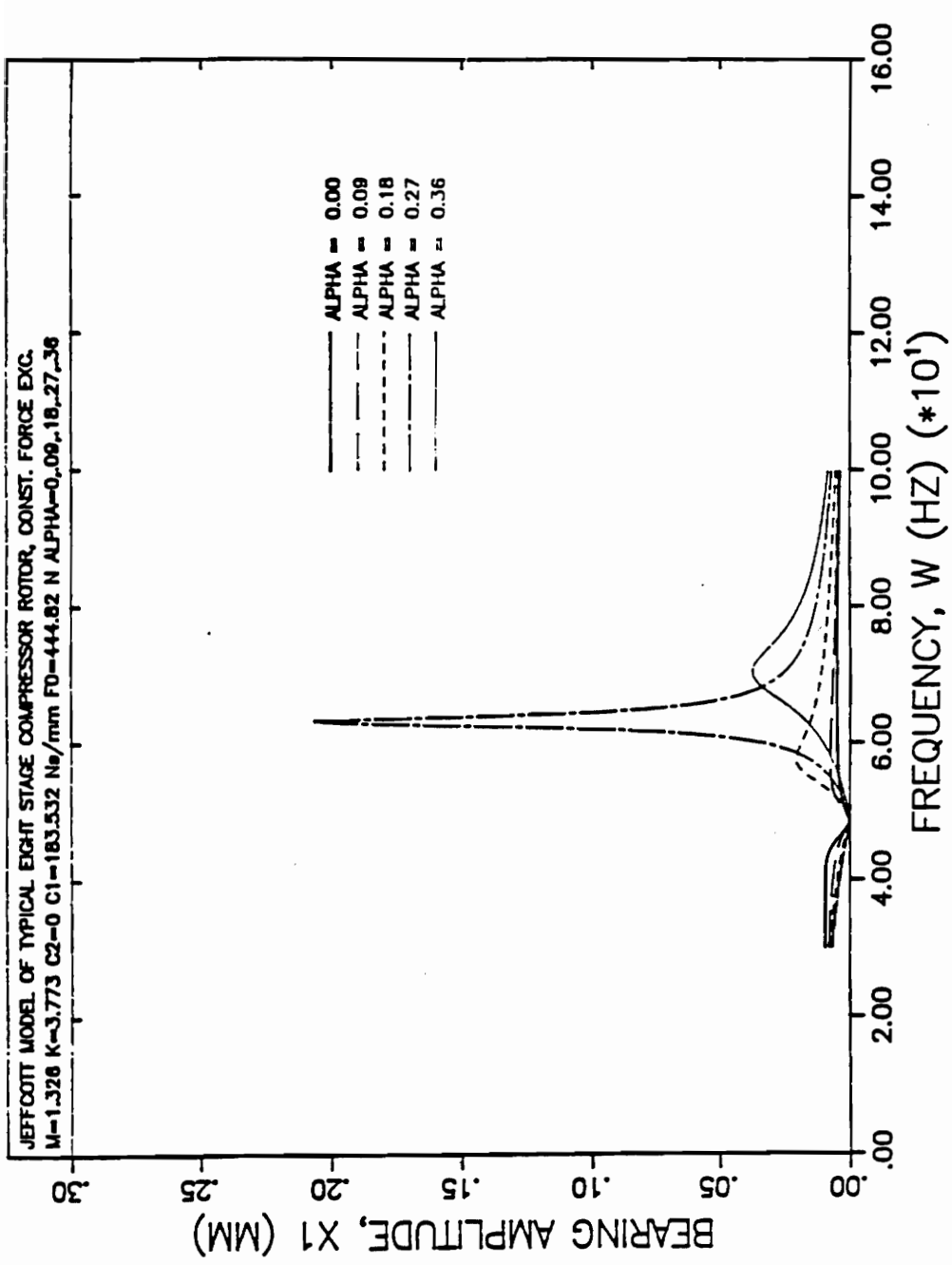

Figure 55.
Jeffcott Approximation of the Light-Stage Compressor Rotor, Planar Excitation, M = 1.326, K = 3.773, Bearing

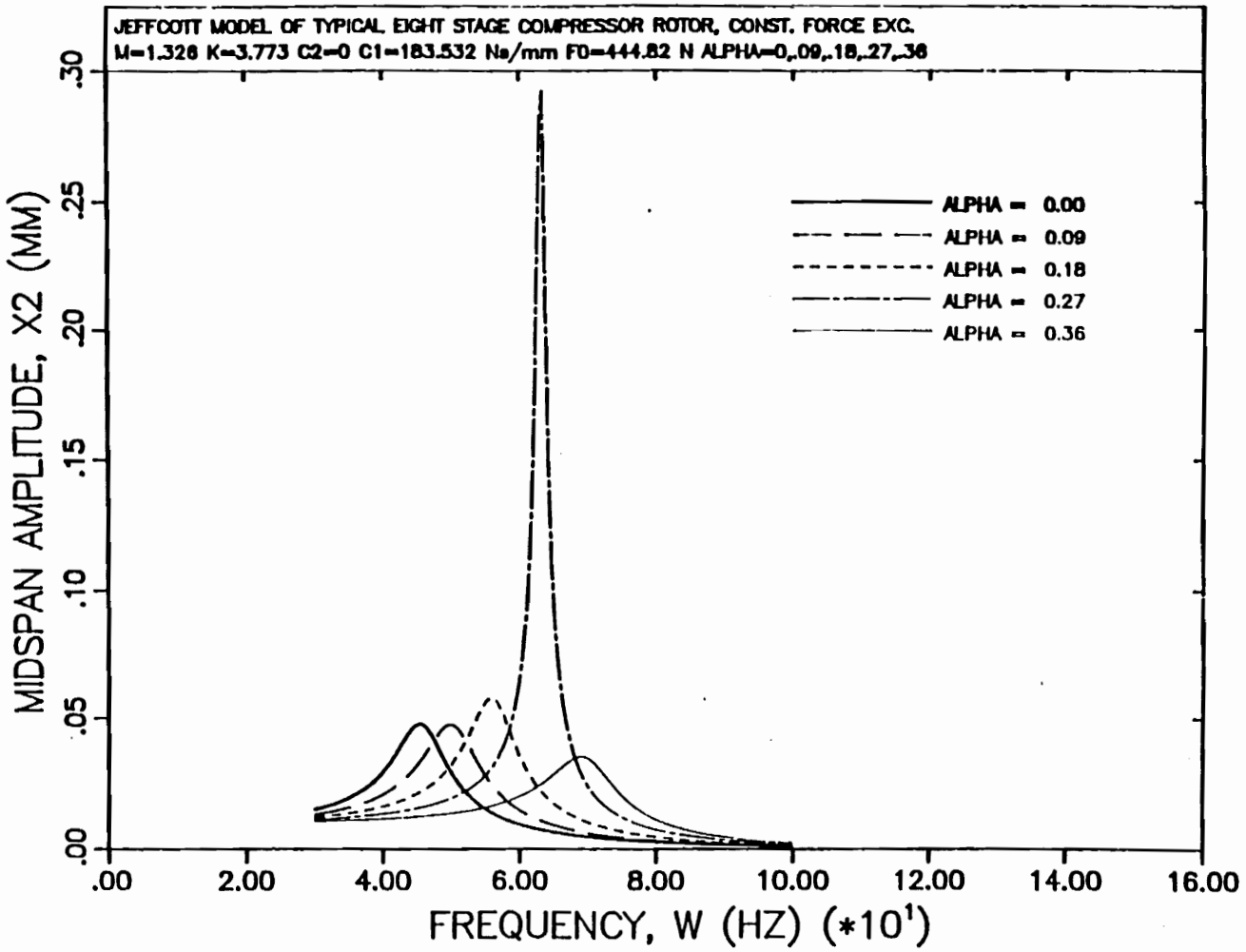

Figure 56.
Jeffcott Approximation of the Eight-Stage Compressor Rotor, Planar Excitation, M = 1.326, K = 3.773, Midspan

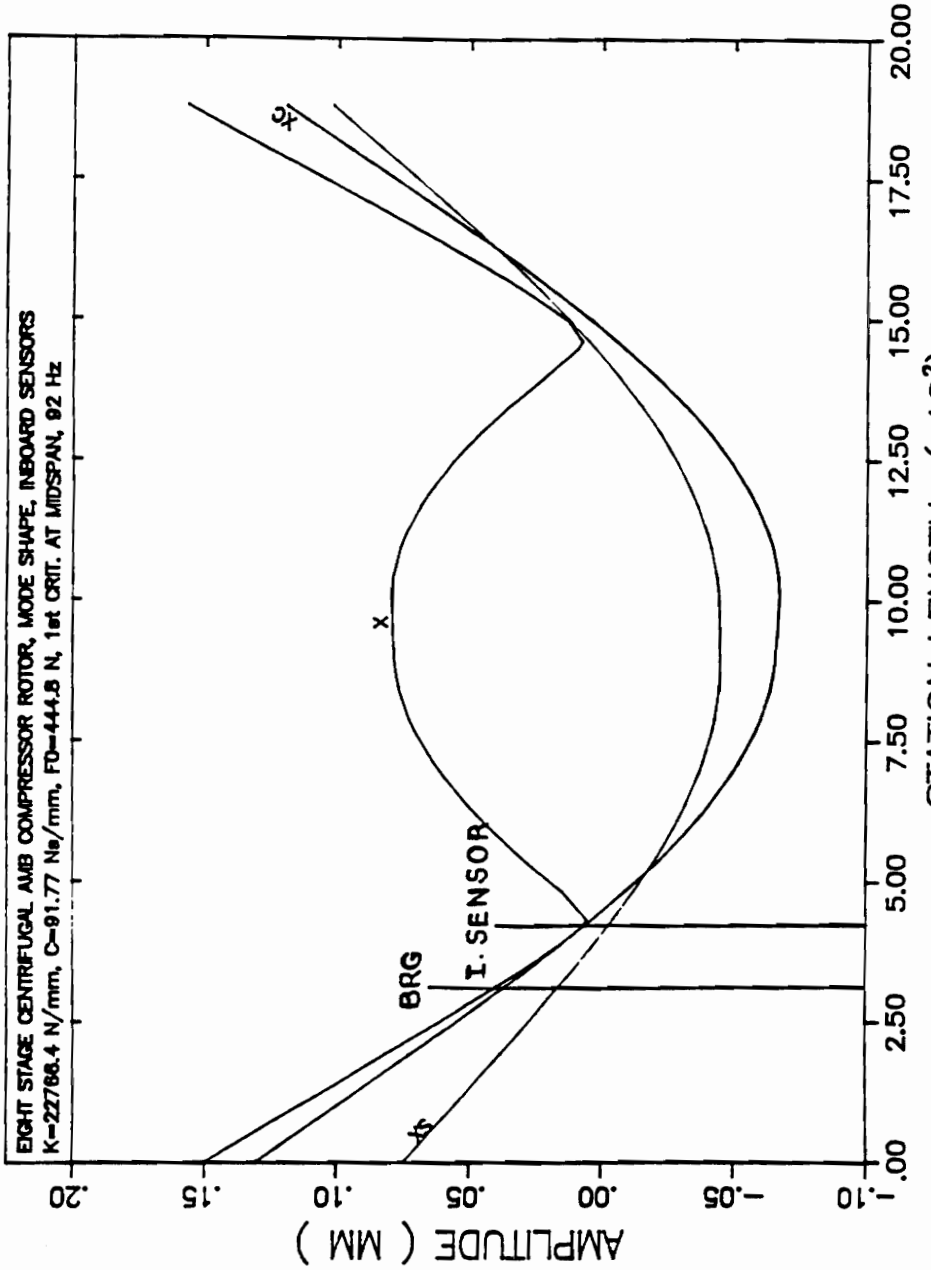

Figure 57.
Sensor Influence on Mode Shapes, Eight-Stage Compressor Rotor, Planar Excitation, First Mode

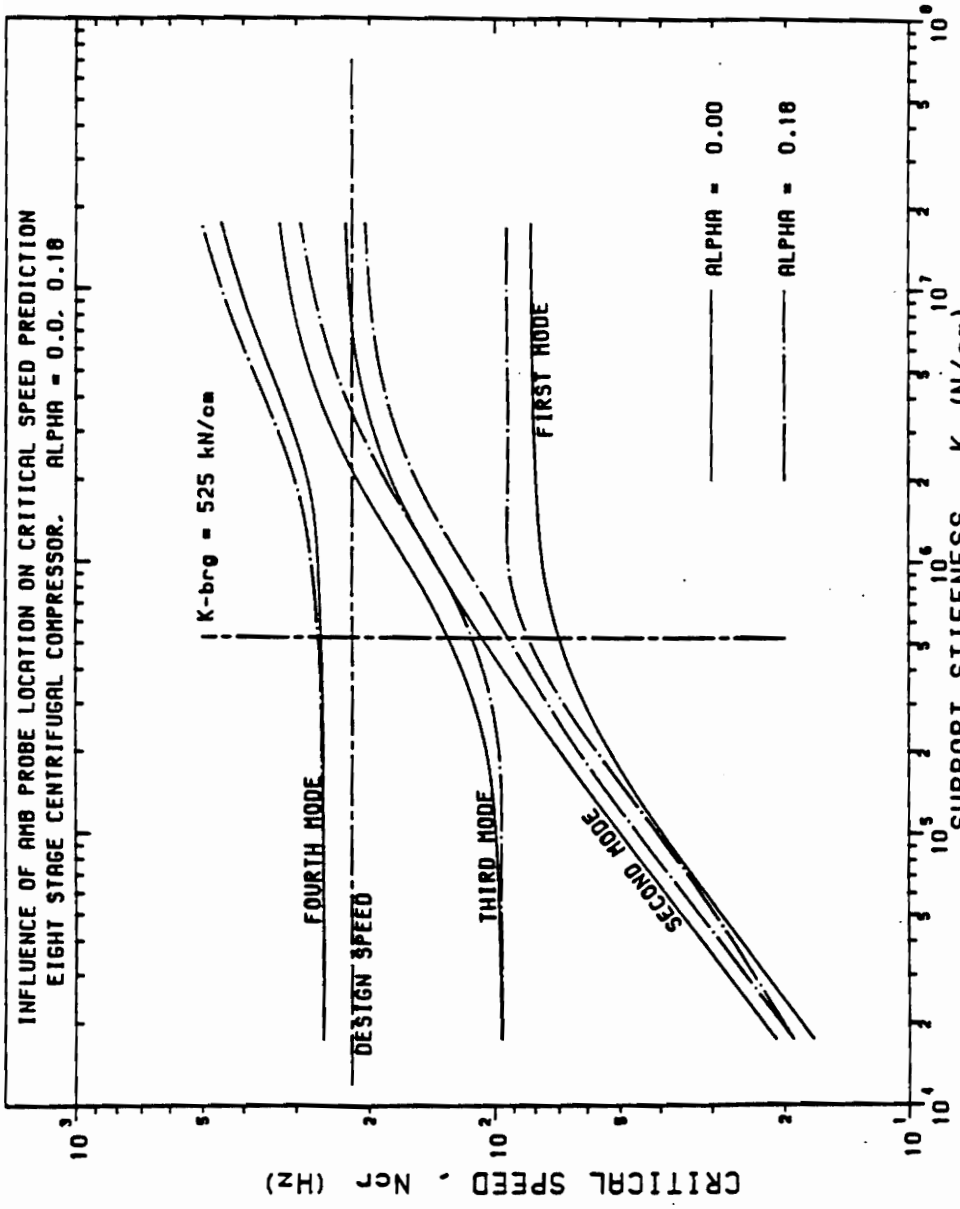

Figure 58.
Influence of Sensor Location on Undamped Critical Speeds for First Four Modes, Eight-Stage Compressor Rotor (Keesee, 1989)

Chapter 4

CONCLUSIONS AND RECOMMENDATIONS

The modification of the rotor dynamics codes to account for sensor non-colocation show a definite change in the vibrational characteristics when the sensors are moved away from the bearing location. The following conclusions can be drawn from this research.

1. The first mode critical frequency increases as the sensor is moved from the outboard location in the direction of the inboard location. This is due to the fact that for the first mode, in most rotor systems the sensors sense a greater deflection as they move inboard and away from the bearing location. This increases the effective stiffness of the active magnetic bearing and results in higher critical frequencies. Because of this effect, it is possible to bypass the first critical by using the inboard sensors while starting the rotor and by using the outboard sensors when the rotational frequency nears the first critical. This is suggested by Keesee (1989). The higher critical frequencies can be handled similarly. Third mode critical frequencies decrease as the sensor is moved from the outboard location towards the inboard location. The amplitude at first critical frequency decreases

as the sensor is moved from the outboard location towards the inboard location. The amplitude at the third critical frequency increases as the sensor is moved from the outboard location towards the inboard location until it reaches a peak for some particular inboard sensor location, after which the amplitude decreases as the sensor is moved further inboard.

2. For specific values of bearing damping amplification factor, mass ratio and stiffness ratio, the first mode transforms into the third mode after going through a transition stage as the sensors are moved from the outboard to the inboard location. For such cases, the first and third critical frequencies coincide at some particular inboard sensor location and large amplitudes are observed when the sensor is placed at or near this particular inboard sensor location. For a rotor system with low amplification factor and high mass ratio, this particular inboard sensor location moves nearer to the bearing location and therefore if the sensors are placed inboard in such a rotor system very large amplitudes would result leading to damage of the rotor system. It would be advisable in such cases to locate the sensors in the outboard position. This phenomena is further aggravated if the stiffness ratio of the rotor system is high since it leads to increased sensitivity of the critical frequencies and amplitudes of the rotor system with regard to changes in the sensor location. It is to be noted that the terms stiffness ratio and mass ratio have meaning only when referred to in the context of an equivalent two-mass model.

3. The results indicate a fairly close agreement between the Jeffcott model and the transfer matrix model. The comparison indicates greater differences in amplitude values compared to critical frequency values and greater deviation in phase angle values compared to amplitude values. Percentage differences between the results of the modified Jeffcott method and the modified transfer matrix method are given in Tables 3 to 6.

4. The behavior of the rotor system, with respect to changes in sensor location, does not indicate any significant deviation when a constant force excitation is used instead of an unbalance force excitation.

The following recommendations can be made for future work in this area:

1. This research assumes that the relationship between the forces applied at the bearing and the shaft deflection sensed by the sensor is linear *i.e.,* the bearing stiffness and damping values are only a function of shaft excitation frequency. However when an active control system is used, it may be essential or advantageous on occasion to control the bearing stiffness and damping as a function of both, the excitation frequency as well as the shaft deflection detected by the sensor. Research needs to be done to understand rotor system behaviour under such circumstances.

2. The stability characteristics of rotor systems with active magnetic bearings need to be studied when the sensor location is changed along the longitudinal axis of the rotor shaft.

3. Only the first and third modes have been studied for the effect of sensor non-colocation on the forced response characteristics of rotors with active magnetic bearings. The effect of sensor non-colocation on other modes of vibration should be studied.

4. The unbalance force has never been considered at a location other than midspan. The effect of placing an unbalance at different locations along the rotor longitudinal axis should be studied. The effect of more than one unbalance should be considered.

5. The existing transfer matrix code can only handle circular synchronous rotation of the rotor system. The solution technique used in this code to handle sensor non-colocation has been verified with the closed-form Jeffcott model and this solution technique needs to be used in a generalized analysis to predict the forced-response behaviour with elliptical motion of the rotor shaft.

BIBLIOGRAPHY

1. Burrows C. R., and Sahinkaya M. N., Sept. 1988, "Control Strategies for use with Magnetic Bearings," *International Conference on Vibrations in Rotating Machinery, Proc. of the Institution of Mechanical Engineers, pp. 23-32.*

2. Hendrickson T. A., Leonard J. S., and Weise D. A., May 1987, "Application of Active Magnetic Bearing Technology for Vibration Free Rotating Machinery," *Naval Engineers Journal, Vol. 99, No. 3, pp. 107-111.*

3. Hustak J., Kirk R.G., and Schoeneck K. A., Jun. 1985, "Active Magnetic Bearings for Optimum Turbomachinery Design," *Instability in Rotating Machinery, NASA Conference Publication 2409, pp. 327-336.*

4. Jeffcott H. H., Mar. 1919, "The Lateral Vibrations of Loaded Shafts in the Neighborhood of a Whirling Speed ... The Effect of Want of Balance," *Phil. Mag. Series 6, Vol. 37, pp. 304-314.*

5. Keesee J. M., Jun. 1989, "Influence of Active Magnetic Bearing Sensor Location on the Calculated Critical Speeds of Turbomachinery," *Masters Thesis, Department of Me-*

chanical Engineering, Virginia Polytechnic Institute and State University, Blacksburg, Virginia.

6. Kirk R. G., and Hustak J. F., and Schoeneck K. A., Sept. 1988, "Analysis and Test Results of two Centrifugal Compressors using Active Magnetic Bearings," *International Conference on Vibrations in Rotating Machinery, Proc. of the Institution of Mechanical Engineers, pp. 93-100.*

7. Lund J. W., May 1965, "Rotor-Bearing Dynamics Design Technology, Part V: Computer Program Manual for Rotor Response and Stability, AFAPL-TR-65-45, Part V, Mech. Tech. Inc.," *Air Force Aero Propulsion Lab., Wright-Patterson Air Force Base, Ohio.*

8. Myklestad N. O., Apr. 1944, "A New Method of Calculation of Natural Modes of Uncoupled Bending Vibration of Airplane Wings and Other Types of Beams," *Journal of Aeronautical Sciences, vol. 11, no. 2, pp. 153-162.*

9. Prohl M. A., Sept. 1945, "A General Method for Calculating Critical Speeds of Flexible Rotors," *Journal of Applied Mechanics, vol. 12, no. 3, pp. 142-148.*

10. Schweitzer G., Jun. 1985, "Magnetic Bearings for Vibration Control," *Instability in Rotating Machinery, NASA Conference Publication 2409, pp. 317-326.*

11. Williams R. D., Keith F. J., and Allaire P.E., Feb. 1990, "Digital control of Active Magnetic Bearings," *IEEE Transactions on Industrial Electronics,* Vol. 37, No. 1., pp. 19-27.

12. Zlotykamien H., Sept. 1988, "The Active Magnetic Bearing enables Optimum Control of Machine Vibrations," *International Conference on Vibrations in Rotating Machinery, Proc. of the Institution of Mechanical Engineers, pp. 41-52.*

Appendix A. DATA FOR THE TWO MASS JEFFCOTT MODEL IN SI UNITS

SYNCHRONOUS UNBALANCE RESPONSE OF A FLEXIBLE ROTOR.
SYMMETRIC BEARINGS AND SUPPORTS, CIRCULAR ORBITS

EXAMPLE TWO MASS ROTOR
STIFFNESS = 763.36 N/mm DAMPING = 0.132 Nsec/mm

STATIONS	NO.BRGS.	NO.UNBAL.	NO.FORCES	PED.FLEX.	BRG MOMENTAL		PLOT STNS
29	2	0	2	0	0	1	3

ROTOR DATA

STATION	WEIGHT	LENGTH	SHAFT DIAMETER		POLAR MOM.	TRANS. MOM.	EX10-6	GX10-6	DENSITY
	N	MM.	OUTSIDE	INSIDE	N-MM**2	N-MM**2	N/MM**2	N/MM**2	N/MM**3
1	.000	25.400	25.400	.000	.000	.1676E-01	.199	.077	.277E-07
2	.000	31.750	25.400	.000	.000	.4444E-01	.199	.077	.277E-07
3	.000	15.875	25.400	.000	.000	.3451E-01	.199	.077	.277E-07
4	.000	15.875	25.400	.000	.000	.1365E-01	.199	.077	.277E-07
5	44.498	15.875	25.400	.000	.000	.1365E-01	.199	.077	.277E-07
6	.000	15.875	25.400	.000	.000	.1365E-01	.199	.077	.277E-07
7	.000	31.750	25.400	.000	.000	.3451E-01	.199	.077	.277E-07
8	.000	38.100	25.400	.000	.000	.7078E-01	.199	.077	.277E-07
9	.000	25.400	25.400	.000	.000	.5985E-01	.199	.077	.277E-07
10	.000	25.400	25.400	.000	.000	.3352E-01	.199	.077	.277E-07
11	.000	25.400	25.400	.000	.000	.3352E-01	.199	.077	.277E-07
12	.000	25.400	25.400	.000	.000	.3352E-01	.199	.077	.277E-07
13	.001	76.200	25.400	.000	.000	.2969	.199	.077	.277E-07
14	.001	38.100	25.400	.000	.000	.3232	.199	.077	.277E-07
15	88.996	38.100	25.400	.000	.000	.8619E-01	.199	.077	.277E-07
16	.001	76.200	25.400	.000	.000	.3232	.199	.077	.277E-07
17	.001	25.400	25.400	.000	.000	.2969	.199	.077	.277E-07
18	.000	25.400	25.400	.000	.000	.3352E-01	.199	.077	.277E-07
19	.000	25.400	25.400	.000	.000	.3352E-01	.199	.077	.277E-07
20	.000	25.400	25.400	.000	.000	.3352E-01	.199	.077	.277E-07
21	.000	38.100	25.400	.000	.000	.5985E-01	.199	.077	.277E-07
22	.000	31.750	25.400	.000	.000	.7078E-01	.199	.077	.277E-07
23	.000	15.875	25.400	.000	.000	.3451E-01	.199	.077	.277E-07
24	.000	15.875	25.400	.000	.000	.1365E-01	.199	.077	.277E-07
25	44.498	15.875	25.400	.000	.000	.1365E-01	.199	.077	.277E-07
26	.000	15.875	25.400	.000	.000	.1365E-01	.199	.077	.277E-07
27	.000	31.750	25.400	.000	.000	.3451E-01	.199	.077	.277E-07
28	.000	25.400	25.400	.000	.000	.4444E-01	.199	.077	.277E-07
29	.000	.000	25.400	.000	.000	.1676E-01	.199	.077	.277E-07
	177.993	812.800							

MASS CENTER 406.40 MM. FROM LEFT END; TOTAL IP .0000 N-MM**2; TOTAL IT .897E+07 N-MM**2

BEARING STATIONS
5 25

BEARING AT STATION NO. 5

KXX	CXX
763.364	.131601

BEARING AT STATION NO. 25

KXX	CXX
763.364	.131601

Appendix B. DATA FOR THE TWO MASS JEFFCOTT MODEL IN ENGLISH UNITS

SYNCHRONOUS UNBALANCE RESPONSE OF A FLEXIBLE ROTOR.
SYMMETRIC BEARINGS AND SUPPORTS, CIRCULAR ORBITS

EXAMPLE TWO MASS ROTOR
STIFFNESS = 4359.14 LB/IN DAMPING = 0.752 LB.SEC/IN

STATIONS	NO.BRGS.	NO.UNBAL.	NO.FORCES	PED.FLEX.	BRG MOMENTAL	NUMERICAL	PLOT STNS
29	2	0	2	0	0	1	3

ROTOR DATA

STATION	WEIGHT	LENGTH	SHAFT DIAMETER		POLAR MOM.	TRANS. MOM.	EX10-6	GX10-6	DENSITY
	LB	IN.	OUTSIDE	INSIDE	LB-IN**2	LB-IN**2	LB/IN**2	LB/IN**2	LB/IN**3
1	.000	1.000	1.000	.000	.000	.5727E-04	28.900	11.100	.100E-02
2	.001	1.250	1.000	.000	.000	.1519E-03	28.900	11.100	.100E-02
3	.001	.625	1.000	.000	.000	.1179E-03	28.900	11.100	.100E-02
4	.001	.625	1.000	.000	.000	.1179E-03	28.900	11.100	.100E-02
5	10.000	.625	1.000	.000	.000	.1179E-03	28.900	11.100	.100E-02
6	.001	.625	1.000	.000	.000	.1179E-03	28.900	11.100	.100E-02
7	.001	1.250	1.000	.000	.000	.1179E-03	28.900	11.100	.100E-02
8	.001	1.500	1.000	.000	.000	.2419E-03	28.900	11.100	.100E-02
9	.001	1.000	1.000	.000	.000	.2045E-03	28.900	11.100	.100E-02
10	.001	1.000	1.000	.000	.000	.2045E-03	28.900	11.100	.100E-02
11	.001	1.000	1.000	.000	.000	.2045E-03	28.900	11.100	.100E-02
12	.001	1.000	1.000	.000	.000	.2045E-03	28.900	11.100	.100E-02
13	.002	3.000	1.000	.000	.000	.1014E-02	28.900	11.100	.100E-02
14	.002	1.500	1.000	.000	.000	.1104E-02	28.900	11.100	.100E-02
15	20.001	1.500	1.000	.000	.000	.2945E-03	28.900	11.100	.100E-02
16	.002	3.000	1.000	.000	.000	.1014E-02	28.900	11.100	.100E-02
17	.002	1.000	1.000	.000	.000	.1014E-02	28.900	11.100	.100E-02
18	.001	1.000	1.000	.000	.000	.1145E-03	28.900	11.100	.100E-02
19	.001	1.000	1.000	.000	.000	.1145E-03	28.900	11.100	.100E-02
20	.001	1.000	1.000	.000	.000	.1145E-03	28.900	11.100	.100E-02
21	.001	1.500	1.000	.000	.000	.2045E-03	28.900	11.100	.100E-02
22	.001	1.250	1.000	.000	.000	.2419E-03	28.900	11.100	.100E-02
23	.001	.625	1.000	.000	.000	.1179E-03	28.900	11.100	.100E-02
24	.000	.625	1.000	.000	.000	.4666E-04	28.900	11.100	.100E-02
25	10.000	.625	1.000	.000	.000	.4666E-04	28.900	11.100	.100E-02
26	.000	.625	1.000	.000	.000	.4666E-04	28.900	11.100	.100E-02
27	.001	1.250	1.000	.000	.000	.1179E-03	28.900	11.100	.100E-02
28	.001	1.000	1.000	.000	.000	.1519E-03	28.900	11.100	.100E-02
29	.000	.000	1.000	.000	.000	.5727E-04	28.900	11.100	.100E-02
	40.025	32.000							

MASS CENTER 16.00 IN. FROM LEFT END; TOTAL IP .0000 LB-IN**2; TOTAL IT .313E+04 LB-IN**2

BEARING STATIONS
5 25

BEARING AT STATION NO. 5

KXX	CXX
4359.14	.751500

BEARING AT STATION NO. 25

KXX	CXX
4359.14	.751500

Appendix C. DATA FOR EIGHT STAGE CENTRIFUGAL COMPRESSOR ROTOR IN SI UNITS

VPI&SU --- --ROTOR DYNAMICS ANALYSIS
CRITICAL SPEEDS OF A FLEXIBLE ROTOR

TWO BEARING CENTRIFUGAL COMPRESSOR
ACTIVE MAGNETIC BEARING SUPPORTS
SENSORS AT BEARING CENTER (4-20-89)

CRTSPD1 - MODAL ANALYSIS VERSION 12/1/76

N = 60 STATIONS NB = 2 BEARINGS NSK= 6 STIFFNESS VALUES NGYR = 0 MASS = 0 DSP= 100.00

STA. NO	Z (CM)	WEIGHT (N)	LENGTH (CM)	WEIGHT OD (CM)	WEIGHT ID (CM)	STIFF. LT (CM)	STIFF. OD (CM)	STIFF. ID (CM)	I (CM**4)	POLAR MOM. (N-CM**2)	TRANS MOM. (N-CM**2)	E * 10-6 (N/CM^2)	DENSITY (N/CM^3)	EXT WGT (N)	G*10-6 (N/CM^2)
1	.000	6.06	2.540	8.890	.000	2.540	8.890	.000	306.6	59.8	23.4	20.34	.077	.00	7.929
2	2.540	18.17	5.080	8.890	.000	5.080	8.890	.000	306.6	179.5	31.1	20.34	.077	.00	7.929
3	7.620	61.54	2.540	25.400	.000	2.540	11.430	.000	837.8	4106.1	1947.8	20.34	.077	.00	7.929
4	10.160	67.60	7.620	8.890	.000	7.620	8.890	.000	306.6	4165.9	1854.0	20.34	.077	.00	7.929
5	17.780	30.28	1.270	17.780	.000	1.270	10.160	.000	523.1	658.0	150.0	20.34	.077	.00	7.929
6	19.050	48.44	3.810	17.780	.000	3.810	10.160	.000	523.1	1914.3	866.0	20.34	.077	.00	7.929
7	22.860	84.78	5.080	17.780	.000	5.080	10.160	.000	523.1	3350.0	1378.8	20.34	.077	.00	7.929
8	27.940	72.67	2.540	17.780	.000	2.540	10.160	.000	523.1	2871.5	1201.3	20.34	.077	.00	7.929
9	30.480	48.44	2.540	17.780	.000	2.540	10.160	.000	523.1	1914.3	905.1	20.34	.077	.00	7.929
10	33.020	72.67	5.080	17.780	.000	5.080	10.160	.000	523.1	2871.5	1201.3	20.34	.077	.00	7.929
11	38.100	84.78	3.810	17.780	.000	3.810	10.160	.000	523.1	3350.0	1378.8	20.34	.077	.00	7.929
12	41.910	48.44	1.270	17.780	.000	1.270	10.160	.000	523.1	1914.3	866.0	20.34	.077	.00	7.929
13	43.180	27.93	5.080	10.160	.000	5.080	10.160	.000	523.1	682.7	270.0	20.34	.077	.00	7.929
14	48.260	31.64	5.080	10.160	.000	5.080	10.160	.000	523.1	408.2	68.0	20.34	.077	.00	7.929
15	53.340	31.64	5.080	10.160	.000	5.080	10.160	.000	523.1	408.2	68.0	20.34	.077	.00	7.929
16	58.420	23.73	2.540	10.160	.000	2.540	10.160	.000	523.1	306.2	76.5	20.34	.077	.00	7.929
17	60.960	12.36	.635	15.240	.000	.635	12.700	.000	1277.0	231.2	106.8	20.34	.077	.00	7.929
18	61.595	57.84	1.905	30.480	.000	1.905	12.700	.000	1277.0	6328.9	3131.9	20.34	.077	.00	7.929
19	63.500	69.21	5.080	10.160	.000	5.080	10.160	.000	523.1	6403.9	3101.6	20.34	.077	.00	7.929
20	68.580	20.27	.635	15.240	.000	.635	12.700	.000	1277.0	333.3	98.3	20.34	.077	.00	7.929

21	69.215	57.84	1.905	30.480	.000	1.905	12.700	.000	1277.0	6328.9	3131.9	20.34	.077	.00	7.929
22	71.120	69.21	5.080	10.160	.000	5.080	10.160	.000	523.1	6403.9	3101.6	20.34	.077	.00	7.929
23	76.200	20.27	.635	15.240	.000	.635	12.700	.000	1277.0	333.3	98.3	20.34	.077	.00	7.929
24	76.835	57.84	1.905	30.480	.000	1.905	12.700	.000	1277.0	6328.9	3131.9	20.34	.077	.00	7.929
25	78.740	69.21	5.080	10.160	.000	5.080	10.160	.000	523.1	6403.9	3101.6	20.34	.077	.00	7.929
26	83.820	20.27	.635	15.240	.000	.635	12.700	.000	1277.0	333.3	98.3	20.34	.077	.00	7.929
27	84.455	57.84	1.905	30.480	.000	1.905	12.700	.000	1277.0	6328.9	3131.9	20.34	.077	.00	7.929
28	86.360	61.30	2.540	10.160	.000	2.540	10.160	.000	523.1	6301.8	3110.1	20.34	.077	.00	7.929
29	88.900	56.35	5.080	17.780	.000	5.080	17.780	.000	4905.6	2016.4	791.3	20.34	.077	.00	7.929
30	93.980	96.89	5.080	17.780	.000	5.080	17.780	.000	4905.6	3828.6	1497.6	20.34	.077	.00	7.929
31	99.060	56.35	2.540	10.160	.000	2.540	10.160	.000	523.1	2016.4	791.3	20.34	.077	.00	7.929
32	101.600	61.30	1.905	30.480	.000	1.905	12.700	.000	1277.0	6301.8	3110.1	20.34	.077	.00	7.929
33	103.505	57.84	.635	15.240	.000	.635	12.700	.000	1277.0	6328.9	3131.9	20.34	.077	.00	7.929
34	104.140	20.27	5.080	10.160	.000	5.080	10.160	.000	523.1	333.3	98.3	20.34	.077	.00	7.929
35	109.220	69.21	1.905	30.480	.000	1.905	12.700	.000	1277.0	6403.9	3101.6	20.34	.077	.00	7.929
36	111.125	57.84	.635	15.240	.000	.635	12.700	.000	1277.0	6328.9	3131.9	20.34	.077	.00	7.929
37	111.760	20.27	5.080	10.160	.000	5.080	10.160	.000	523.1	333.3	98.3	20.34	.077	.00	7.929
38	116.840	69.21	1.905	30.480	.000	1.905	12.700	.000	1277.0	6403.9	3101.6	20.34	.077	.00	7.929
39	118.745	57.84	.635	15.240	.000	.635	12.700	.000	1277.0	6328.9	3131.9	20.34	.077	.00	7.929
40	119.380	20.27	5.080	10.160	.000	5.080	10.160	.000	523.1	333.3	98.3	20.34	.077	.00	7.929
41	124.460	69.21	1.905	30.480	.000	1.905	12.700	.000	1277.0	6403.9	3101.6	20.34	.077	.00	7.929
42	126.365	57.84	.635	15.240	.000	.635	12.700	.000	1277.0	6328.9	3131.9	20.34	.077	.00	7.929
43	127.000	12.36	2.540	10.160	.000	2.540	10.160	.000	523.1	231.2	106.8	20.34	.077	.00	7.929
44	129.540	23.73	5.080	10.160	.000	5.080	10.160	.000	523.1	306.2	76.5	20.34	.077	.00	7.929
45	134.620	31.64	5.080	10.160	.000	5.080	10.160	.000	523.1	408.2	68.0	20.34	.077	.00	7.929
46	139.700	31.64	5.080	10.160	.000	5.080	10.160	.000	523.1	408.2	68.0	20.34	.077	.00	7.929
47	144.780	27.93	1.270	17.780	.000	1.270	10.160	.000	523.1	682.7	270.0	20.34	.077	.00	7.929
48	146.050	48.44	3.810	17.780	.000	3.810	10.160	.000	523.1	1914.3	866.0	20.34	.077	.00	7.929
49	149.860	84.78	5.080	17.780	.000	5.080	10.160	.000	523.1	3350.0	1378.8	20.34	.077	.00	7.929
50	154.940	72.67	2.540	17.780	.000	2.540	10.160	.000	523.1	2871.5	1201.3	20.34	.077	.00	7.929
51	157.480	48.44	2.540	17.780	.000	2.540	10.160	.000	523.1	1914.3	905.1	20.34	.077	.00	7.929
52	160.020	72.67	5.080	17.780	.000	5.080	10.160	.000	523.1	2871.5	1201.3	20.34	.077	.00	7.929
53	165.100	84.78	3.810	17.780	.000	3.810	10.160	.000	523.1	3350.0	1378.8	20.34	.077	.00	7.929
54	168.910	48.44	1.270	17.780	.000	1.270	10.160	.000	523.1	1914.3	866.0	20.34	.077	.00	7.929
55	170.180	27.93	5.080	10.160	.000	5.080	10.160	.000	523.1	682.7	270.0	20.34	.077	.00	7.929
56	175.260	23.73	2.540	10.160	.000	2.540	10.160	.000	523.1	306.2	76.5	20.34	.077	.00	7.929
57	177.800	25.70	2.540	15.240	.000	2.540	15.240	.000	2647.9	618.7	281.7	20.34	.077	.00	7.929
58	180.340	53.39	5.080	15.240	.000	5.080	15.240	.000	2647.9	1549.9	602.8	20.34	.077	.00	7.929
59	185.420	85.02	2.540	25.400	.000	2.540	17.780	.000	4905.6	5019.8	2303.6	20.34	.077	.00	7.929
60	187.960	49.53	.003	25.400	.000	.003	17.780	.000	4905.6	3990.5	1942.1	20.34	.077	.00	7.929

		2955.66													

```
TOTAL ROTOR ASSEMBLY C.G. =  96.60 CENTIMETERS FROM STA. 1.


BEARING REACTION AT STA.   9 =  1416.94 N
BEARING REACTION AT STA.  51 =  1538.72 N


        BEARING STATIONS     9    51
        BEARING  1, SENSOR AT STA.    6   12
        BEARING  2, SENSOR AT STA.   48   54
```

Appendix D. DATA FOR EIGHT STAGE CENTRIFUGAL COMPRESSOR ROTOR IN ENGLISH UNITS

VPI&SU ---- ROTOR DYNAMICS ANALYSIS
CRITICAL SPEEDS OF A FLEXIBLE ROTOR

TWO BEARING CENTRIFUGAL COMPRESSOR
ACTIVE MAGNETIC BEARING SUPPORTS
TWO SENSORS PER BEARING (4-20-89)

CRTSPD1 - MODAL ANALYSIS VERSION 12/1/76

N = 60 STATIONS NB = 2 BEARINGS NSK= 6 STIFFNESS VALUES NGYR = 0 MASS = 0 DSP= 100.00

STA. NO	Z (IN)	WEIGHT (LB)	LENGTH (IN)	WEIGHT OD (IN)	WEIGHT ID (IN)	STIFF. LT (IN)	STIFF. OD (IN)	STIFF. ID (IN)	I (IN**4)	POLAR MOM. (LB-IN**2)	TRANS MOM. (LB-IN**2)	E * 10-6 (LB/IN 2)	DENSITY (LB/IN 3)	EXT WGT (LB)	G*10-6 (LB/IN 2)
1	.000	1.36	1.000	3.500	.000	1.000	3.500	.000	7.4	2.1	.8	29.50	.283	.00	11.500
2	1.000	4.08	2.000	3.500	.000	2.000	3.500	.000	7.4	6.3	1.1	29.50	.283	.00	11.500
3	3.000	13.84	1.000	10.000	.000	1.000	4.500	.000	20.1	143.1	67.9	29.50	.283	.00	11.500
4	4.000	15.20	3.000	3.500	.000	3.000	3.500	.000	7.4	145.2	64.6	29.50	.283	.00	11.500
5	7.000	6.81	.500	7.000	.000	.500	4.000	.000	12.6	22.9	5.2	29.50	.283	.00	11.500
6	7.500	10.89	1.500	7.000	.000	1.500	4.000	.000	12.6	66.7	30.2	29.50	.283	.00	11.500
7	9.000	19.06	2.000	7.000	.000	2.000	4.000	.000	12.6	116.7	48.0	29.50	.283	.00	11.500
8	11.000	16.34	1.000	7.000	.000	1.000	4.000	.000	12.6	100.1	41.9	29.50	.283	.00	11.500
9	12.000	10.89	1.000	7.000	.000	1.000	4.000	.000	12.6	66.7	31.5	29.50	.283	.00	11.500
10	13.000	16.34	2.000	7.000	.000	2.000	4.000	.000	12.6	100.1	41.9	29.50	.283	.00	11.500
11	15.000	19.06	1.500	7.000	.000	1.500	4.000	.000	12.6	116.7	48.0	29.50	.283	.00	11.500
12	16.500	10.89	.500	7.000	.000	.500	4.000	.000	12.6	66.7	30.2	29.50	.283	.00	11.500
13	17.000	6.28	2.000	4.000	.000	2.000	4.000	.000	12.6	23.8	9.4	29.50	.283	.00	11.500
14	19.000	7.11	2.000	4.000	.000	2.000	4.000	.000	12.6	14.2	2.4	29.50	.283	.00	11.500
15	21.000	7.11	2.000	4.000	.000	2.000	4.000	.000	12.6	14.2	2.4	29.50	.283	.00	11.500
16	23.000	5.33	1.000	4.000	.000	1.000	4.000	.000	12.6	10.7	2.7	29.50	.283	.00	11.500
17	24.000	2.78	.250	6.000	.000	.250	5.000	.000	30.7	8.1	3.7	29.50	.283	.00	11.500
18	24.250	13.00	.750	12.000	.000	.750	5.000	.000	30.7	220.5	109.1	29.50	.283	.00	11.500
19	25.000	15.56	2.000	4.000	.000	2.000	4.000	.000	12.6	223.2	108.1	29.50	.283	.00	11.500
20	27.000	4.56	.250	6.000	.000	.250	5.000	.000	30.7	11.6	3.4	29.50	.283	.00	11.500

21	27.250	13.00	.750	12.000	.000	.750	5.000	.000	30.7	220.5	109.1	29.50	.283	.00	11.500
22	28.000	15.56	2.000	4.000	.000	2.000	4.000	.000	12.6	223.2	108.1	29.50	.283	.00	11.500
23	30.000	4.56	.250	6.000	.000	.250	5.000	.000	30.7	11.6	3.4	29.50	.283	.00	11.500
24	30.250	13.00	.750	12.000	.000	.750	5.000	.000	30.7	220.5	109.1	29.50	.283	.00	11.500
25	31.000	15.56	2.000	4.000	.000	2.000	4.000	.000	12.6	223.2	108.1	29.50	.283	.00	11.500
26	33.000	4.56	.250	6.000	.000	.250	5.000	.000	30.7	11.6	3.4	29.50	.283	.00	11.500
27	33.250	13.00	.750	12.000	.000	.750	5.000	.000	30.7	220.5	109.1	29.50	.283	.00	11.500
28	34.000	13.78	1.000	4.000	.000	1.000	4.000	.000	12.6	219.6	108.4	29.50	.283	.00	11.500
29	35.000	12.67	2.000	7.000	.000	2.000	7.000	.000	117.9	70.3	27.6	29.50	.283	.00	11.500
30	37.000	21.78	2.000	7.000	.000	2.000	7.000	.000	117.9	133.4	52.2	29.50	.283	.00	11.500
31	39.000	12.67	1.000	4.000	.000	1.000	4.000	.000	12.6	70.3	27.6	29.50	.283	.00	11.500
32	40.000	13.78	.750	12.000	.000	.750	5.000	.000	30.7	219.6	108.4	29.50	.283	.00	11.500
33	40.750	13.00	.250	6.000	.000	.250	5.000	.000	30.7	220.5	109.1	29.50	.283	.00	11.500
34	41.000	4.56	2.000	4.000	.000	2.000	4.000	.000	12.6	11.6	3.4	29.50	.283	.00	11.500
35	43.000	15.56	.750	12.000	.000	.750	5.000	.000	30.7	223.2	108.1	29.50	.283	.00	11.500
36	43.750	13.00	.250	6.000	.000	.250	5.000	.000	30.7	220.5	109.1	29.50	.283	.00	11.500
37	44.000	4.56	2.000	4.000	.000	2.000	4.000	.000	12.6	11.6	3.4	29.50	.283	.00	11.500
38	46.000	15.56	.750	12.000	.000	.750	5.000	.000	30.7	223.2	108.1	29.50	.283	.00	11.500
39	46.750	13.00	.250	6.000	.000	.250	5.000	.000	30.7	220.5	109.1	29.50	.283	.00	11.500
40	47.000	4.56	2.000	4.000	.000	2.000	4.000	.000	12.6	11.6	3.4	29.50	.283	.00	11.500
41	49.000	15.56	.750	12.000	.000	.750	5.000	.000	30.7	223.2	108.1	29.50	.283	.00	11.500
42	49.750	13.00	.250	6.000	.000	.250	5.000	.000	30.7	220.5	109.1	29.50	.283	.00	11.500
43	50.000	2.78	1.000	4.000	.000	1.000	4.000	.000	12.6	8.1	3.7	29.50	.283	.00	11.500
44	51.000	5.33	2.000	4.000	.000	2.000	4.000	.000	12.6	10.7	2.7	29.50	.283	.00	11.500
45	53.000	7.11	2.000	4.000	.000	2.000	4.000	.000	12.6	14.2	2.4	29.50	.283	.00	11.500
46	55.000	7.11	2.000	4.000	.000	2.000	4.000	.000	12.6	14.2	2.4	29.50	.283	.00	11.500
47	57.000	6.28	.500	7.000	.000	.500	4.000	.000	12.6	23.8	9.4	29.50	.283	.00	11.500
48	57.500	10.89	1.500	7.000	.000	1.500	4.000	.000	12.6	66.7	30.2	29.50	.283	.00	11.500
49	59.000	19.06	2.000	7.000	.000	2.000	4.000	.000	12.6	116.7	48.0	29.50	.283	.00	11.500
50	61.000	16.34	1.000	7.000	.000	1.000	4.000	.000	12.6	100.1	41.9	29.50	.283	.00	11.500
51	62.000	10.89	1.000	7.000	.000	1.000	4.000	.000	12.6	66.7	31.5	29.50	.283	.00	11.500
52	63.000	16.34	2.000	7.000	.000	2.000	4.000	.000	12.6	100.1	41.9	29.50	.283	.00	11.500
53	65.000	19.06	1.500	7.000	.000	1.500	4.000	.000	12.6	116.7	48.0	29.50	.283	.00	11.500
54	66.500	10.89	.500	7.000	.000	.500	4.000	.000	12.6	66.7	30.2	29.50	.283	.00	11.500
55	67.000	6.28	2.000	4.000	.000	2.000	4.000	.000	12.6	23.8	9.4	29.50	.283	.00	11.500
56	69.000	5.33	1.000	4.000	.000	1.000	4.000	.000	12.6	10.7	2.7	29.50	.283	.00	11.500
57	70.000	5.78	1.000	6.000	.000	1.000	6.000	.000	63.6	21.6	9.8	29.50	.283	.00	11.500
58	71.000	12.00	2.000	6.000	.000	2.000	6.000	.000	63.6	54.0	21.0	29.50	.283	.00	11.500
59	73.000	19.12	1.000	10.000	.000	1.000	7.000	.000	117.9	174.9	80.3	29.50	.283	.00	11.500
60	74.000	11.14	.001	10.000	.000	.001	7.000	.000	117.9	139.1	67.7	29.50	.283	.00	11.500

		666.60													

```
TOTAL ROTOR ASSEMBLY C.G.= 38.03 INCHES FROM STA. 1.

BEARING REACTION AT STA.   9 =   318.56 LB
BEARING REACTION AT STA.  51 =   345.93 LB

          BEARING STATIONS    9   51
          BEARING  1, SENSOR AT STA.    6  12
          BEARING  2, SENSOR AT STA.   48  54
```

Appendix E. MODIFIED JEFFCOTT ANALYSIS PROGRAM CODE

```
      complex k11,k12,k21,k22,x1,x2,det,gamma,xs
      real m1,m2,k1,k2,c1,c2,ebar,w,wlow,whigh,wstep,alpha
      real kr,mr,wcr,twopi,f0,magxs,phixs
      real beta,magx1,magx2,phi1,phi2,alplow,alphigh,alpstep
      character*30 outputfile

      open(unit=1,file='frespdat.in')
      read(1,1) m2,k2,kr,mr,c1,ebar,f0
      read(1,1) alplow,alphigh,alpstep,wlow,whigh,wstep

1     format(7f10.3)
      close(1)

      twopi=3.1415927*2.
      m2=m2/386.
      m1=mr*m2
      k1=kr*k2
      c2=0.0
      wcr=sqrt(k2/m2)
      wlow=wlow/60.*twopi
      whigh=whigh/60.*twopi
      wstep=wstep/60.*twopi

      write(*,*) ' give a name for the output file'
      read(*,3) outputfile
3     format(a30)
      open(unit=2,file=outputfile)
```

```
      do 40 alpha = alplow,alphigh,alpstep
      beta = sin(acos(-1.)*alpha/2.)
      write(2,50) alpha
50    format('  alpha is  ',f6.2)

      do 10 w = wlow,whigh,wstep
            k12 = cmplx((k2-k1*beta),(w*(c2-c1*beta)))
            k21 = cmplx(k2,w*c2)
            k11 = cmplx(-m2*w*w,0) + k21
            gamma = cmplx((-m1*w*w + k1),w*c1)
            k22 = gamma + k12
            det = k22*k11-k21*k12
            if (det.eq.0.) then
                  write(2,*) 'no solution exists'
            else
                  x1 = (k11*f0 + k12*m2*ebar*w*w)/det
                  x2 = (k21*f0 + k22*m2*ebar*w*w)/det
                  xs = x1 + (x2-x1)*beta
                  magx1 = cabs(x1)
                  magx2 = cabs(x2)
                  magxs = cabs(xs)
                  if (magx1.ne.0.) then
                     phi1 = acos(real(x1)/magx1)*180./acos(-1.)
                     if (aimag(x1).lt.0.) phi1 = 360.-phi1
                     phi1 = 360.-phi1
                  else
                        phi1 = 0
                  endif
```

```
            if (magx2.ne.0.) then
               phi2 = acos(real(x2)/magx2)*180./acos(-1.)
               if (aimag(x2).lt.0.) phi2 = 360.-phi2
               phi2 = 360.-phi2
            else
                phi2 = 0
            endif
            if (magxs.ne.0.) then
               phixs = acos(real(xs)/magxs)*180./acos(-1.)
               if (aimag(xs).lt.0.) phixs = 360.-phixs
               phixs = 360.-phixs
            else
                phixs = 0
            endif

      write(2,30) w/twopi,magx1*25.4,phi1,magx2*25.4
     +           ,phi2,magxs*25.4,phixs
30    format(f10.3,f10.6,f10.3,f10.6,f10.3,f10.6,f10.3)

          endif

10     continue
       write(2,*)
40     continue

       write(2,20)
20     format(' ',' w Hz  ',' x1  mm  ',
     + 'ph-x1(deg)',' x2  mm  ','ph-x2(deg)',' xs  mm  ',
     + 'ph-xs(deg)')
```

```
      write(2,70)
70    format(|,'  ',' m2  N  ',' k2 N/mm ',' k1/k2  ',
     + ' m1/m2  ',' c/ Ns/mm ',' ebar mm ','excitation N')
      write(2,60) m2*386.*4.4482,k2*4.4482/25.4,kr,mr,
     +            c1*4.4482/25.4,ebar*25.4,f0*4.4482
60    format(|,7f10.3)

      close(2)

      stop
      end
```

Appendix F. GUIDE FOR RUNNING THE MODIFIED TRANSFER MATRIX PROGRAM

The modified transfer matrix program is called FLXK and two versions are provided to obtain the output in different units. FLXKSI and FLXKFPS are on the disk titled FRESP. FRESP includes the following programs on it.

1. JEFFSI.FOR
2. FPSJEFF.FOR
3. FRESPDAT.IN
4. FLXKSI.EXE
5. FLXKFPS.EXE
6. SUBR.EXE

7. EQS.EXE

8. INVERT.EXE

9. P1SHAFT.EXE

10. SAMP1.IN

11. SAMP2.IN

All the output files generated by running FLXKSI or FLXKFPS, with the example input files are on the disk titled OUTPUT. These files are as follows:

1. UTLPLT.EXE

2. SAMP1OUT.1

3. SAMP1OUT.2

4. SAMP1OUT.3

5. SAMP1OUT.4

6. SAMP1OUT.5

7. SAMP1OUT.6

8. SAMP2OUT.1

9. SAMP2OUT.2

10. SAMP2OUT.3

11. SAMP2OUT.4

12. SAMP2OUT.5

13. SAMP2OUT.6

Use the program FLXKSI if you want the output file results in SI units. Use the program FLXKFPS if you want the output file results in British units. However in both cases, the input file data should be in British units. This is so, because the same input file can be run with the two programs without any modifications.

The disk FRESP does not contain any system DOS program to boot the computer. The computer must be started with a separate disk, or a start up program may be added to the FRESP disk.

For getting plots from the output data files on a plotter, the program UTLPLT must be invoked. This is the plotting program which accepts an input file with a suitable format and makes the required plots on an HP plotter.

GENERATION OF THE INPUT DATA FILE FOR PROGRAM FLXK

Given below is a brief description of the parameters that are required from the user to generate the input data file in the correct manner. The input is described as a card image file. When format is specified as list directed, the values may be seperated by blanks, commas or slashes.

Card 1 (List-directed)

LCNO Arbitrary number to identify case being run.

HPRIN 0 Do not print energy balance data.

1 Print energy balance data.

Cards 2 & 3. (20A4) Any descriptive information.

Card 4. (List directed)

NS Number of rotor stations. Program dimensions will accomodate up to 60 stations only.

NB Number of bearings. Program dimensions will accomodate up to 10 bearings.

NU Number of unbalance locations.

NF Number of constant excitation forces.

NP Number of stations where amplitude data is printed. (NC < = 5)

NMS Number of frequencies where mode shape data is printed. (NMS < = 5)

Card 5. (List directed)

TOL Tolerance value for the convergence to solution given as a percentage. 1E-6 is a good tolerance value.

Card 6. (3G10.3)

E Rotor elastic modulus*1E-6, lb/in**2.

G Rotor shear modulus*1E-6, lb/in**2. (program sets G = 11.1 if zero is input.

RHO Rotor density, lb/in**3. (program sets RHO = 0.283 if zero is input)

Card(s) 7. (6F10.3,2F7.3,F6.3) (One for each rotor station)

(If DO = 0 then DO = MDO. If RL = 0 then RL = MRL)

	WE	Additional mass at rotor station, lb. (program calculates mass and inertias from rotor dimensions and adds to WE, RP, and RT)
	MRL	Section length, in. (= 0 for last station)
	MDO	Outside mass diameter, in.
	MDI	Inside mass diameter, in.
	RP	Additional polar moment of inertia, lb in**2.
	RT	Additional transverse moment of inertia, lb in**2.
	DO	Outside stiffness diameter, in.
	DI	Inside stiffness diameter, in.
	RL	Stiffness length, in.

Card(s) 7a. (3G10.3) (One for each rotor station but only if E = 0)

	E(I)	Rotor elastic modulus*1E-6, lb/in**2. (program sets E = 30 if zero is input.
	G(I)	Rotor shear modulus*1E-6, lb/in**2. (program sets G = 11.1 if zero is input.
	RHO(I)	Rotor density, lb/in**3 (program sets RHO = 0.283 if 0 is input)

Card 8. (List directed) Station numbers of bearing locations.

Card(s) 9. (3I10) (One for each bearing)

	NSEN	Number of sensors at that particular bearing. (Either 0, 1 or 2)
	LSEN1	Station number where the first sensor is located.
	LSEN2	Station number where the second sensor is located.

Card 10. (List directed) Station numbers for which output is printed.

Card 11. (List directed) Frequency values for which mode shape data

is printed.

Card(s) 12. (I5, 2G10.3) (One for each of NU unbalance locations)

LU	Unbalance station number.
UX	Unbalance in x-direction (in rotor coordinates), oz in.
UY	Unbalance in y-direction (in rotor coordinates), oz in.

Card(s) 13. (I5, 2G10.3) (One for each of NF excitation force locations)
(If NF is non zero, NU is set to zero)

LF	Excitation force station number.
FX	Excitation force cosine component in the x-direction, lb.
FY	Excitation force sine component in the x-direction, lb.

Card 14. (4G10.2)

SPST	Initial rotor excitation frequency, rpm.
SPFN	Final rotor excitation frequency, rpm.
SPINC	Excitation frequency increment, rpm.
SPIN	Rotor spinning frequency, rpm. (if = -1 then same as excitation frequency). (If NU is non zero, SPIN is set to -1)

Card(s) 15. (I5) (If JFLAG(1) > 0 then one for each bearing)

JFLAG(I) Indicates no. of speed points used for the bearing properties table JFLAG(1) decides whether bearing properties change with changes in the excitation frequency. If JFLAG(1) = 0, bearing properties remain constant else bearing properties are interpolated from a table listing the properties for JFLAG(I) excitation frequency values. (Max. JFLAG(I) = 20)

Card(s) 16. (2G10.3) (One for each bearing, but only if JFLAG(1) = 0)

BKXX Bearing stiffness. lb/in.

BCXX Bearing damping. lb sec/in.

Card(s) 17. (3G10.3) (One for each of JFLAG(I) excitation frequency values, but only if JFLAG(1) > 0. The whole set is repeated for each bearing.)

SPDF Excitation frequency value, rpm.

BKXX Bearing stiffness. lb/in.

BCXX Bearing damping. lb sec/in.

INTERPRETATION AND USE OF THE OUTPUT FILES

Running the program FLXKSI (or FLXKFPS) with an input data file generates 6 output data files, the names of which are given by the user at the prompting of the program.

The first file generated (whose name is asked first) contains all the rotor property data, sensor location information and the excitation imposed. This file also contains the amplitude and the phase angle data for each rotor station where output was required, for each particular excitation frequency in the frequency range.

The second file generated, contains in a tabular form, the bearing forces on each bearing for each excitation frequency. This file also contains information about the excitation frequencies at which maximum amplitudes are reached (ie. critical frequencies), and the corresponding phase angles and bearing forces.

The third file is a plot file, which when used in conjunction with the UTLPLT program, generates plots of amplitude vs. frequency for each of the rotor stations where output was generated.

The fourth file is also a plot file which makes plots of phase angles vs. frequency for each output rotor station, when used with the UTLPLT program.

The fifth file contains information about the shear and moment residuals at each excitation frequency. The shear and moment residuals are used to check the correctness of the transfer matrix analysis. These residuals should be very small and ideally should be zero. However, generally they may be of an order varying from 1E-3 to 1E-6.

The sixth and last output file generated is a plot file. This file when used with the UTLPLT program, will generate plots of the mode shapes for the specified excitation frequencies. Three mode shape curves are produced for each excitation frequency. The curve titled XC represents the cosine component of the amplitude. The curve titles XS represents the sine component of the amplitude. However, as the vibration is circular synchronous, XC and XS may be interpreted as the deflections along the X and Y axis respectively. The curve titled X represents the total magnitude of the deflection along the rotor longitudinal axis.

USING THE UTLPLT PROGRAM

The UTLPLT program is invoked by typing in "utlplt". This program asks a number of questions, as follows and generates the plots on an HP plotter or the computer screen depending upon the user response to these questions. For more information on using the UTLPLT program, please refer to the program manual which is available seperately from this package.

Enter data file:

The user specifies the name of the appropriate plotting file. This file will be either the third, fourth or the sixth output file generated by the FLXK program.

Enter Output device or filename:

Type in "nul" at this place.

Enter LDEV (0:CON, 1:LPT1, 2:COM1):

Type in "0" if you want to see the display on the screen. Type in "2" if you want the curves plotted on the plotter.

Origin placement in inches - XORG, YORG:

Type in "1,1" at this question.

Enter rotation option (0: 0 deg, 1: 90 deg):

Type in "1" for this question.

Enter plotting ratio:

Type in "1" for this question.

Remove legend at bottom of plot (Y/N):

Enter "Y" for this query.

At this point the program should start making the plot.

Appendix G. ADDITIONAL PLOTS ILLUSTRATING SENSOR INFLUENCE ON VIBRATIONAL CHARACTERISTICS OF THE TWO-MASS MODEL

The plots in Figs. 59-90 illustrate the effect of a change in sensor location on the vibrational characteristics of the two-degree-of-freedom rotor system. The different line types indicate amplitudes or phase angles for different cases of sensor location. The plots are made for the data:

mass ratios $(M_1/M_2) = 1 , 0.25$

stiffness ratios $(K_1/K_2) = 0.1 , 2$

α values $-0.2 , -0.1 , 0.0 , 0.1 , 0.2$

The bearing damping is fixed at 0.263 Nsec/mm and therefore the bearing amplification factor of the rotor system varies from 3.535 for a mass ratio of 0.25 and a stiffness ratio of 0.5 to

14.14 for a mass ratio of 1 and a stiffness ratio of 2. Figures 59-74 show sensor influence on rotor vibrational characteristics when an unbalance excitation of 6.78 Nmm is applied to the midspan mass, while Figs. 75-90 show sensor influence on rotor vibrational characteristics when a constant force excitation of 88.96 N is applied to both the journal masses at the bearing locations.

Figures 59-66 show bearing amplitudes (Figs. 59-62) and midspan amplitudes (Figs. 63-66) for different values of mass ratios and stiffness ratios and the application of unbalance force excitation. Figures 67-74 show the effect of sensor location on bearing phase angles (Figs. 67-70) and midspan phase angles (Figs. 71-74) for different values of mass and stiffness ratios with the application of unbalance force excitation. The phase angles are lagging phase angles.

Figures 75-82 show sensor influence on bearing amplitudes (Figs. 75-78) and midspan amplitudes (Figs. 79-82) for different values of mass ratios and stiffness ratios and the application of an excitation force in one plane. Figures 83-90 show sensor influence on bearing phase angles (Figs. 83-86) and midspan phase angles (Figs. 87-90) for different mass and stiffness ratios with the application of an excitation force in one plane.

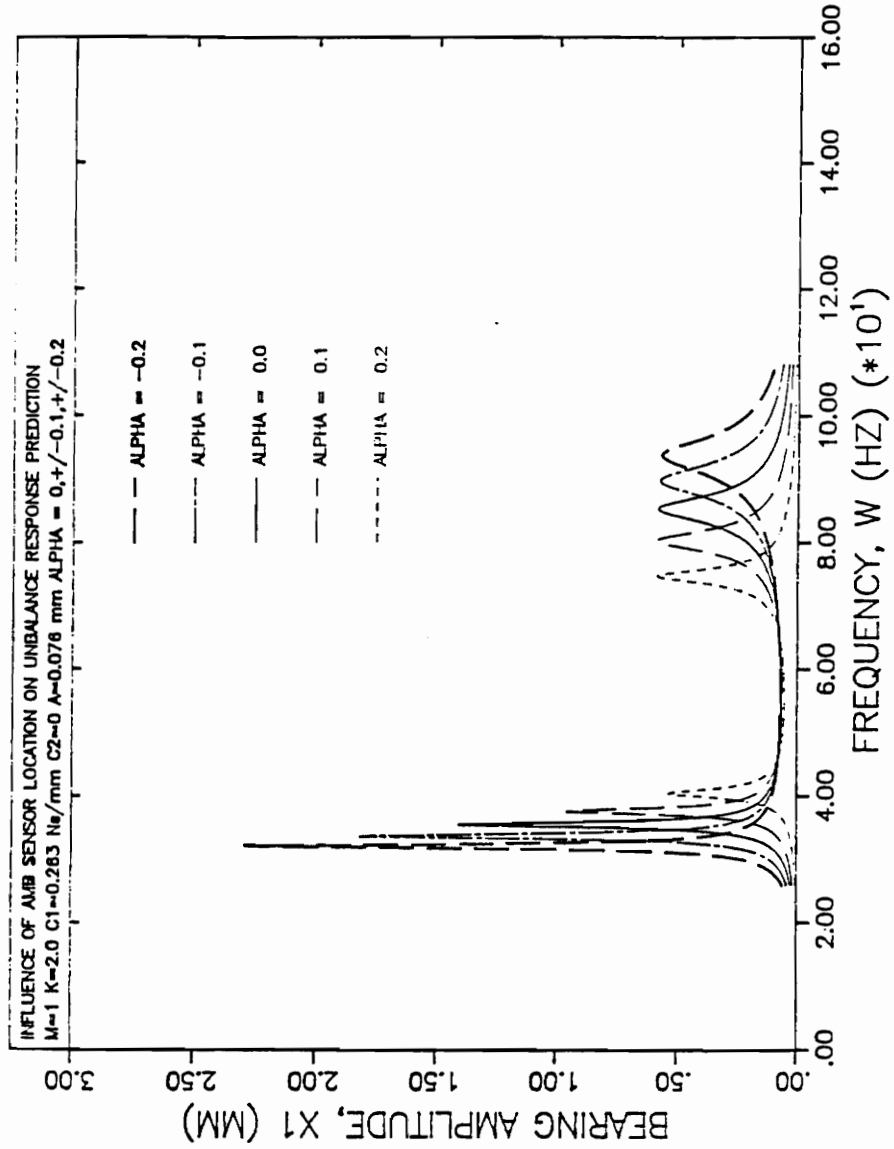

Figure 59.
Sensor Influence on Bearing Amplitude, Unbalance Excitation, M = 1, K = 2

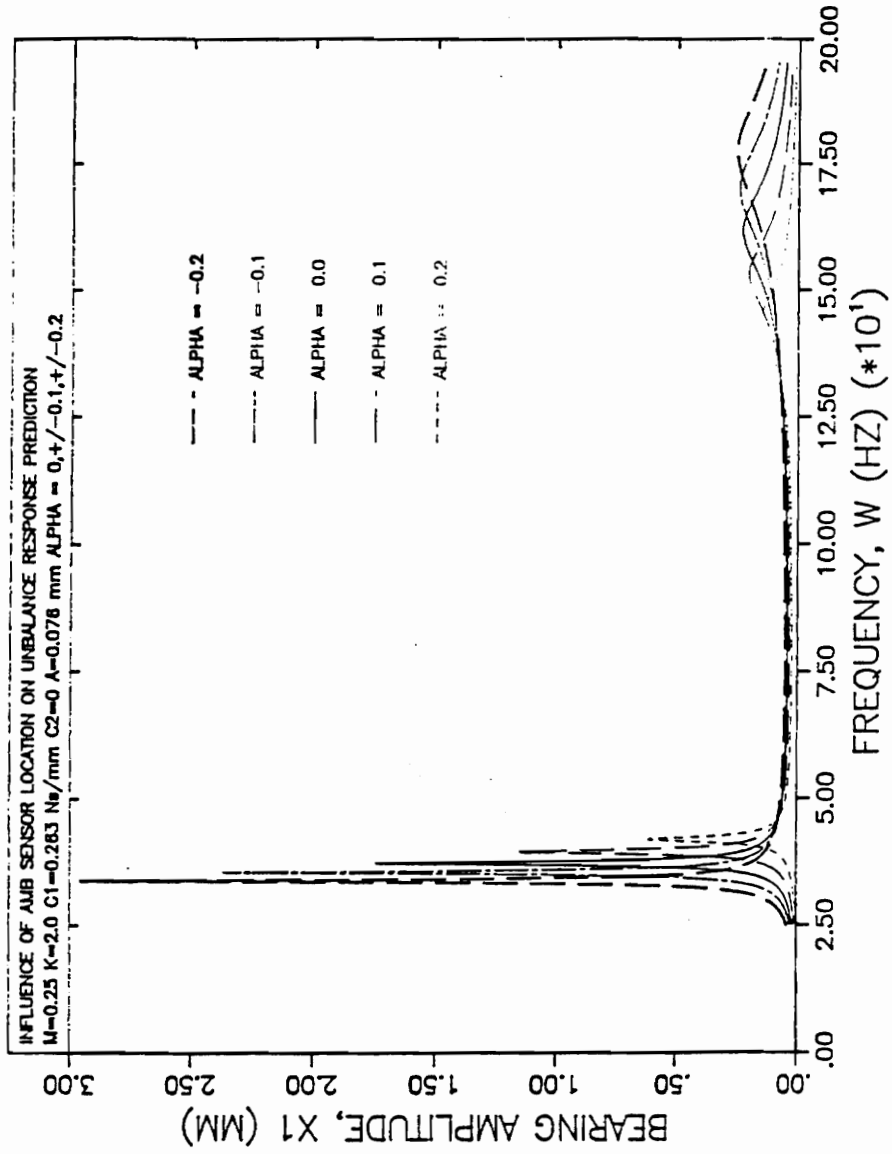

Figure 60.
Sensor Influence on Bearing Amplitude, Unbalance Excitation, M = 0.25, K = 2

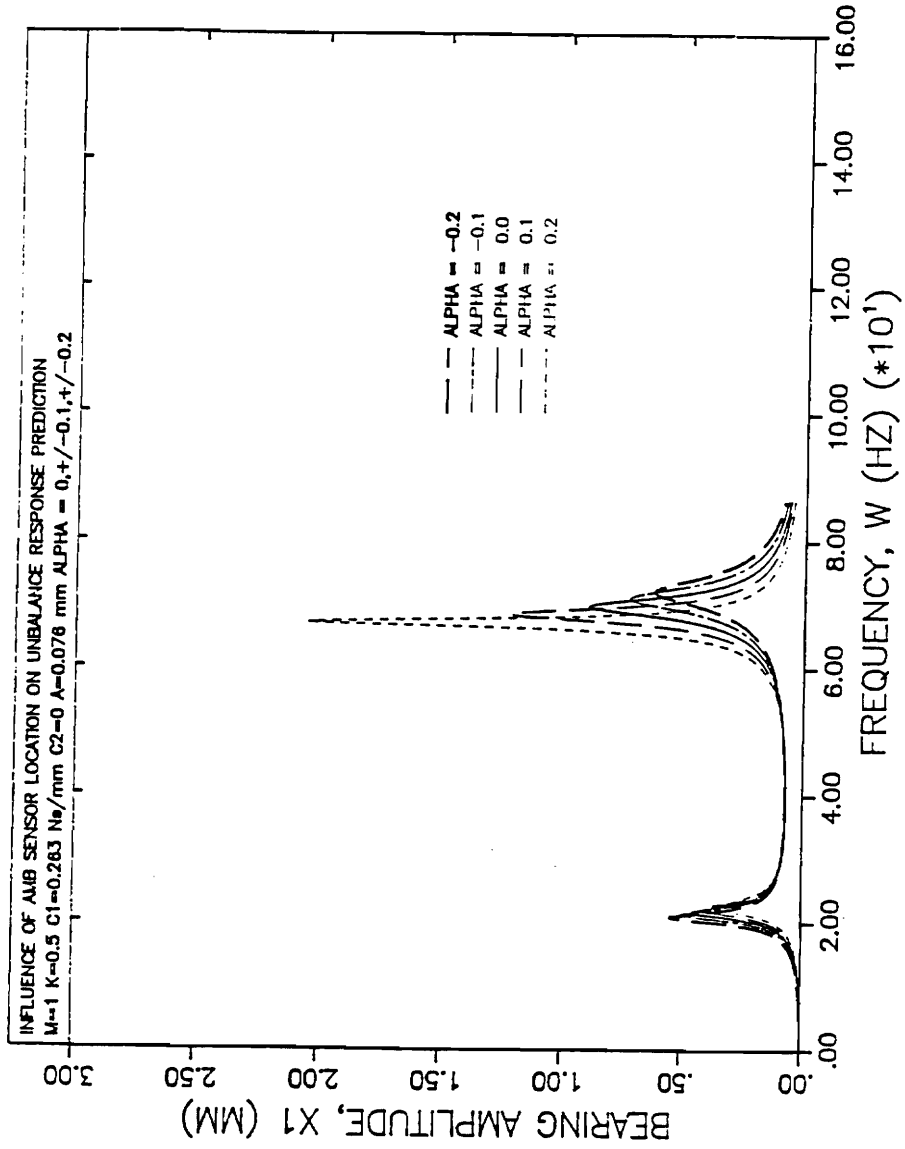

Figure 61.
Sensor Influence on Bearing Amplitude, Unbalance Excitation, M = 1, K = 0.5

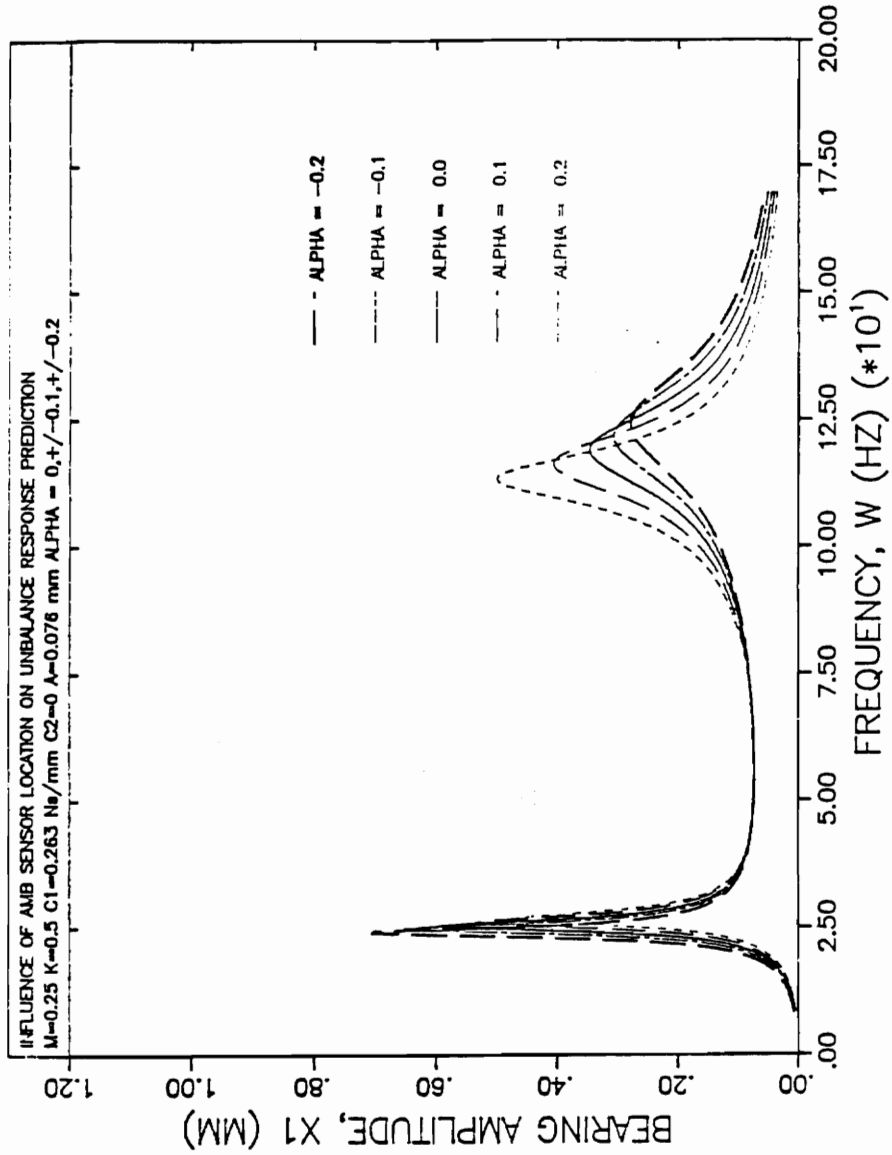

Figure 62.
Sensor Influence on Bearing Amplitude, Unbalance Excitation, M = 0.25, K = 0.5

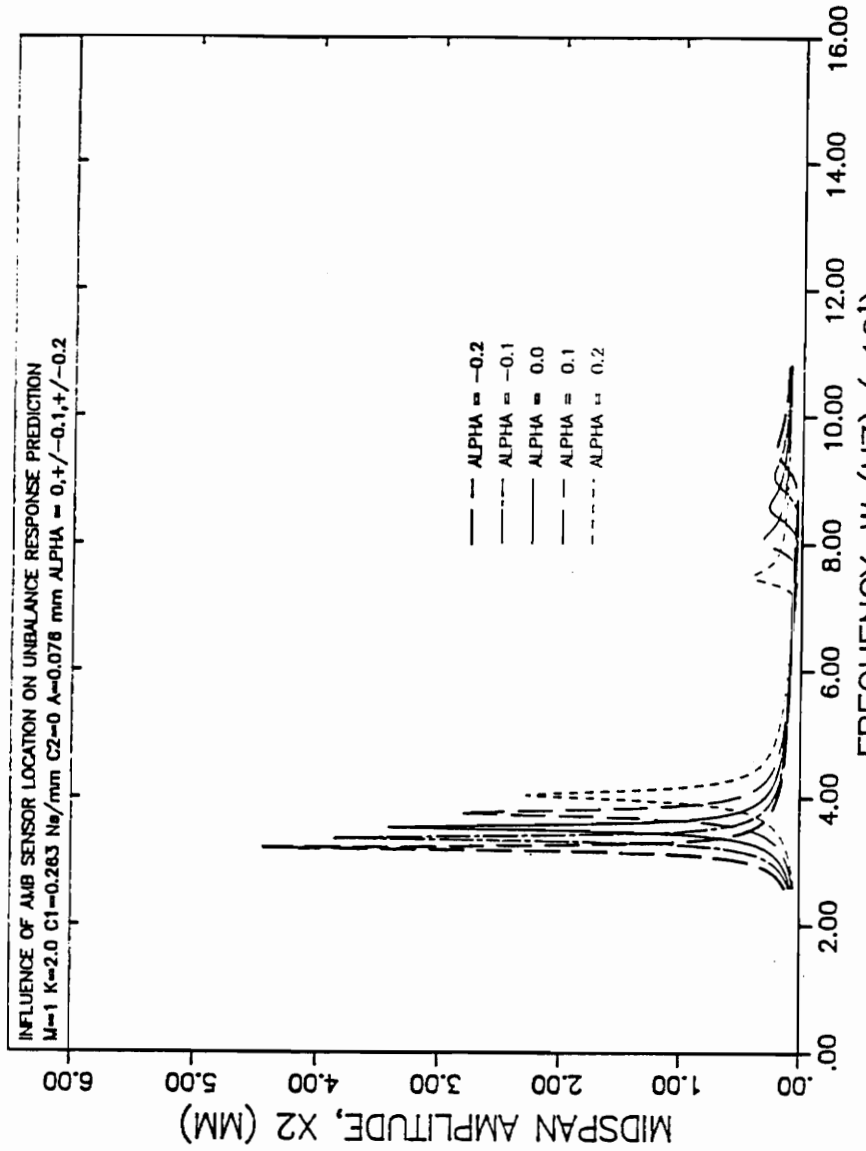

Figure 63.

Sensor Influence on Midspan Amplitude, Unbalance Excitation, M = 1, K = 2

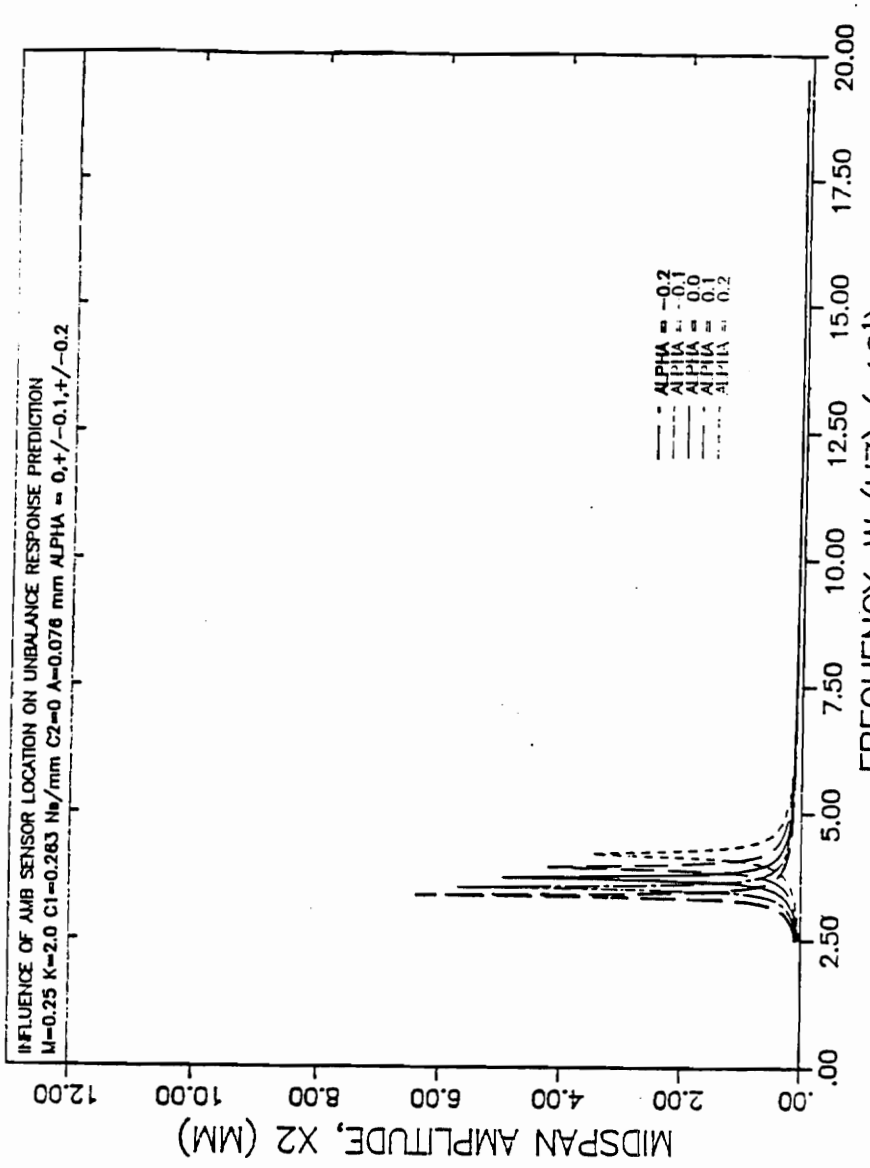

Figure 64.
Sensor Influence on Midspan Amplitude, Unbalance Excitation, M = 0.25, K = 2

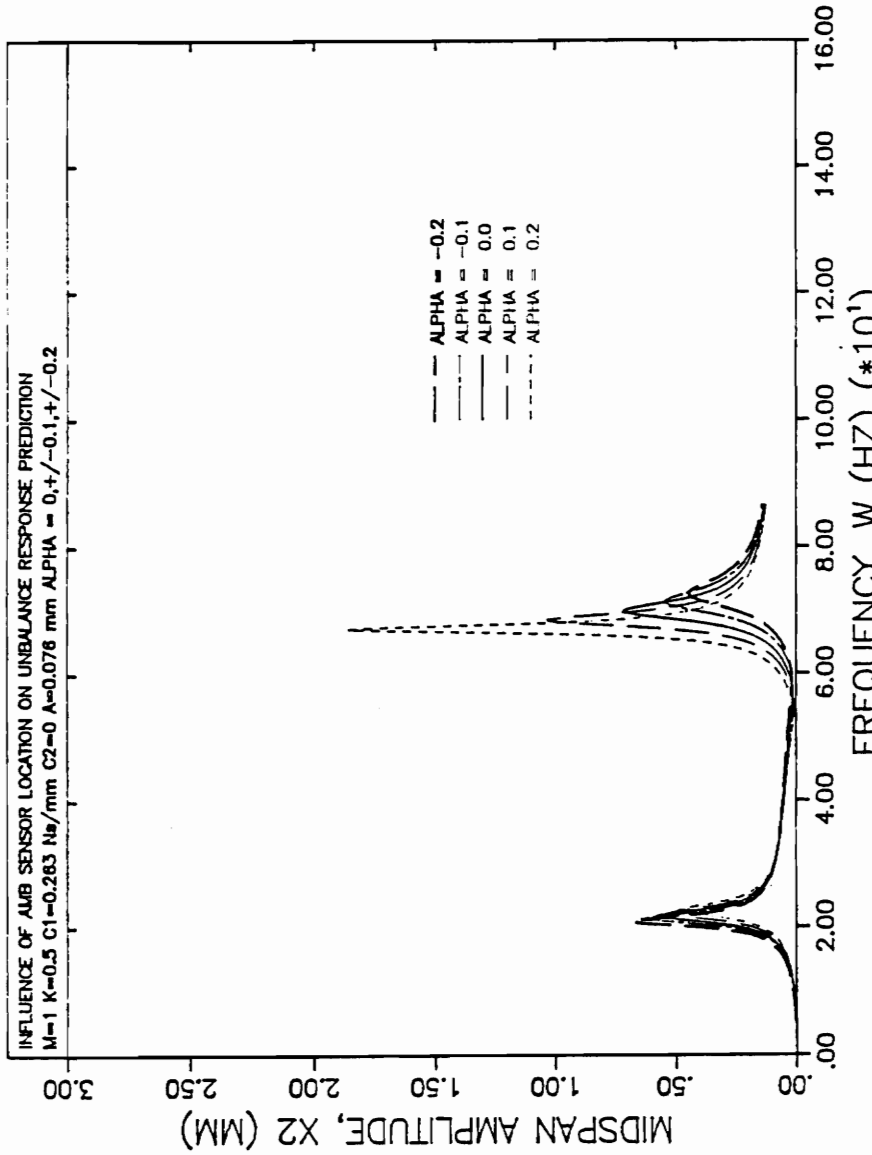

Figure 65.
Sensor Influence on Midspan Amplitude, Unbalance Excitation, M = 1, K = 0.5

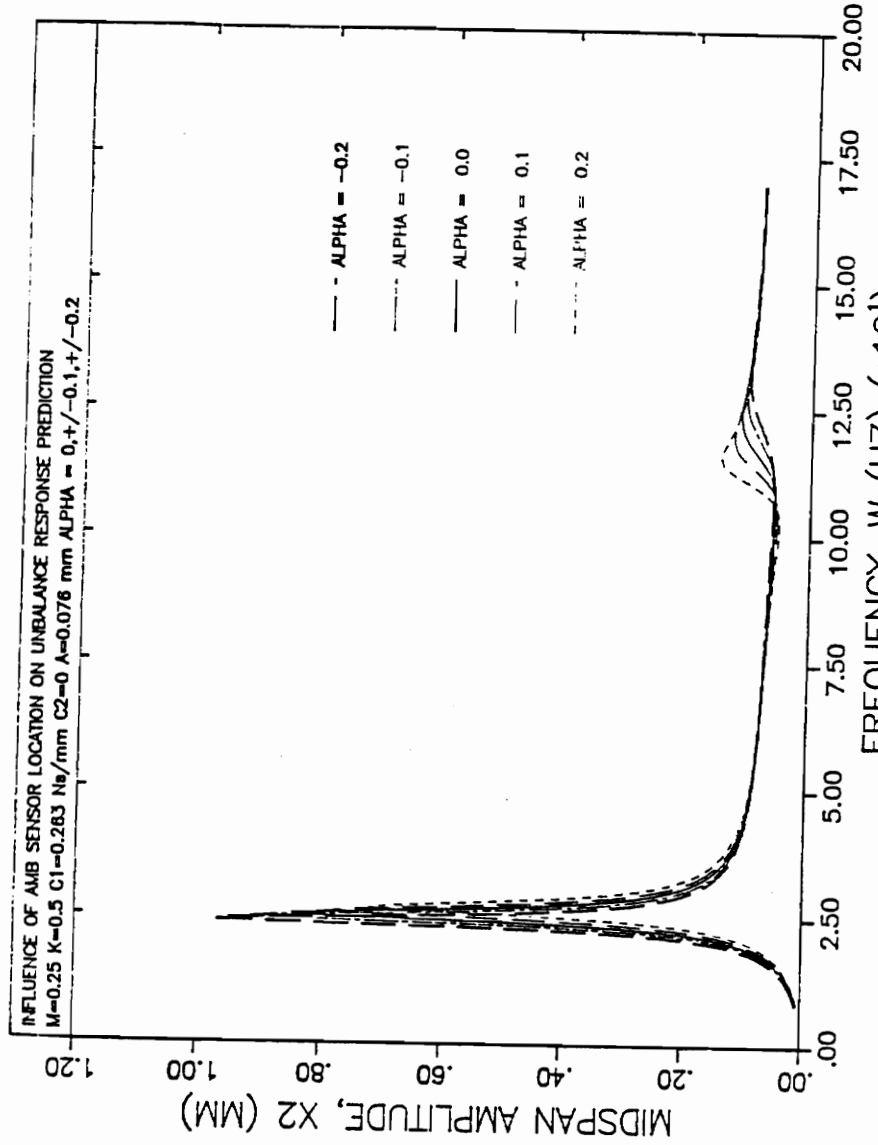

Figure 66.

Sensor Influence on Midspan Amplitude, Unbalance Excitation, M = 0.25, K = 0.5

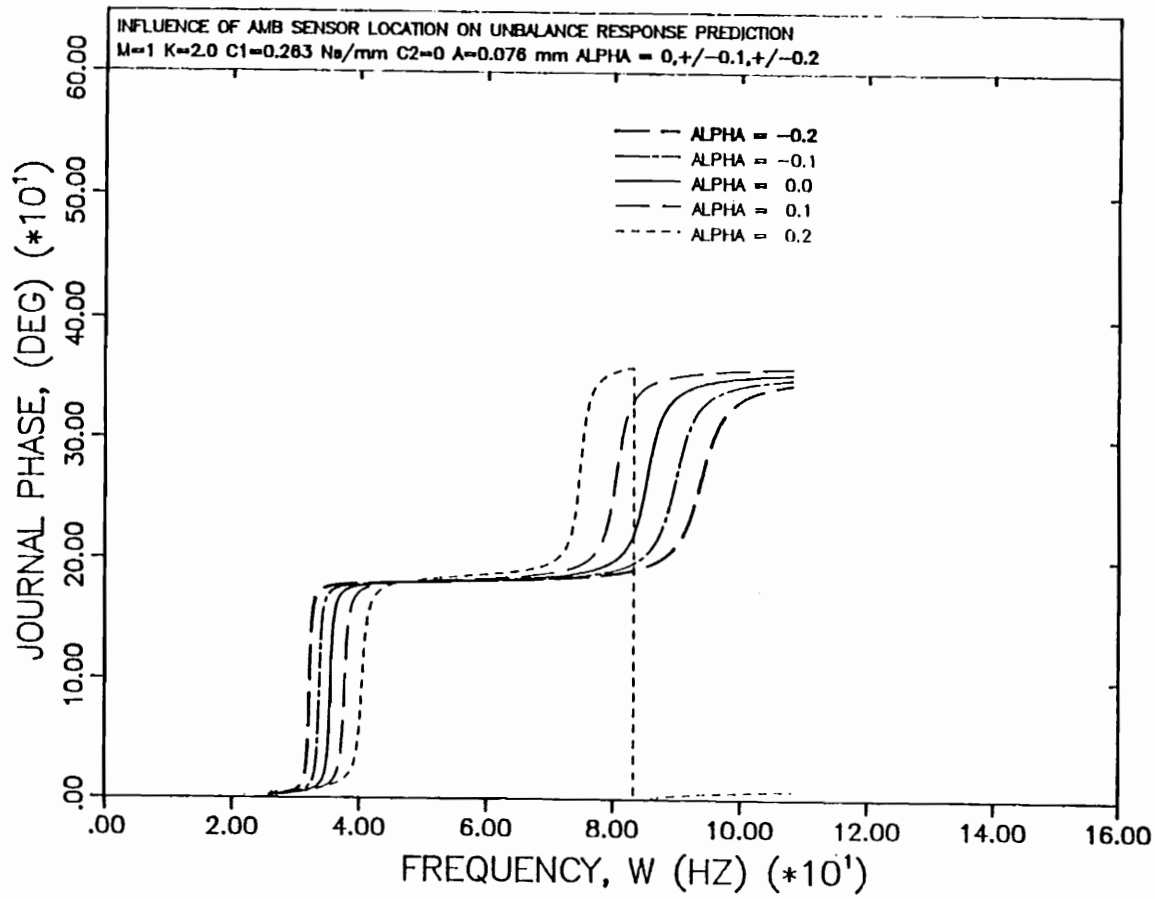

Figure 67.
Sensor Influence on Bearing Phase, Unbalance Excitation, M = 1, K = 2

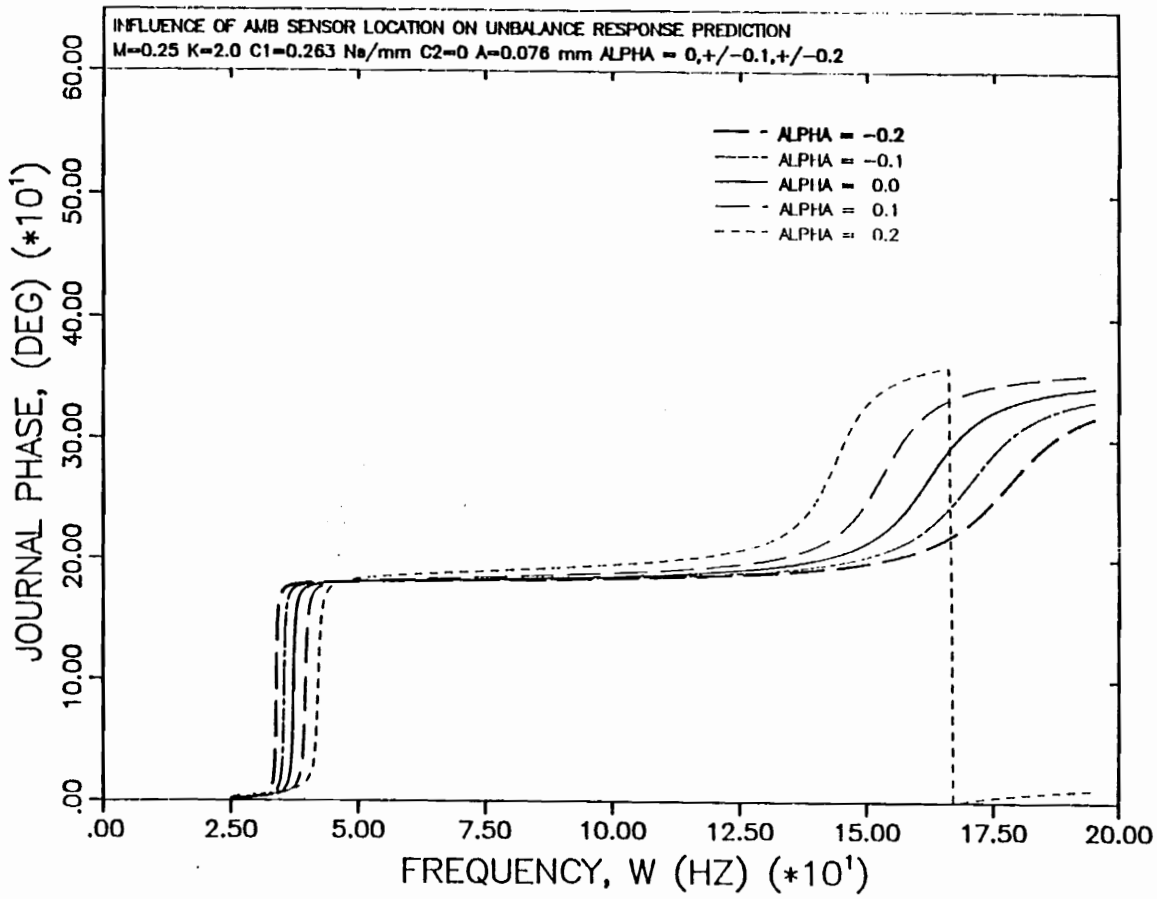

Figure 68.
Sensor Influence on Bearing Phase, Unbalance Excitation, M = 0.25, K = 2

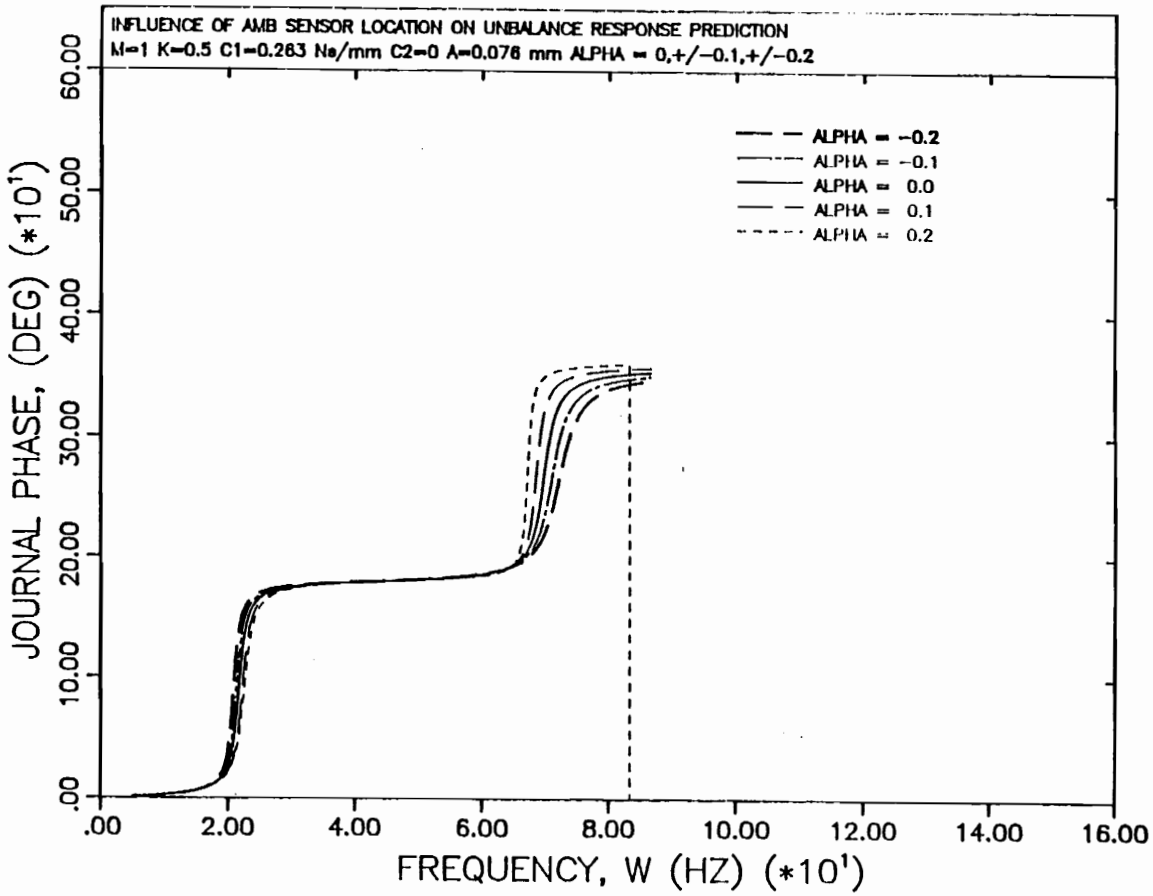

Figure 69.

Sensor Influence on Bearing Phase, Unbalance Excitation, M = 1, K = 0.5

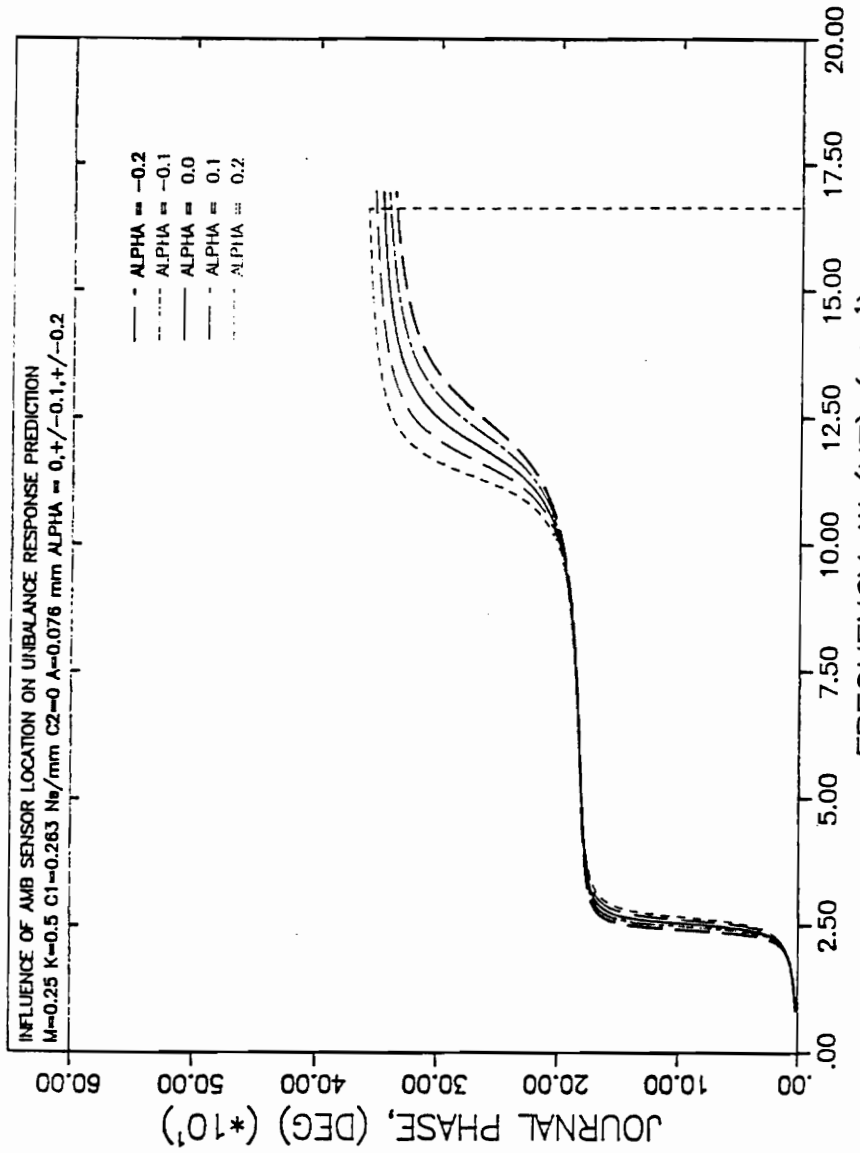

Figure 70.

Sensor Influence on Bearing Phase, Unbalance Excitation, M = 0.25, K = 0.5

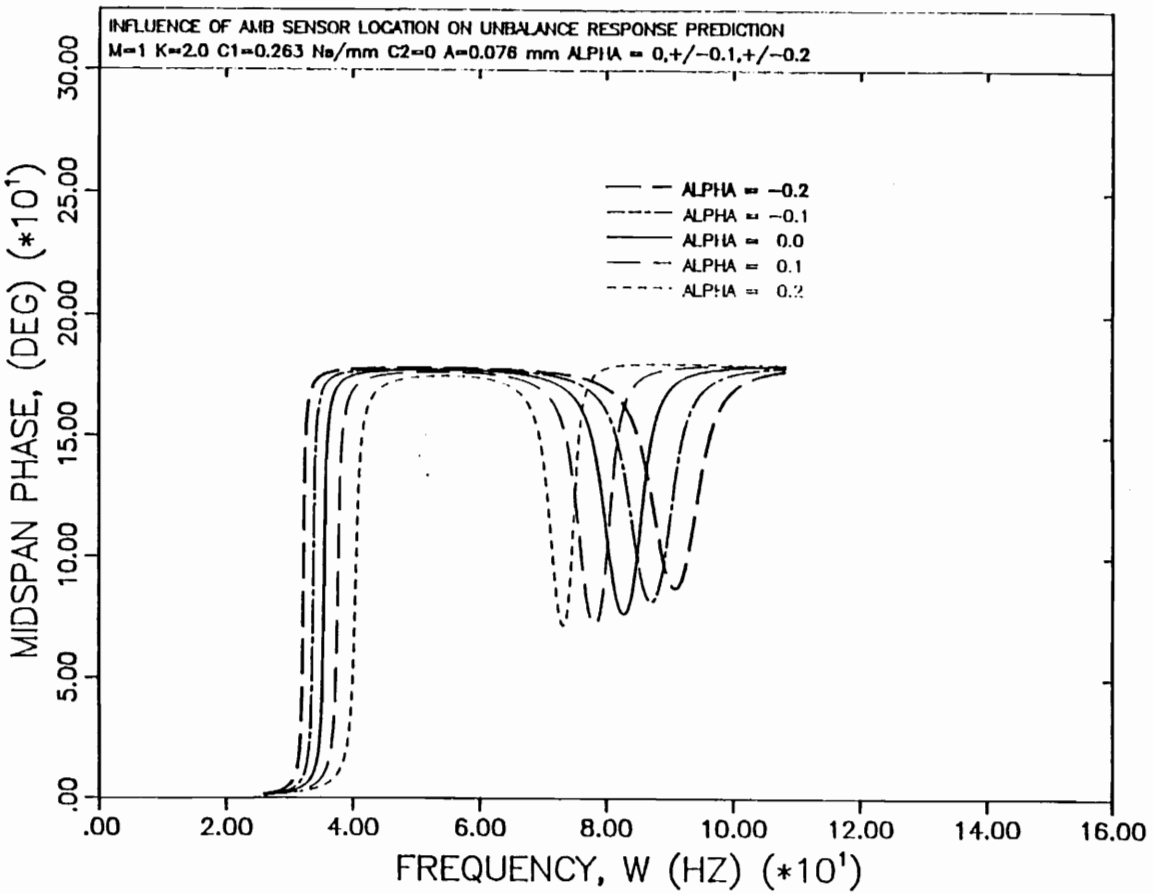

Figure 71.
Sensor Influence on Midspan Phase, Unbalance Excitation, M = 1, K = 2

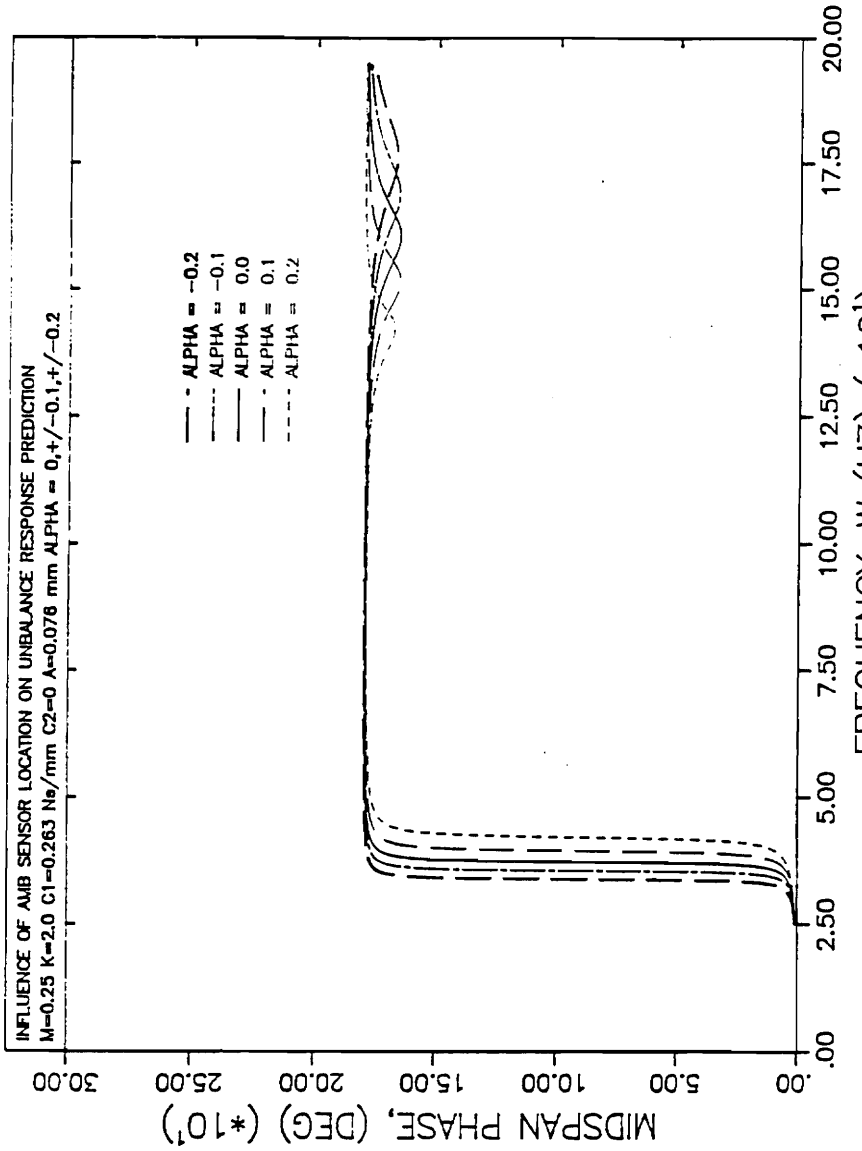

Figure 72.
Sensor Influence on Midspan Phase, Unbalance Excitation, M = 0.25, K = 2

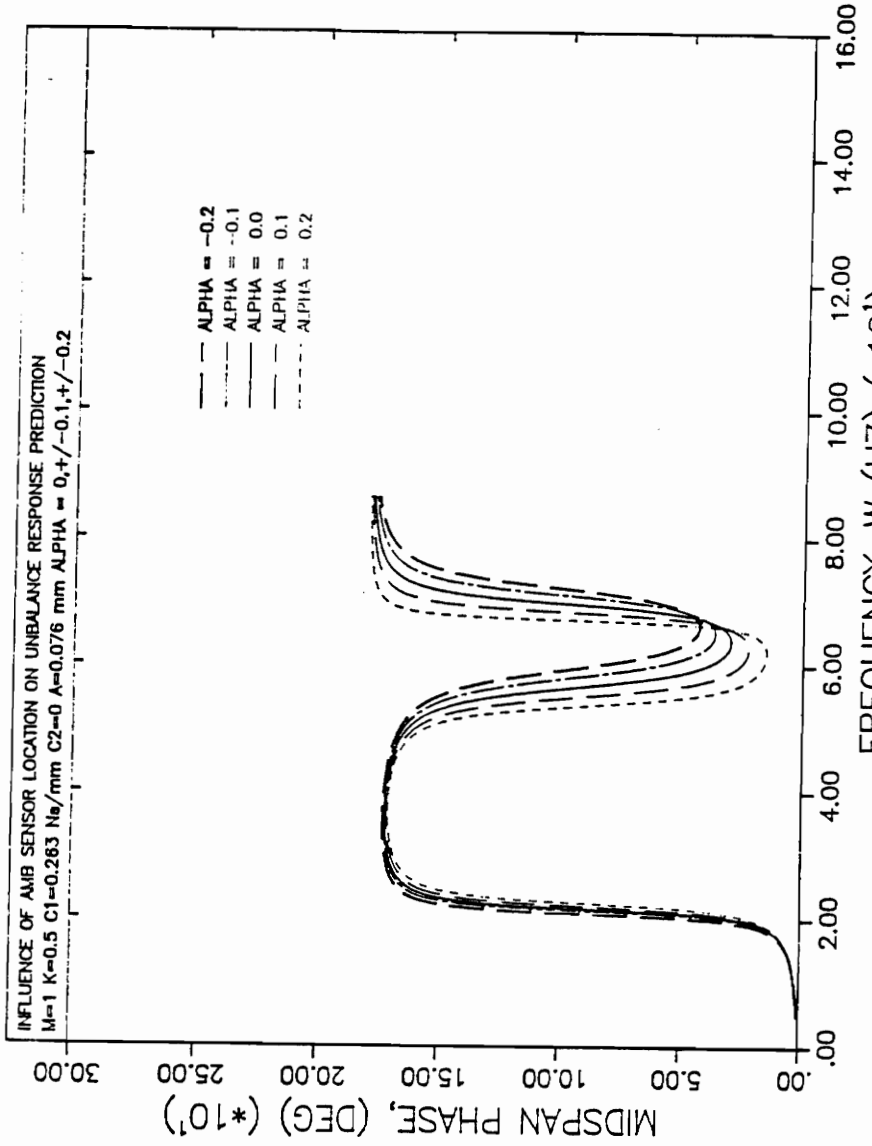

Figure 73.
Sensor Influence on Midspan Phase, Unbalance Excitation, M = 1, K = 0.5

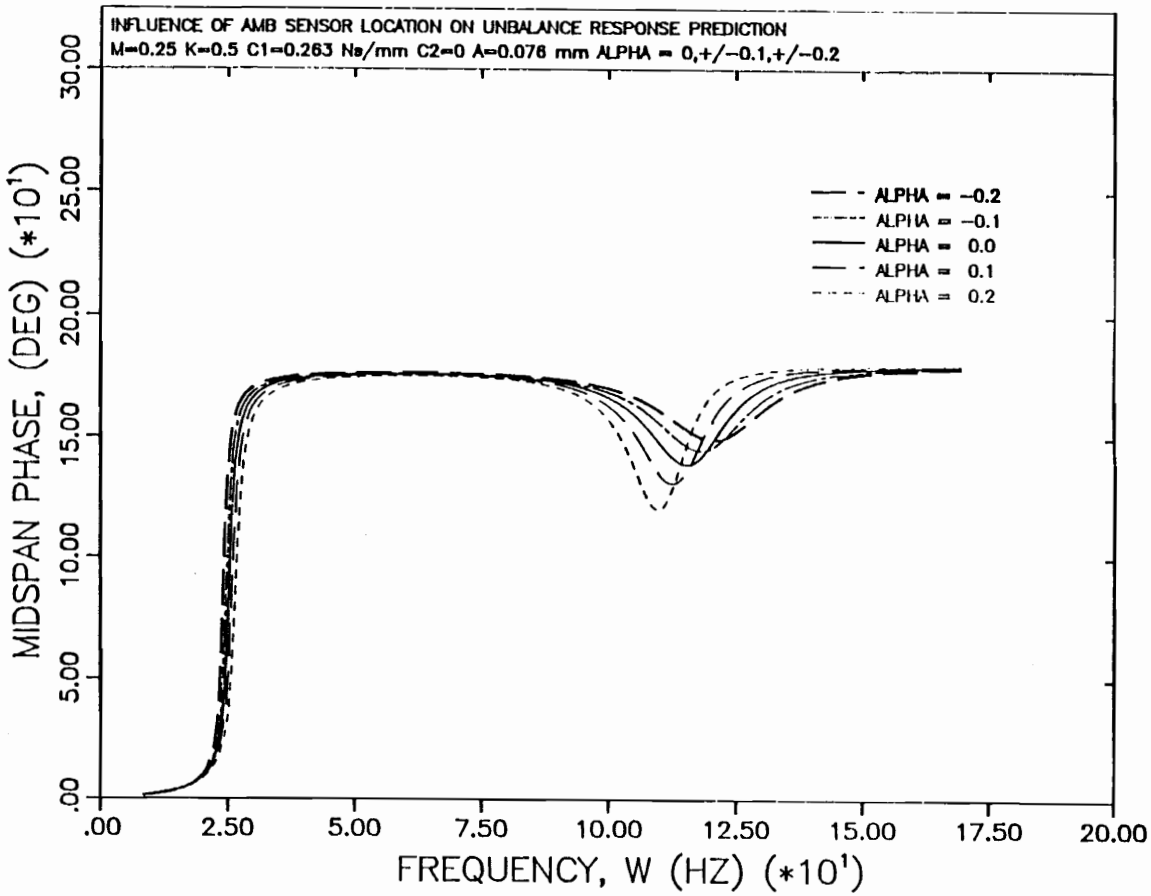

Figure 74.

Sensor Influence on Midspan Phase, Unbalance Excitation, M = 0.25, K = 0.5

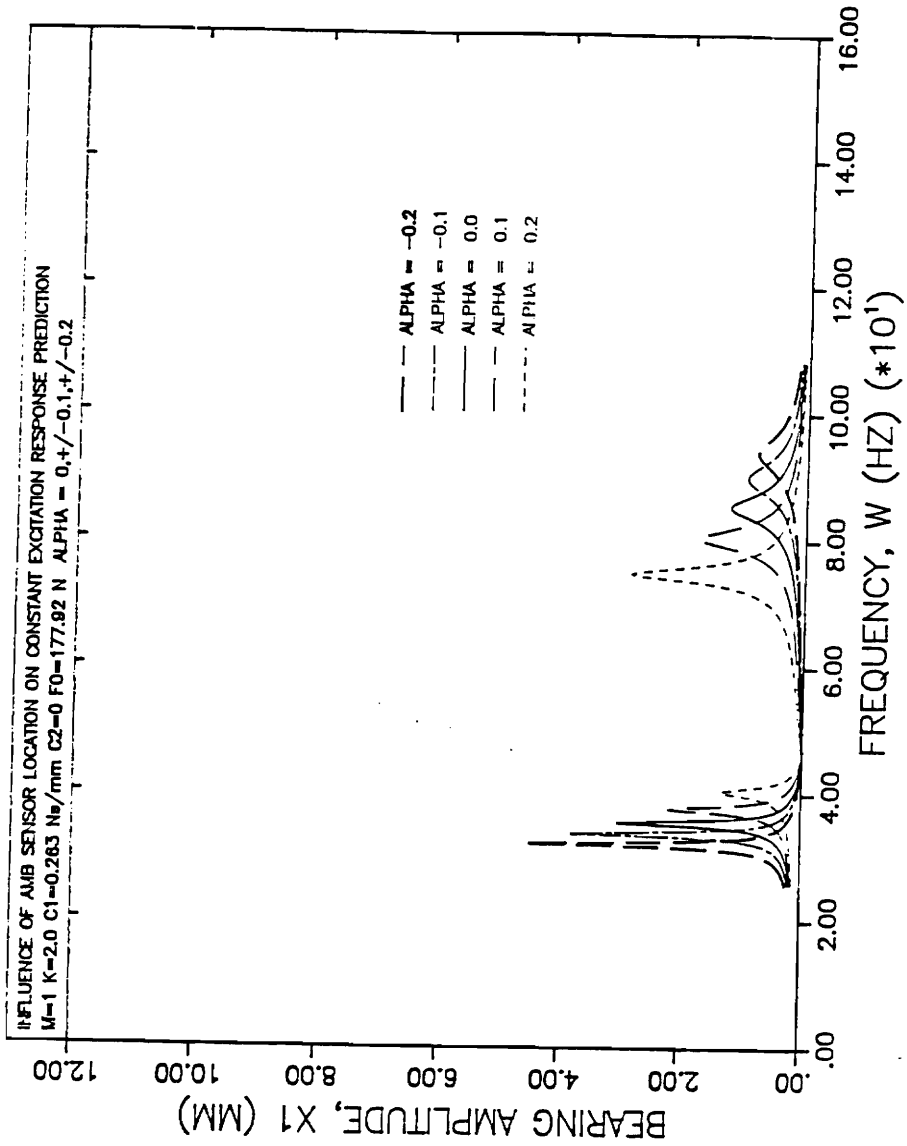

Figure 75.
Sensor Influence on Bearing Amplitude, Planar Excitation, M = 1, K = 2

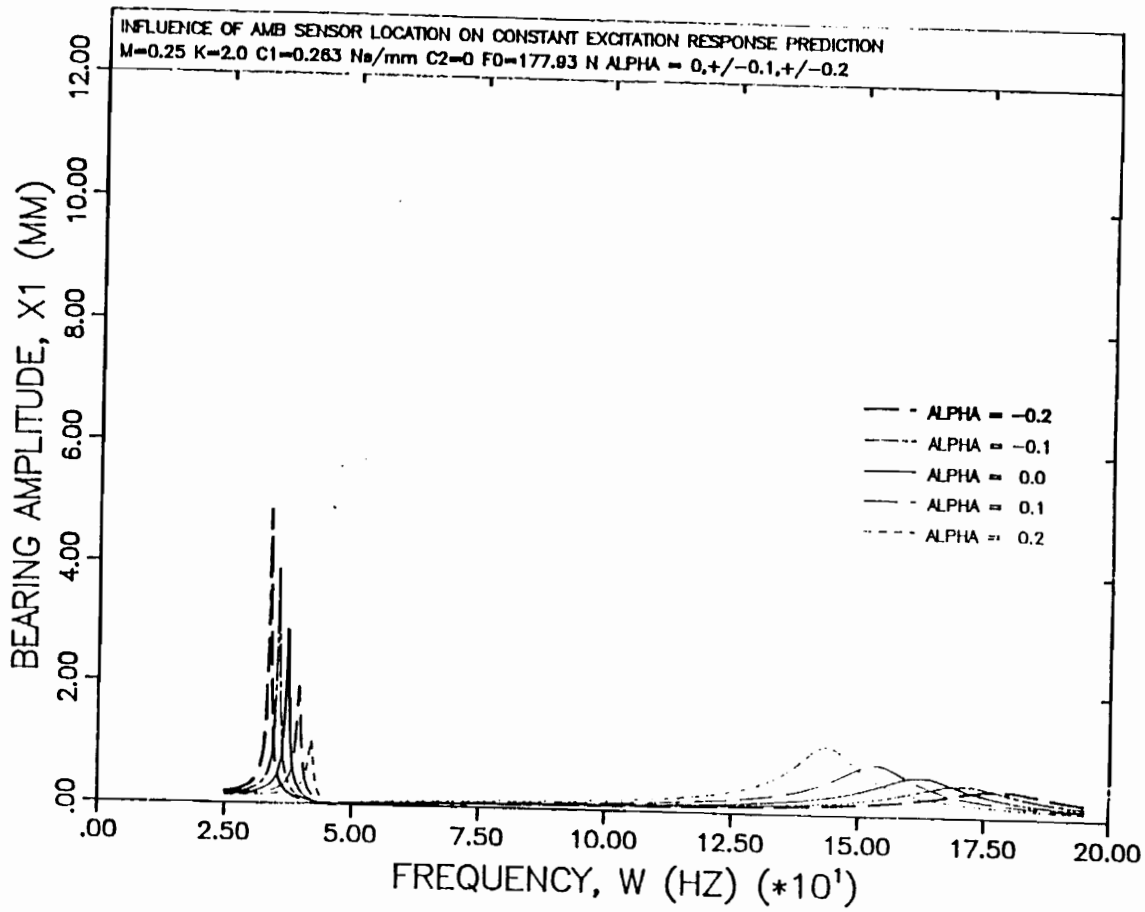

Figure 76.

Sensor Influence on Bearing Amplitude, Planar Excitation, M = 0.25, K = 2

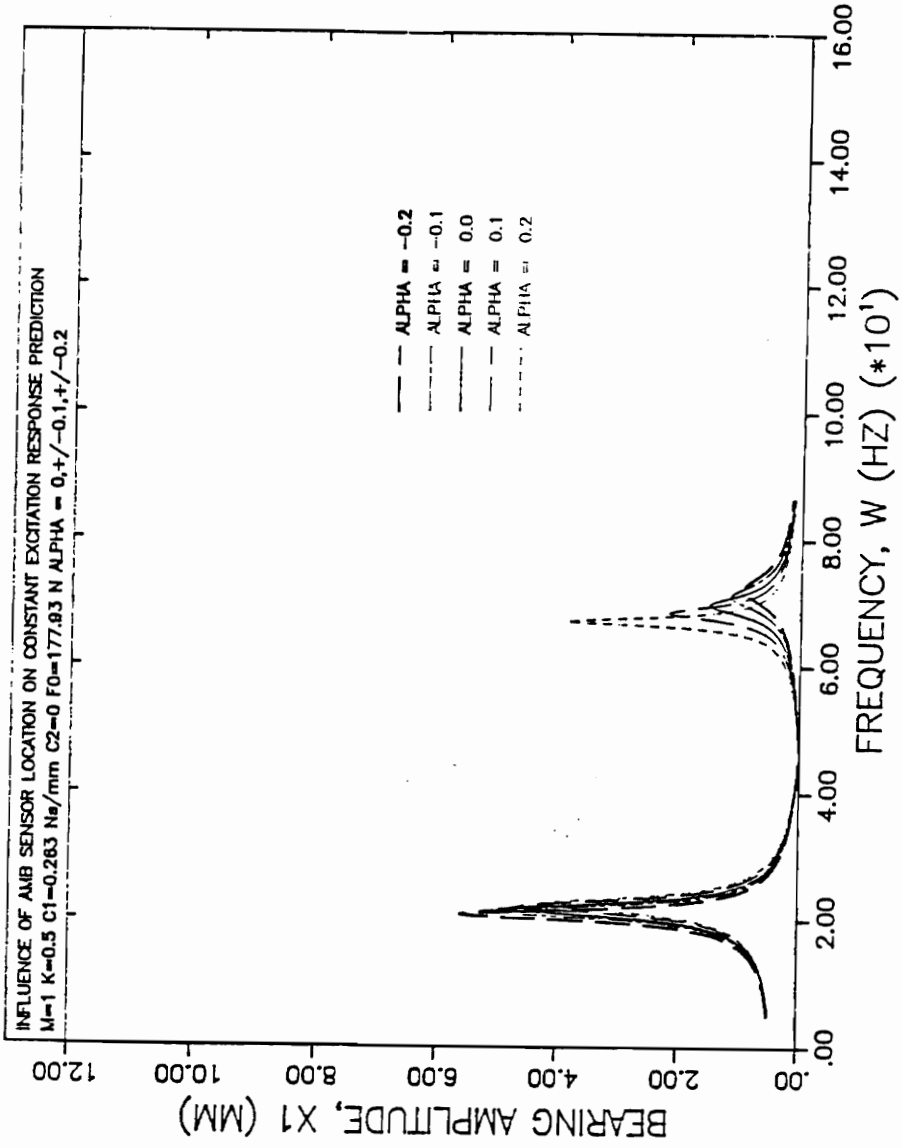

Figure 77.
Sensor Influence on Bearing Amplitude, Planar Excitation, M = 1, K = 0.5

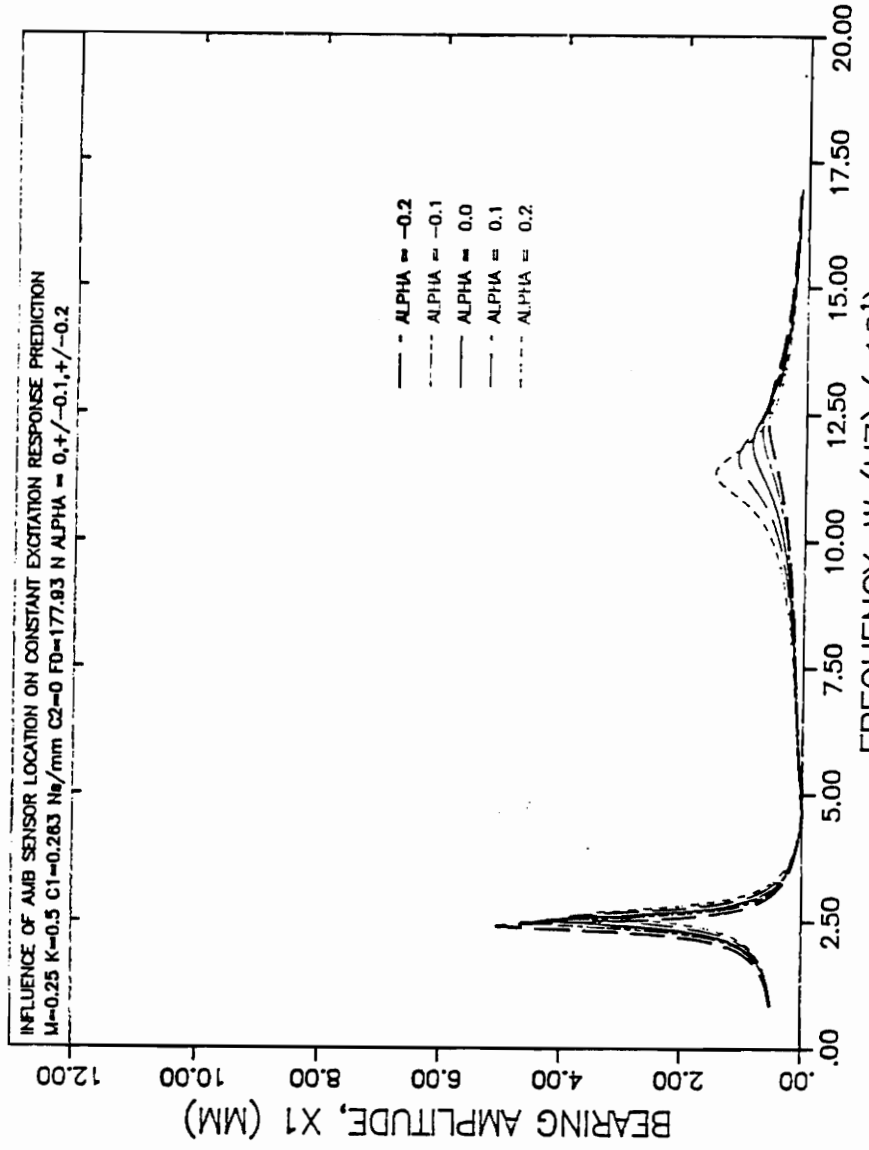

Figure 78.

Sensor Influence on Bearing Amplitude, Planar Excitation, M = 0.25, K = 0.5

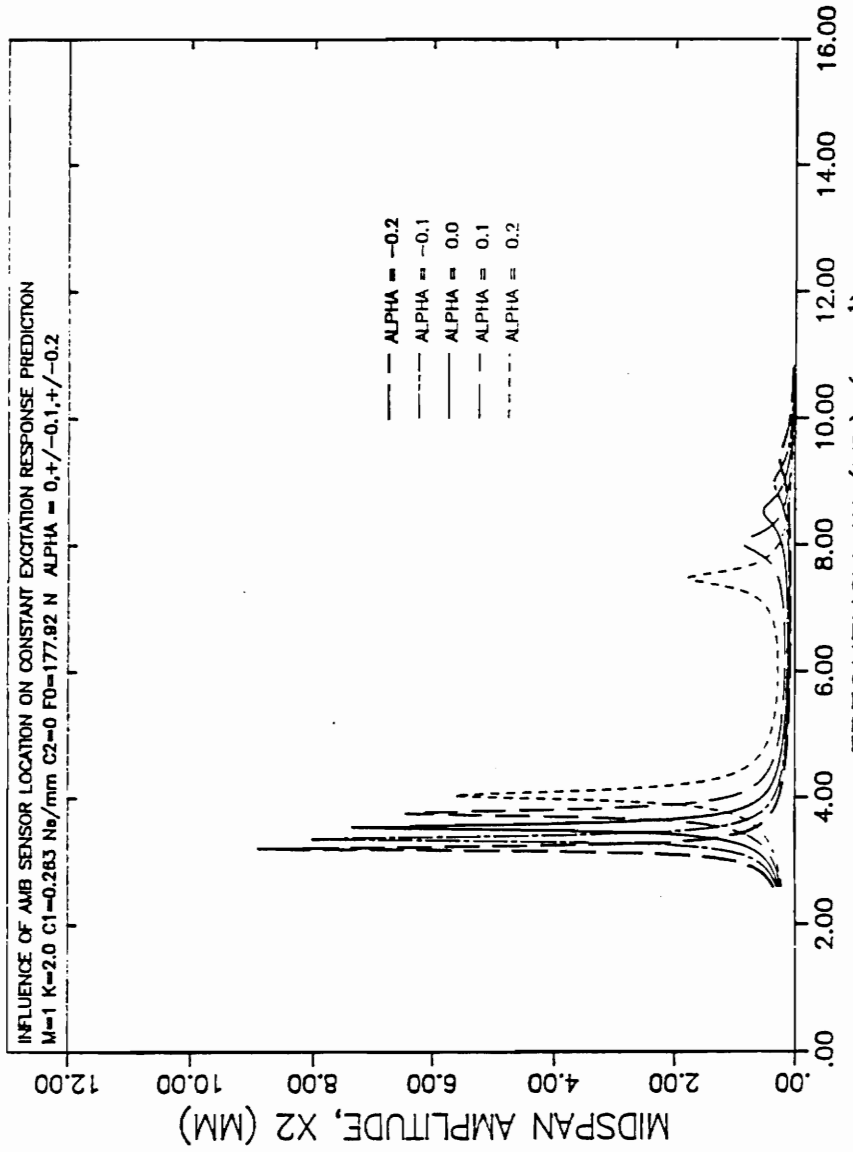

Figure 79.
Sensor Influence on Midspan Amplitude, Planar Excitation, M = 1, K = 2

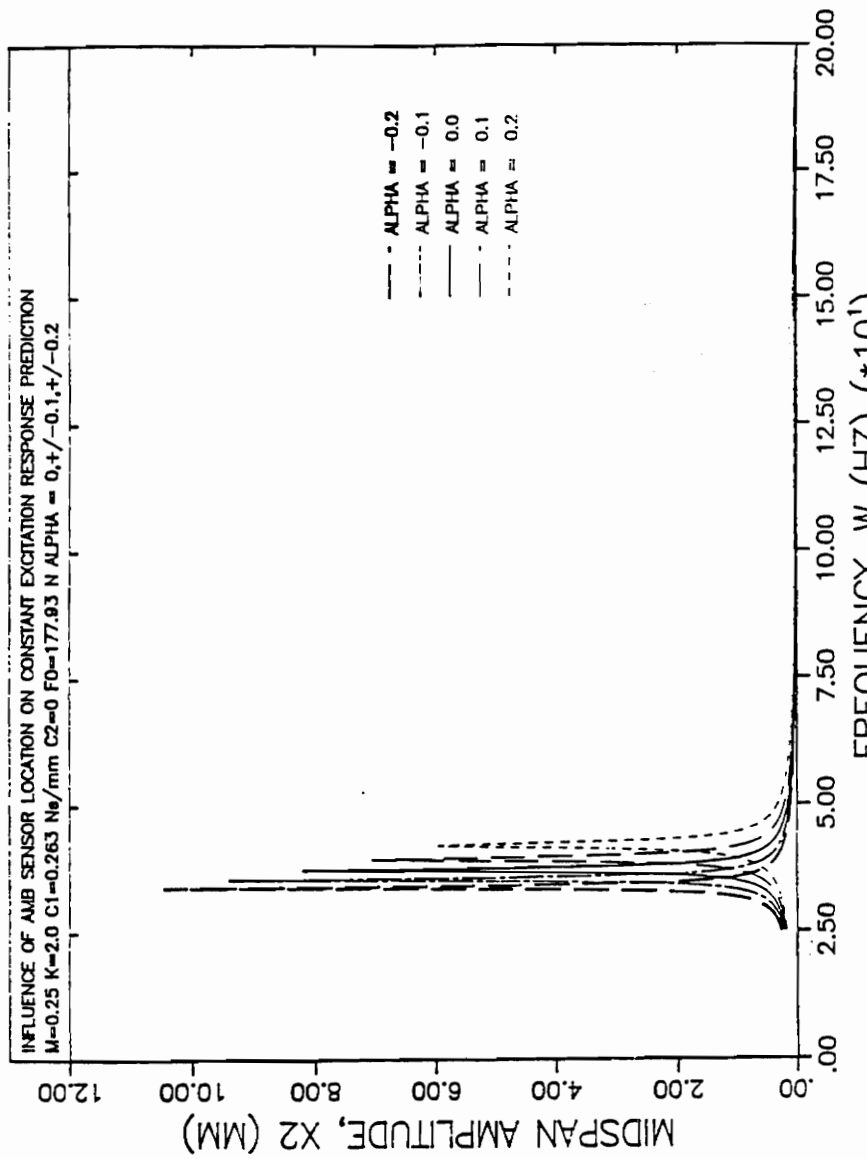

Figure 80.

Sensor Influence on Midspan Amplitude, Planar Excitation, M = 0.25, K = 2

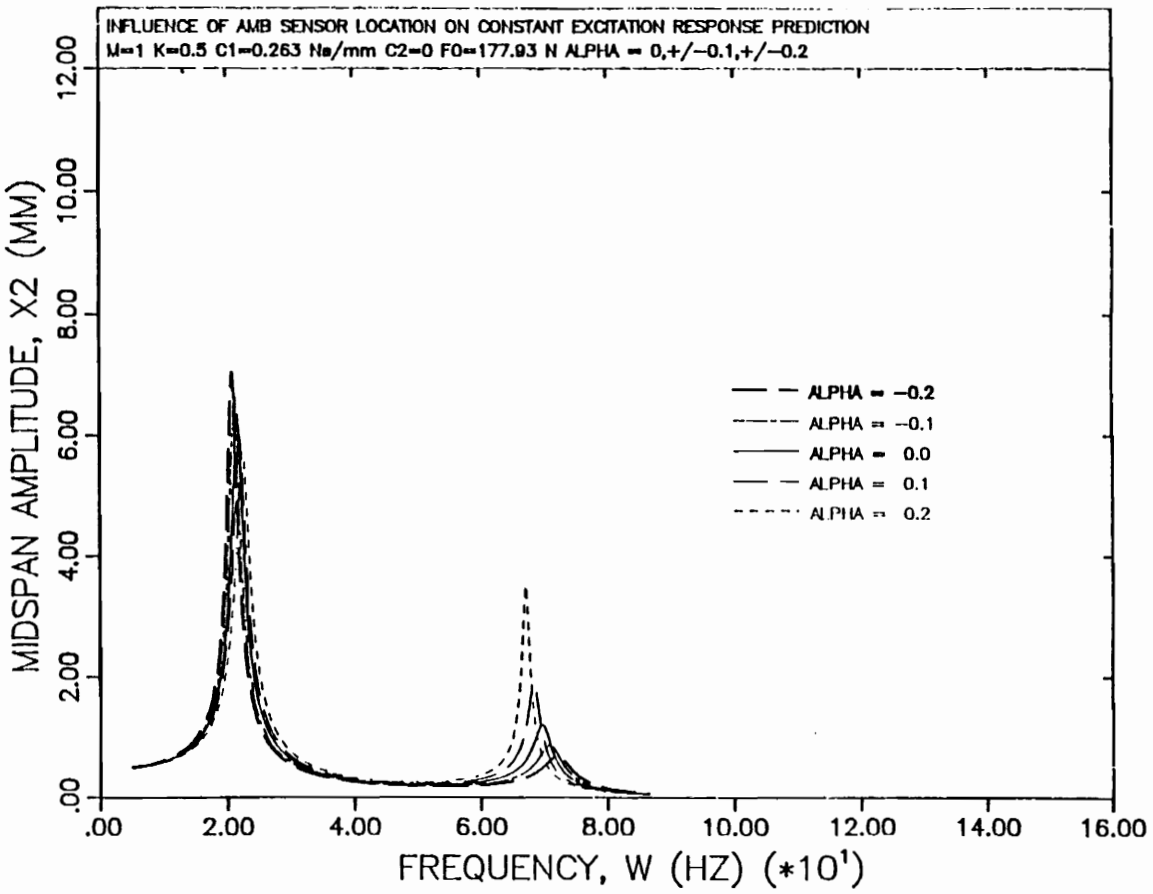

Figure 81.
Sensor Influence on Midspan Amplitude, Planar Excitation, M = 1, K = 0.5

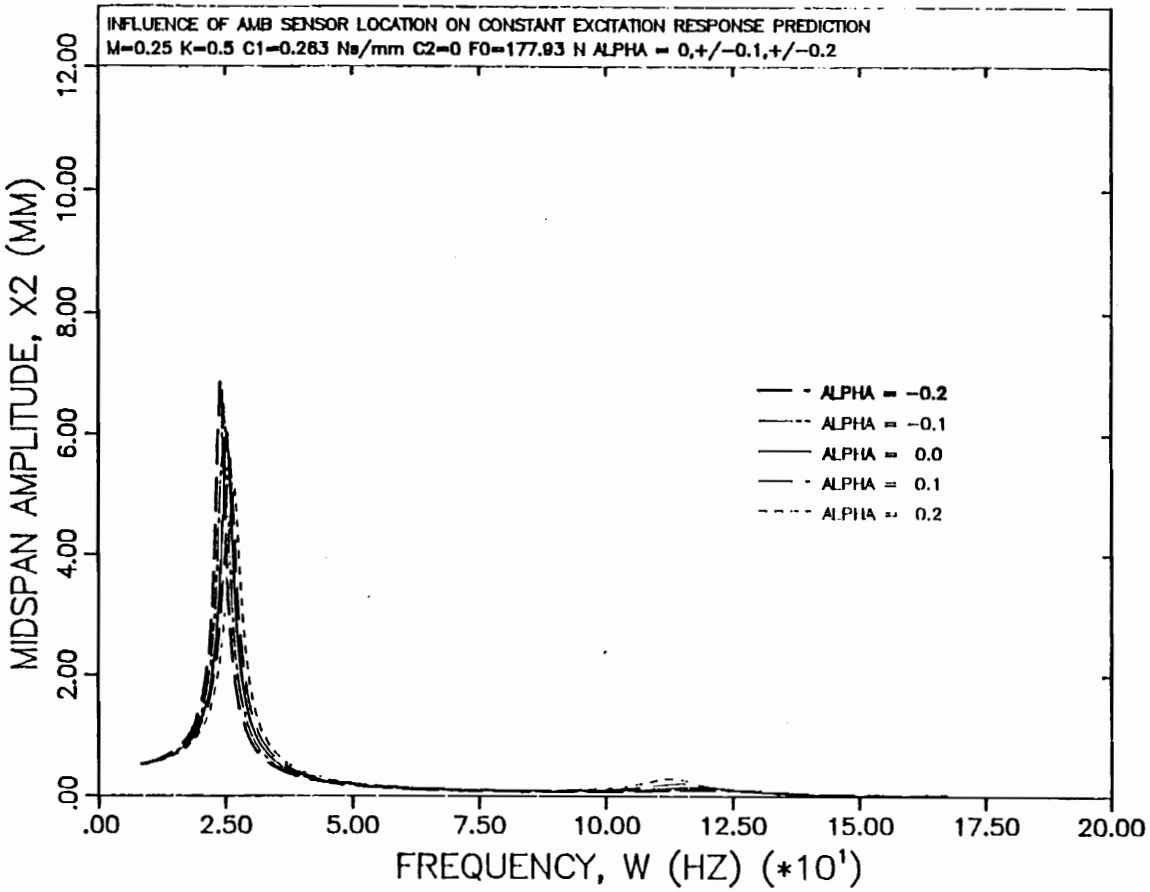

Figure 82.

Sensor Influence on Midspan Amplitude, Planar Excitation, M = 0.25, K = 0.5

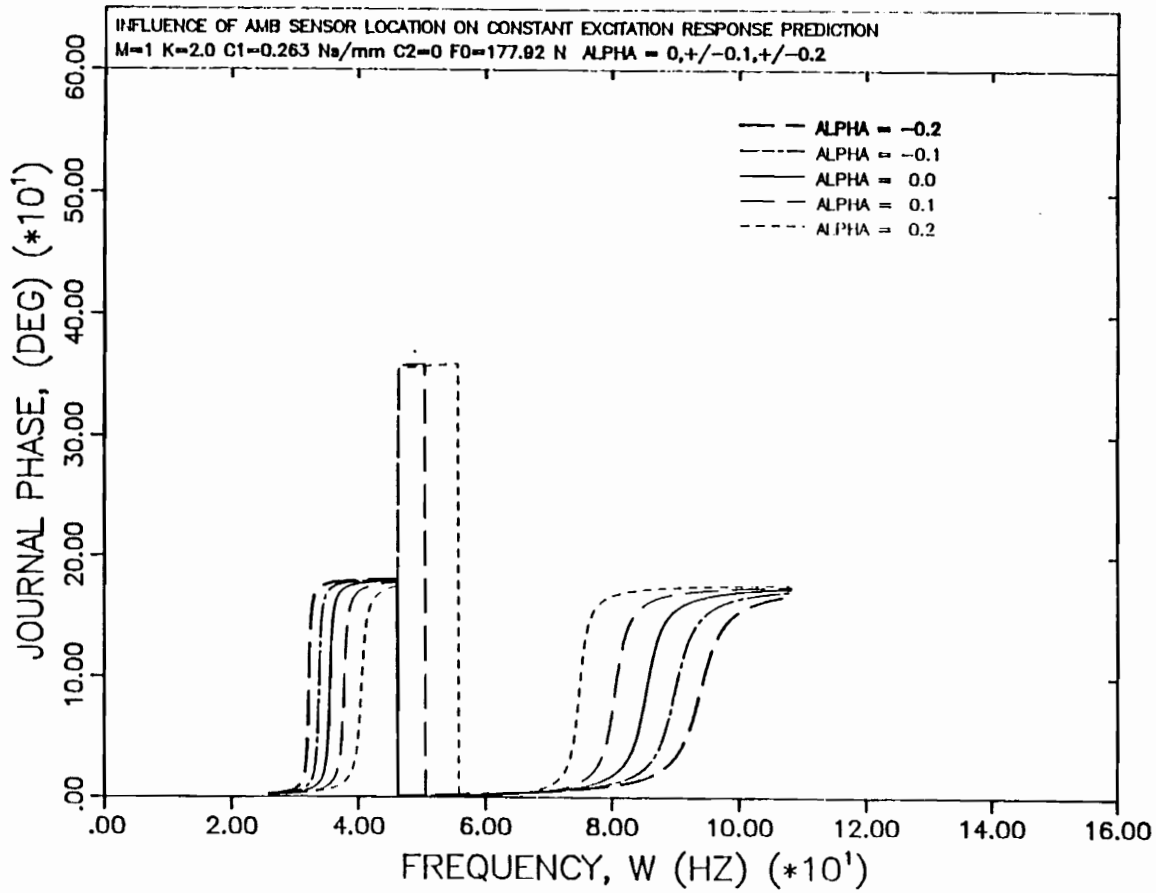

Figure 83.
Sensor Influence on Bearing Phase, Planar Excitation, M = 1, K = 2

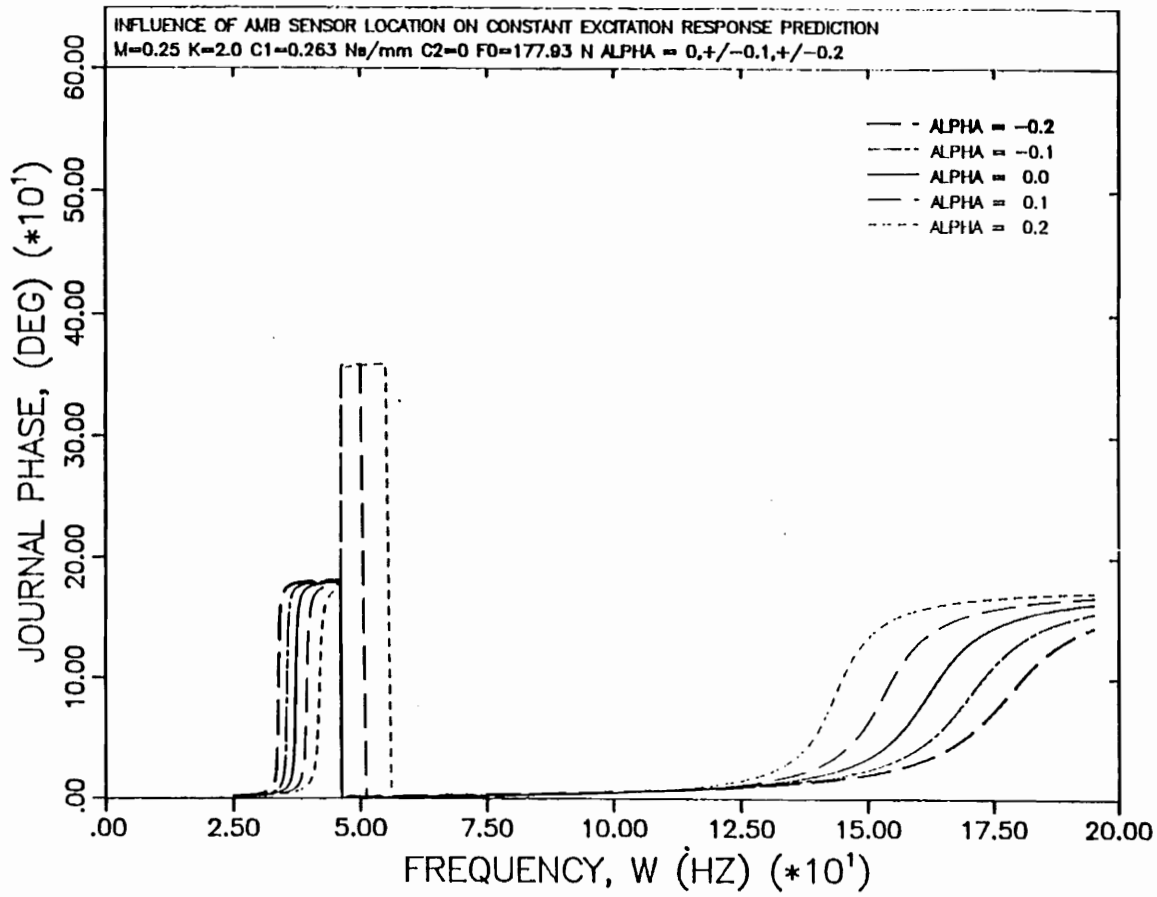

Figure 84.

Sensor Influence on Bearing Phase, Planar Excitation, M = 0.25, K = 2

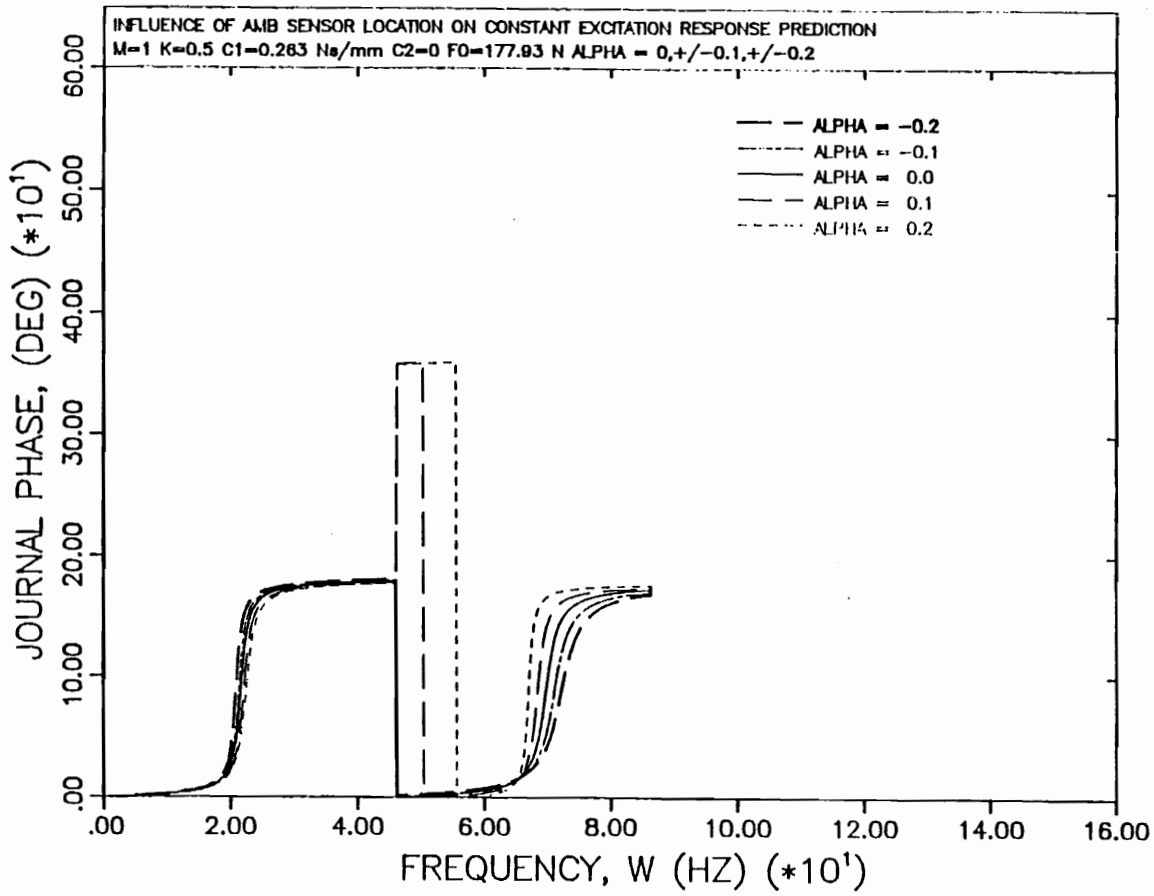

Figure 85.
Sensor Influence on Bearing Phase, Planar Excitation, M = 1, K = 0.5

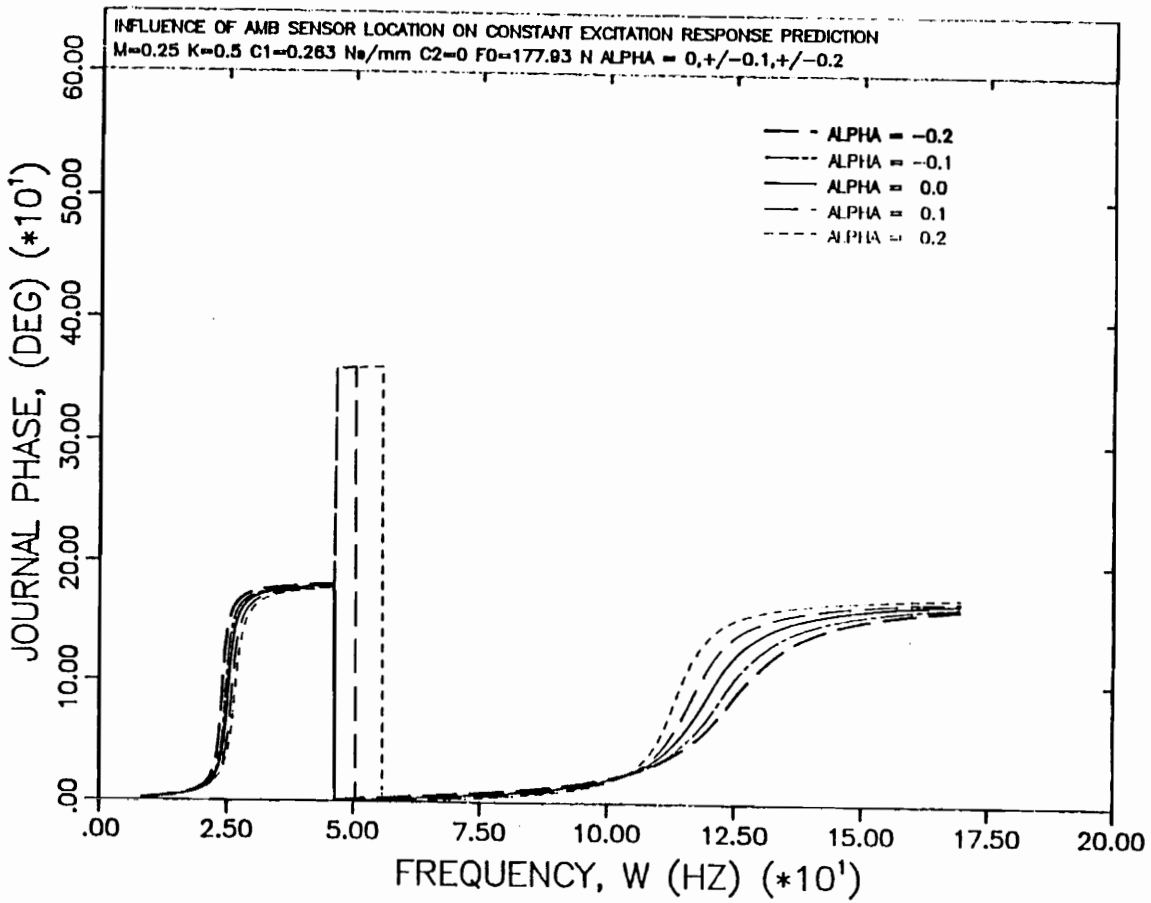

Figure 86.

Sensor Influence on Bearing Phase, Planar Excitation, M = 0.25, K = 0.5

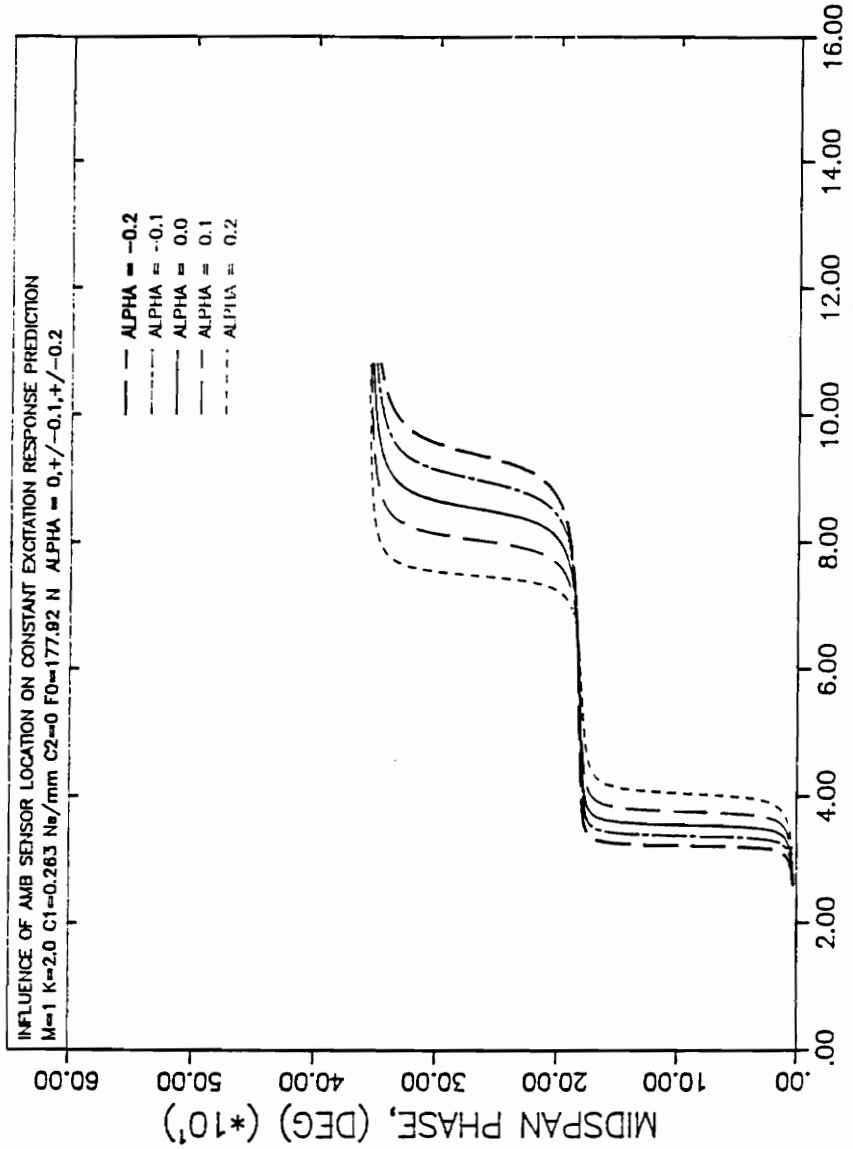

Figure 87.
Sensor Influence on Midspan Phase, Planar Excitation, M = 1, K = 2

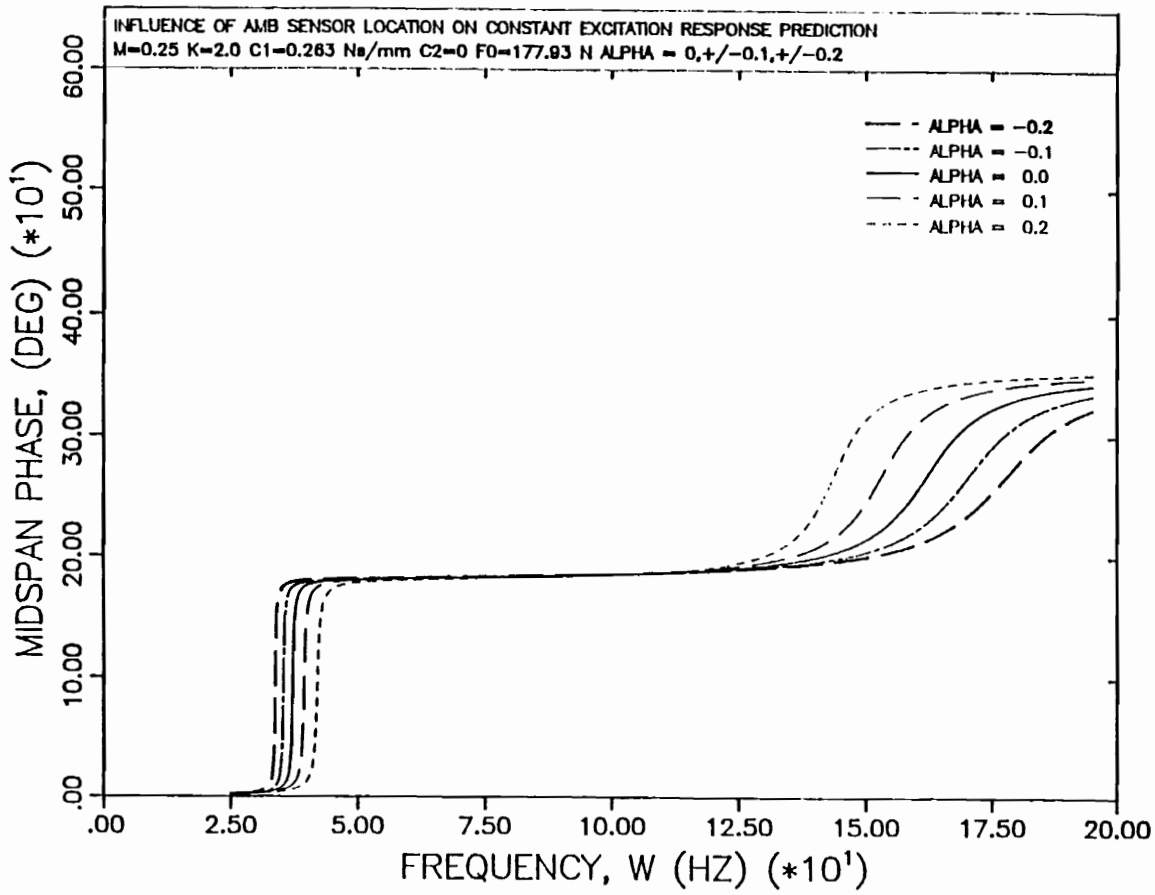

Figure 88.

Sensor Influence on Midspan Phase, Planar Excitation, M = 0.25, K = 2

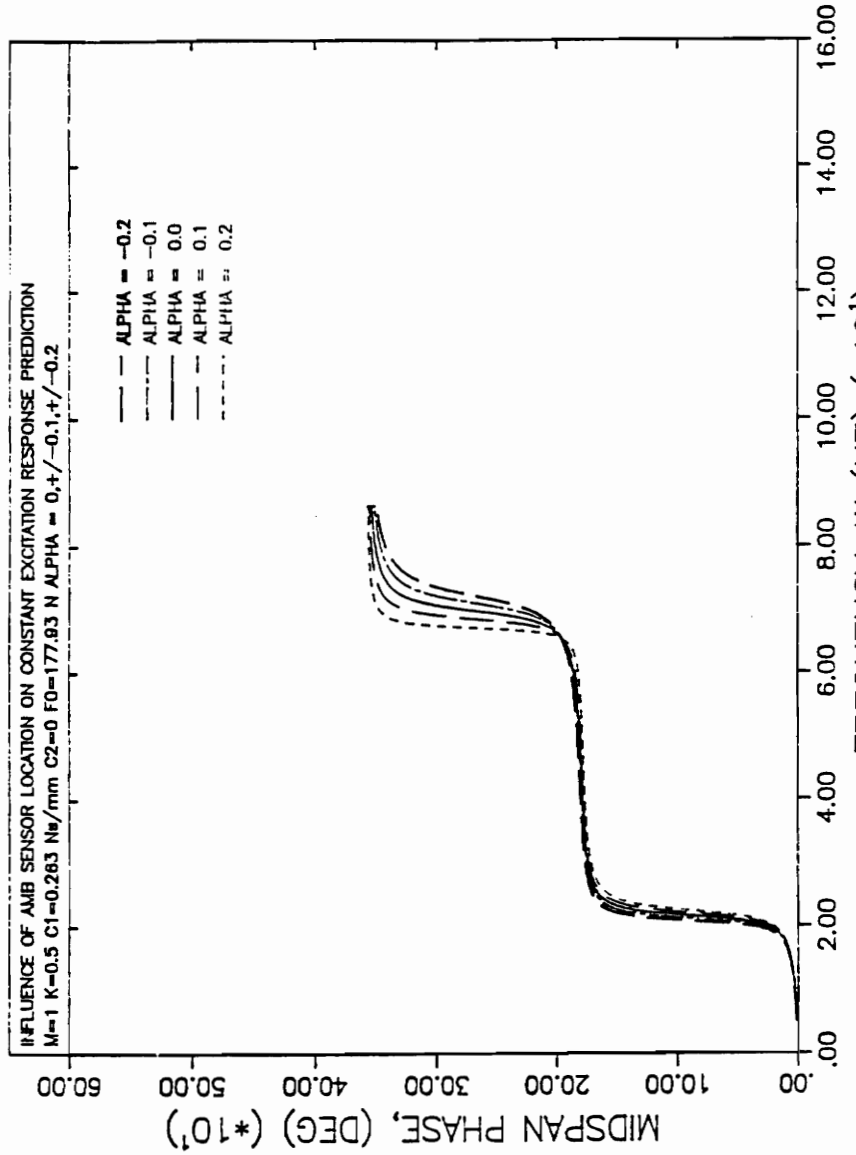

Figure 89.
Sensor Influence on Midspan Phase, Planar Excitation, M = 1, K = 0.5

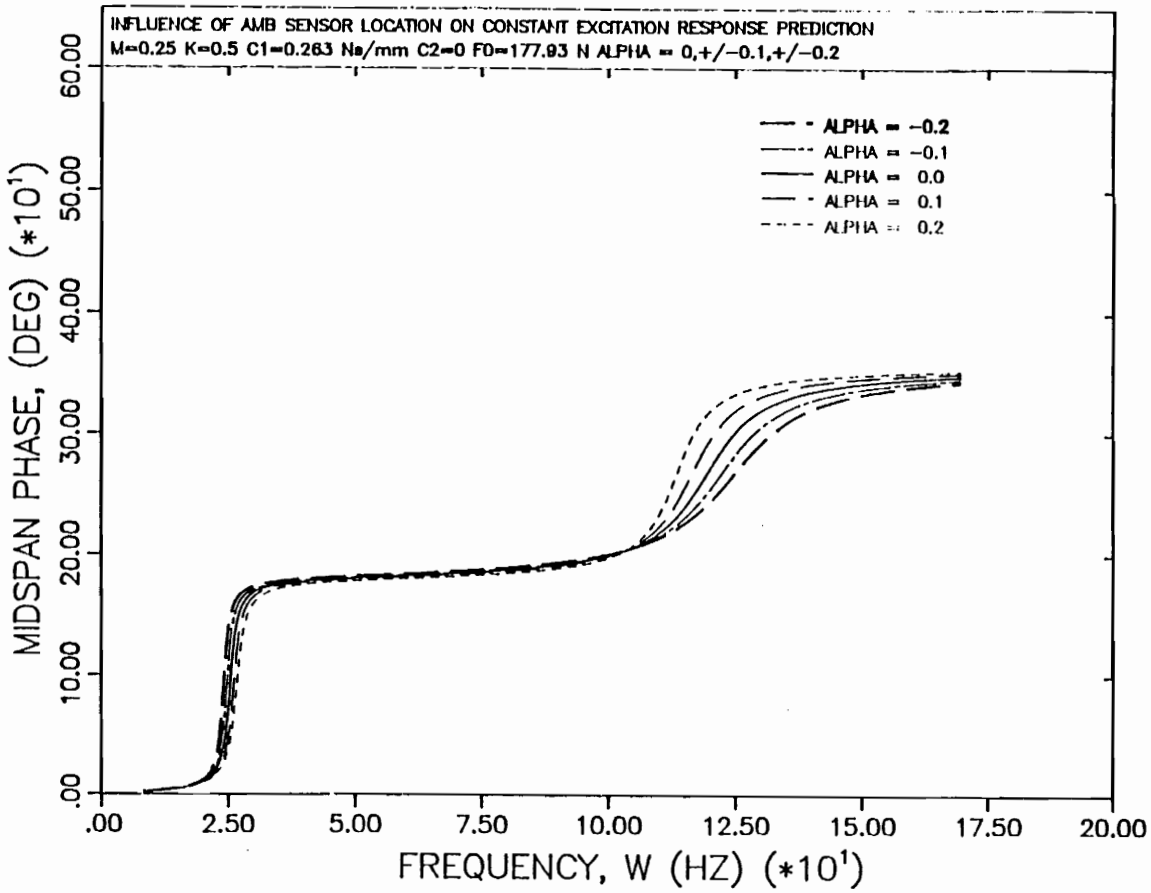

Figure 90.

Sensor Influence on Midspan Phase, Planar Excitation, M = 0.25, K = 0.5

VITA

The author was born on Jan 20, 1966 in North Gujarat, India and completed his high school education in Bombay in March 1981. After completing his higher secondary education in Ahmedabad in August 1983 he joined the Lalbhai Dalpatbhai College of Engineering, Gujarat University and graduated with a Bachelor's Degree in Civil Engineering in June 1988. Since August 1988 the author has been working towards a Master's Degree in Mechanical Engineering at the Virginia Polytechnic Institute and State University. He has also worked as a research assistant with the rotor-dynamics laboratory at Virginia Tech. from August 1989 to August 1990.